1st Asian Workshop on Molecular Spectroscopy

Program and Abstracts

May 20–21, 2017

Kyoto University, Japan

1st Asian Workshop on Molecular Spectroscopy

20 May (Saturday)

8 : 45 — 9 : 00 Opening Remarks Jon T. Hougen (NIST, USA)

9 : 00 — 9 : 15 A01 Shoko Okuda and Hiroyuki Sasada (Keio University, Japan)
"Relative Intensity of a Cross-over Resonance to Lamb Dips in the ν_3 Band of Methane"

9 : 15 — 9 : 30 A02 Christian Schröter, Jong Chan Lee, and Thomas Schultz (UNIST, Ulsan, Korea)
"Rotational Raman Spectroscopy with 5 THz Bandwidth, 3 MHz resolution, and sub-kHz accuracy"

9 : 30 — 9 : 45 A03 Kensuke Harada and Keiichi Tanaka (Kyushu University, Japan)
"Millimeter-wave spectroscopy of He-HCN and He-DCN:
Energy levels near the dissociation limit"

9 : 45 — 10 : 00 A04 Yu Zhai and Hui Li (Jilin University, China)
"Intermolecular Potential Energy Surfaces for HCN-H_2 van der Waals Complex and their applications in the research of HCN-(pH$_2$)N clusters"

---------- Coffee break ----------

10 : 15 — 10 : 30 A05 Yasuki Endo, Carlos Cabezas, and Jean-Claude Guillemin
(National Chiao Tung University, Taiwan)
"FTMW spectroscopy of substituted Criegee intermediates"

10 : 30 — 10 : 45 A06 Jou-Wei Su, Chen-An Chung, and Yuan-Pern Lee
(National Chiao Tung University, Taiwan)
"Infrared Absorption Spectrum of Hydroperoxymethyl Formate [HC(O)OCH$_2$OOH] Produced in the Reaction of the Criegee Intermediate CH$_2$OO with HCOOH

10 : 45 — 11 : 00 A07 Yoshiyuki Kawashima, Ken Ajiki, and Eizi Hirota
(Kanagawa Institute of Technology, The Graduate University for Advanced Studies, Japan)
"Fourier Transform Microwave spectroscopy of CF_3SF_5"

11 : 00 — 11 : 15 A08 Takayoshi Amano
(Jet Propulsion Laboratory, California Institute of Technology, USA)
"Some theoretical considerations on the microwave three-wave mixing experiments"

---------- Coffee break ----------

11 : 30 — 11 : 45 A09 Yu-Jong Wu (National Synchrotron Radiation Research Center, Taiwan)
"Infrared Spectrum of Hydrogen Fluoride Anion Isolated in Solid Argon"

11 : 45 — 12 : 00 A10 Rafael Escribano, Pedro C. Gomez, Victor J. Herrero, and Naoki Watanabe
(Universidad Complutense de Madrid, Madrid, Spain, and Hokkaido University, Japan)
"Variation of H-bond properties with density in astrophysical ice structures"

12 : 00 — 12 : 15 A11 Yu-Hsuan Chen, Masashi Tsuge, and Yuan-Pern Lee
(National Chiao Tung University, Taiwan)
"Infrared spectra of protonated aniline in solid para-hydrogen"

12 : 15 — 12 : 30 A12 Koichiro Yamakawa, S. Azami, and Ichiro Arakawa
(Gakushuin University, Japan)
"Phonon-mediated nuclar spin relaxation of H_2O trapped in Ar matrix"

12 : 30 — 12 : 45 A13 Nobukimi Ohashi and Jon T. Hougen
(Kanazawa University, Japan, and NIST, Gaithersburg, USA)
"Cross-contamination of the fitting parameters in multidimensional tunneling treatments"

---------- Lunch ----------

14 : 00 — 14 : 15 A14 Yeon Guk Seong, Cheol Joo Moon, Ahreum Min, Ahreum Ahn, and Myong Yong Choi
(Gyeongsang National University, Chungbuk National University, Korea)
"Conformational Structures of Indole-3-acetic Acid by
UV-UV hole-burning and IR-dip spectroscopy"

14 : 15 — 14 : 30 A15 Cheol Joo Moon, Yeon Guk Seong, Ahreum Min, Ahreum Ahn, and Myong Yong Choi
(Gyeongsang National University, Chungbuk National University, Korea)
"Rapid Non-radiative Decay of Jet-cooled 2-hydroxyformanilide:
IR-dip Spectroscopy and Computational Studies"

14 : 30 — 14 : 45 A16 Yoshihiro Nakashima, Kensuke Harada, Keiichi Tanaka, and Takehiko Tanaka
(Kyushu University, Japan)
"High-resolution Fourier transform emission spectroscopy of the $A\,^2\Pi - X\,^2\Pi$ band of
the OCS^+ ion"

14 : 45 — 15 : 00 A17 Zhen-Dong Sun (Shandong University, China)
"Quantum Zeno effect in field-free methanol gas"

---------- Coffee Break ----------

15 : 15 — 15 : 30 A18 Li-Hong Xu, E. M. Reid, B. Guislain, J. T. Hougen, E. A. Alekseev, and I. Krapivin
(University of New Brunswick, Canada, NIST, USA, Institute of Radioastronomy of National Academy of Sciences of Ukraine, Ukraine, and V.N. Karazin Kharkiv National University, Ukraine)
"Ab Initio Calculations of Torsionally Mediated Hyperfine Splittings in E States of Acetaldehyde"

15 : 30 — 15 : 45 A19 Chen-Wen Wang, Chaoyuan Zhu, and Sheng-Hsien Lin
(National Chiao Tung University, Taiwan)
"Molecular Vibronic Spectra in Solution Simulated by Damped Franck-Condon Factors"

15 : 45 — 16 : 00 A20 Dongho Kim (Yonsei University, Korea)
"Unravelling of Baird's Rule via Spectroscopic Analysis: Reversal of Hückel Aromaticity in the Excited Singlet and Triplet States of Hexaphyrins"

16 : 00 — 16 : 15 A21 Takayoshi Ishimoto, Masaaki Baba, Naofumi Nakayama, and Umpei Nagashima
(Hiroshima University, Kyoto University, Conflex Corporation, FOCUS, Japan)
"Theoretical Study on Geometrical Isotope Effect and Rotational Constants of Polyatomic Molecules"

---------- Coffee Break ----------

16 : 30 — 16 : 45 A22 Ahreum Min, Ahreum Ahn, Cheol Joo Moon, Yeon Guk Seong, and Myong Yong Choi
(Chungbuk National University, Gyeongsang National University, Korea)
"Conformational structures of jet-cooled acetaminophen-water clusters: a gas phase spectroscopic and computational study"

16 : 45 — 17 : 00 A23 Yi-Jen Wang and Yen-Chu Hsu
(Institute of Atomic and Molecular Sciences, Academia Sinica, Taiwan)
"Vibrational Predissociation of the Ã state of the C_3Ar complex in the excitation energy region of 25410 − 25535 cm^{-1}"

17 : 00 — 17 : 15 A24 Kaito Takahashi
(Institute of Atomic and Molecular Sciences, Academia Sinica, Taiwan)
"Variations in the electron detachment spectra of F...H_2O Anion induced by proton motion"

17 : 15 — 17 : 30 A25 Taewan Kim, Wonwoo Park, and Oh-Hoon Kwon (UNIST, Ulsan, Korea)
"Photoinduced Proton Transfer of N-methyl-Hydroxyquinolinium to Small Water Clusters"

18 : 00 — 20 : 00 Picnic

21 May (Sunday)

9 : 00 — 9 : 15 B01 Sachi Kunishige, Takaya Yamanaka, Masaaki Baba, Masakazu Nakajima, Yasuki Endo, and Yasuhiro Ohshima
(Kyoto University, Institute for Molecular Science, University of Tokyo, Tokyo Institute of Technology, Japan)
"High-resolution Spectroscopy of Deuterated Benzenes"

9 : 15 — 9 : 30 B02 Yu-Chan Guan, Yung-Hsiang Chang, Yi-Chieh Liao, and Jow-Tsong Shy
(National Tsing Hua University, Taiwan)
"Precision Saturated Absorption Spectrsocopy of H_3^+ "

9 : 30 — 9 : 45 B03 Akiko Nishiyama, Kazuki Nakashima, Masatoshi Misono, and Masaaki Baba
(Fukuoka University, University of Electro-Communications, Kyoto University, Japan)
"Doppler-free two-photon absorption spectroscopy of vibronic excited states of naphthalene with reference to an optical frequency comb"

9 : 45 — 10 : 00 B04 Akiko Nishiyama, Satoru Yoshida, Takuya Hariki, Yoshiaki Nakajima, and Kaoru Minoshima
(University of Electro-Communications, JST, ERATO MINOSHIMA, Intelligent Optical Synthesizer (IOS) Project, Japan)
"High-sensitive and precise measurement of Doppler-free two-photon absorption spectra of Rb using dual-comb spectroscopy"

---------- Coffee break ----------

10 : 15 — 10 : 30 B05 Yao-Chin Huang, Yu-Chan Guan, Jow-Tsong Shy, and Li-Bang Wang
(National Tsing Hua University, Taiwan)
"Absolute frequency measurement of the molecular iodine hyperfine transition at 647 nm"

10 : 30 — 10 : 45 B06 Peng Kang, Jin Wang, Lei-gang Tao, Yu Robert Sun, An-wen Liu, Tian-peng Hua, and Shui-ming Hu
(Univesity of Science and Technology of China, China)
"Precise line parameters from laser-locked cavity ring-down spectroscopy"

10 : 45 — 11 : 00 B07 D.N. Patel, Tzu-Han Su, Hsiang-Chen Chui, and Jow-Tsong Shy
(National Tsing Hua University, National Cheng Kung University, Taiwan)
"Mid-infrared saturated absorption spectroscopy inside the hollow fiber using difference frequency generation source"

11 : 00 — 11 : 15 B08 L. F. Tsang, Man-Chor Chan, Wenli Zou, and Allan S-C. Cheung
(University of Hong Kong, China)
"Electronic transitions of tungsten monosulfide"

---------- Coffee break ----------

11 : 30 — 11 : 45 B09 Chiao-Wei Chen, Anthony J. Merer , and Yen-Chu Hsu
(Institute of Atomic and Molecular Sciences, Academia Sinica, Taiwan)
"The low-lying electronic states of scandium monocarbide, ScC"

11 : 45 — 12 : 00 B10 Kyohei Watanabe, Kaori Kobayashi, Fusakazu Matsushima, Yoshiki Moriwaki, and Stephen C. Ross
(University of Toyama, Japan, and University of New Brunswick, Canada)
"Laser spectroscopic study of the B/B' $^2\Sigma^+$ v = 9, 10, 11 and 18 levels of CaH"

12 : 00 — 12 : 15 B11 Sang Kuk Lee
(Pusan National University, Korea)
"Vibronic Emission Spectroscopy of Jet-cooled Benzyl-type Radicals Generatedfrom Corona Discharge of Chloro-Substituted o-Xylenes"

12 : 15 — 12 : 30 B12 Kohei Tada, Michihiro Hirata, Shunji Kasahara, Takashi Ishiwata, and Eizi Hirota
(Kyoto University, Kobe University, Hiroshima City University, and The Graduate University for Advanced Studies, Japan)
"High-resolution laser spectroscopy and Zeeman effect of nitrate radical"

12 : 30 — 12 : 45 B13 Masaru Fukushima and Takashi Ishiwata
(Hiroshima City University, Japan)
"Vibronic coupling in the X $^2A_2'$ state of NO_3"

12 : 45 — 13 : 00 B14 Kaori Kobayashi, Wataru Nakamura, Tatsuro Matsushima, Shozo Tsunekawa, and Nobukimi Ohashi (University of Toyama, Kanazawa University, Japan)
"The Microwave Spectroscopy of Ground State CD_3SH"

---------- Lunch ----------

14 : 00 — 14 : 15 B15 Sheng-Yuan Tzeng and Wen-Bih Tzeng
(Institute of Atomic and Molecular Sciences, Academia Sinica, Taiwan)
"Mass-Analyzed Threshold Ionization Spectroscopy of Some Sandwich Molecules"

14 : 15 — 14 : 30 B16 Yu-Che Sun and Wen-Bih Tzeng
(Institute of Atomic and Molecular Sciences, Academia Sinica, Taiwan)
"Study of 2-Chloro-4-fluoroanisole by Two-Color Resonant Two-Photon Mass-Analyzed Threshold Ionization Spectroscopy"

14 : 30 — 14 : 45 B17 Yu Ran Lee, Hong Lae Kim, and Chan Ho Kwon
(Kangwon National University, Korea)
"One-photon mass-analyzed threshold ionization (MATI) spectroscopy of thietane cation"

14 : 45 — 15 : 00 B18 Sung Man Park, Hong Lae Kim, Chan Ho Kwon
(Kangwon National University, Korea)
"One-photon vacuum ultraviolet mass-analyzed threshold ionization (VUV-MATI) spectroscopy of crotonaldehyde"

---------- Coffee break ----------

15 : 15 — 15 : 30 B19 Yu Ran Lee, Hong Lae Kim, and Chan Ho Kwon
(Kangwon National University, Korea)
"Conformer-specific ion spectroscopy of isobutanal"

15 : 30 — 15 : 45 B20 Do Won Kang, Hong Lae Kim, Chan Ho Kwon
(Kangwon National University, Korea)
"Vacuum ultraviolet mass-analyzed threshold ionization spectroscopy of hydrazoic acid"

15 : 45 — 16 : 00 B21 Sung Man Park, Chan Ho Kwon, and Hong Lae Kim
(Kangwon National University, Korea)
"VUV-MATI spectroscopy of tetrahydrofuran"

16 : 00 — 16 : 15 B22 Itaru Kurusu, Reona Yagi, Ryota Kato, Yasutoshi Kasahara, and Haruki Ishikawa
(Kitasato University)
"Temperature effect on the microscopic hydration structures of phenol cation"

---------- Coffee break ----------

16 : 30 — 16 : 45 B23 Ye-Jin Kim and Oh-Hoon Kwon
(Ulsan National Institute of Science and Technology, Korea)
"Proton diffusion dynamics along a diol as a proton-conducting wire in a photo-amphiprotic model system"

16 : 45 — 17 : 00 B24 So Young Eom, Hong Lae Kim, and Chan Ho Kwon
(Kangwon National University, Korea)
"Orientation change and structure according to the various pH conditions of 4-amino-4'-cyanobiphenyl on silver surfaces: SERS and DFT study"

17 : 00 — 17 : 15 B25 Young Jae Kim, Byeong Sung Lee, Tae Hyeon Yoo, and Oh-Hoon Kwon
(Ulsan National Institute of Science and Technology, Korea)
"Hydrogen-bonding energetics and dynamics of biological water using ultrafast electronic spectroscopy"

17 : 15 — 17 : 30 B26 Sung-Sik Lee, Soojin Park, Xianglei Kong, Sungyul Lee, and Han Bin Oh
(Kyung Hee University, Korea)
"Chiral Differentiation of Protonated L- and D-Amino Acids by Permethylated β-cyclodextrin: Experiments and Theory"

---------- Coffee break ----------

17 : 45 — 18 : 00 B27 Seongchul Park, Joohyang Shin, Changwon Yang, Youngshang Pak, and Manho Lim
(Pusan National University, Korea)
"Photodissociation of CF_2ICF_2I and CF_2I_2 in solution probed by femtosecond infrared spectroscopy"

18 : 00 — 18 : 15 B28 Jaeheon Park, Hak-Won Nho, and Oh-Hoon Kwon
(Ulsan National Institute of Science and Technology, Korea)
"Hydration characteristics of a water pool in a nano-confined system probed by a superphotoacid"

18 : 15 — 18 : 30 B29 Yang Cong and Hui Li
(Jilin University, China)
"Local Mode-Based Infrared Probe Spectra: a Case Study of Formic Acid-Water Clusters and Solutions"

18 : 30 — 18 : 45 Closing Remarks Masaaki Baba (Kyoto University, Japan)

Relative Intensity of a Cross-Over Resonance to Lamb Dips in the ν_3 Band of Methane

(Keio Univ., JST, ERATO MINOSHIMA IOS) Shoko Okuda and Hiroyuki Sasada

We have extensively observed sub-Doppler resolution Stark-modulation spectra in the ν_3 band of methane (CH_4) from 87.7 to 92.8 THz (2925 to 3096 cm^{-1}) using a comb-referenced difference-frequency-generation spectrometer. In the analysis, the vibration- and rotation-induced permanent electric dipole moments have been precisely determined for the vibrational excited and ground states [1]. In the course of the study, we have found that the relative intensity of a cross-over resonance to Lamb dips depends on the transition branch.

Figure 1 depicts three saturated absorption spectra under the Stark field perpendicular to the optical electric field. The dispersion-type line profiles are caused by the Stark-modulation detection. Figure 1 (a), (b) and (c) correspond to the P-, Q- and R-branch transitions between the $|v = 0, J'' = 4, E, |M''|=0 \text{ or } 2>$ and $|v_3 = 1, J', E, |M'|=1>$ levels, respectively, where vs are the vibrational quantum numbers, Js are the total angular momentum quantum numbers, Ms are the projection of $\boldsymbol{J}$ along the applied electric field, and E is the doubly degenerate irreducible representation of the T_d point group. The double and single primes present the vibrational ground and exited states. The horizontal axis indicates the frequency deviation from each zero-field transition frequency, ν_0, reported in Refs. [2,3]. Each triplet contains a cross-over resonance at the center and two Lamb dips. Figure 2 illustrates the energy level diagram of Fig. 1 (a) with zero (a)and nonzero external fields (b). The relative intensity of the Lamb dips agrees with the prediction from the corresponding Clebsch-Gordan coefficients. However, the relative intensity of a cross-over resonance to the larger Lamb dip depends on the transition branches. In particular, the cross-over resonance is the strongest among the components of the triplet for the Q- and R-branch transitions. This characteristic behavior has also been seen for most of the observed transitions, $P(4)\ E$, …, $P(7)\ E$, $P(8)\ E^{(2)}$ and $P(9)\ E$, $Q(2)\ E$, $Q(4)\ E$, …,$Q(7)\ E$ and $Q(8)\ E^{(2)}$, and $R(2)\ E$ and $R(4)$

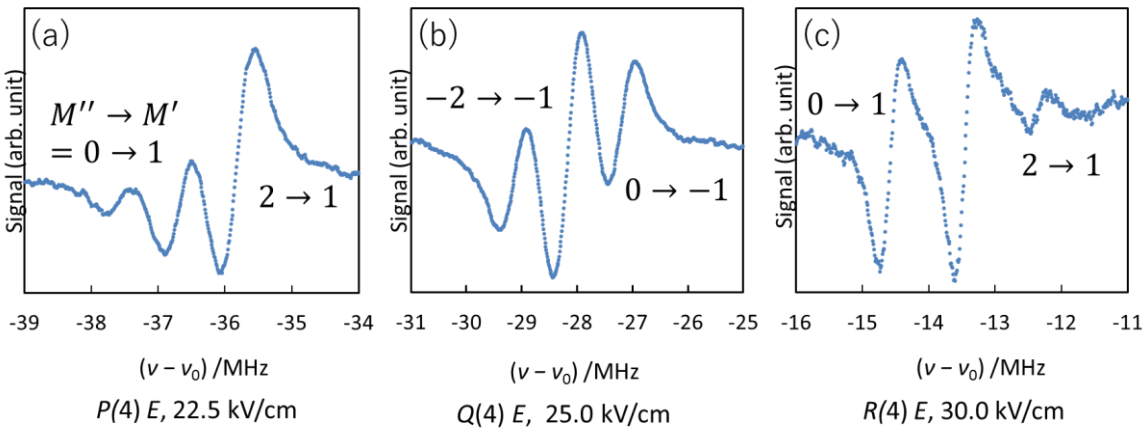

Figure 1. Observed Stark modulation spectra in the ν_3 band of methane. (a) shows the $P(4)\ E$ transition with the external field of 22.5 kV/cm, (b) and (c) are $Q(4)\ E$ with 25.0 kV/cm and $R(4)\ E$ with 30.0 kV/cm, respectively. In each figure, the center spectral component is a cross-over resonance and the others are the associated Lamb dips.

E, …, $R(7)$ E. This is often observed in atomic spectra but never in molecular spectra, as far as we know.

We have analyzed the intensity of the cross-over resonance and the Lamb dips using the rate equation, which was developed for saturated absorption spectroscopy of atoms [4], where the spontaneous emission is the dominant relaxation process. It is revealed that the intensity of the triplet agrees with the atomic theory for the Q-branch transitions, whereas that for the P- and R-branch transitions is apart from it. We attribute this to the difference in the transition dipole moments of the branches and the collisional relaxation rates.

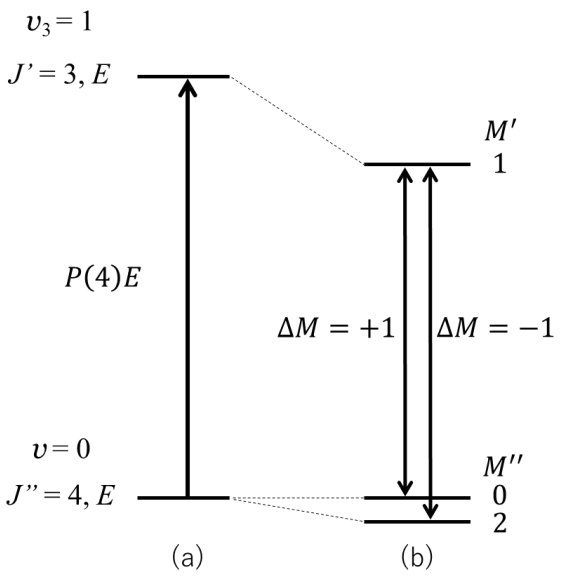

Figure 2. Energy level diagram of the $P(4)E$ transition in Fig. 1 (a) in the absence of the external electric field (a) and in the presence of it (b).

[1] S. Okuda and H. Sasada, 71st International Symposium on Molecular Spectroscopy, The University of Illinois at Urbana-Champaign, TJ09 (2016).

[2] S. Okubo, H. Nakayama, K. Iwakuni, H. Inaba, and H. Sasada, Opt. Express **19**, 23878 (2011).

[3] M. Abe, K. Iwakuni, S. Okubo, and H. Sasada, J. Opt. Soc. Am. B **30**, 1027 (2013).

[4] S. Nakayama, Jpn. J. Appl. Phys. **23**, 879 (1984).

Rotational Raman Spectroscopy with 5 THz Bandwidth, 3 MHz resolution, and sub-kHz accuracy.

(UNIST, 50 UNIST-gil, Eonyang-eup, Ulju-gun, Ulsan, 44919, REP. OF KOREA)
Christian Schröter, Jong Chan Lee, Thomas Schultz (schultz@unist.ac.kr)

Scientific progress is always based on the observation of the natural world. In the field of spectroscopy, we construct ever more powerful spectroscopic tools to increase the fidelity and accuracy of our observations. Modern spectroscopy often operates at the physical limits of observation, e.g., the quantum limit of observing single particles or the precision limit of the Heisenberg uncertainty principle. Further progress requires ingenious measurement concepts, such as the correlation of observables in multidimensional NMR,[1] or the direct coupling of optical frequencies to high-precision clocks in extreme-resolution frequency-comb atomic spectroscopy.[2]

We correlated high-resolution rotational spectra with observables from ultra-fast laser spectroscopy in the technique of correlated rotational alignment spectroscopy (CRASY).[3] As in multidimensional NMR, we coherently excite and probe angular momentum wave packets in the time domain. Instead of nuclear spins, our experiment excites and probes molecular rotations using short optical laser pulses. As in frequency-comb measurements, we couple our experiment to a high-precision clock to obtain absolute frequency results without systematic errors.

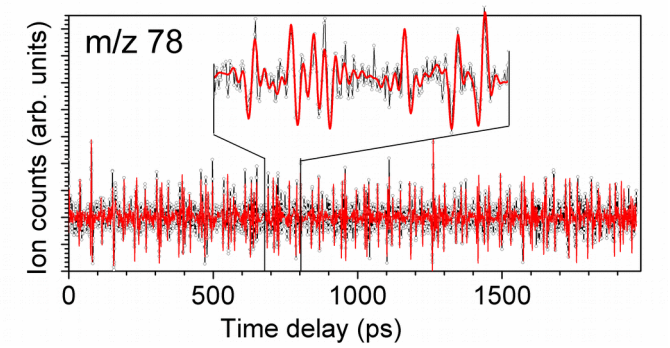

Figure 1: Rotational coherence trace for the $^{32}S^{12}C^{34}S$ isotope (m/z 78). Signal modulations are due to a rotationally coherent wave-packet excited at time delay 0. Extending range of observed time delays increases the spectroscopic resolution of the Fourier-domain spectrum (cf. Figure 2).

Figure 1 shows the measured rotational coherence signal for a mass-selected isotope of carbon disulfide. An 800 nm picosecond laser pulse excited a rotationally coherent wave packet in a beam of neutral, cold molecules. The temporal evolution of the wave packet was probed by 200 nm photoexcitation and photoionization. The formed ions were detected in a mass spectrometer.

The spectroscopic resolution of rotational spectra measured by CRASY, or by

the related methods of rotational coherence spectroscopy (RCS),[3] is fundamentally limited by Heisenberg's uncertainty principle $\Delta E \cdot \Delta t \geq \hbar/2$. The observation time Δt corresponds to the length of the delay range over which we observe the rotational coherence modulations. Our experiment operates at the Heisenberg limit and any increase in observation range directly results in a proportionally higher resolution. To reduce the energy uncertainty, our new spectroscopic set-up at UNIST employs electronic pulse-picking of femtosecond oscillator pulses. This extends the delay range Δt into the sub-microsecond regime, a factor 50 beyond the best published RCS data.

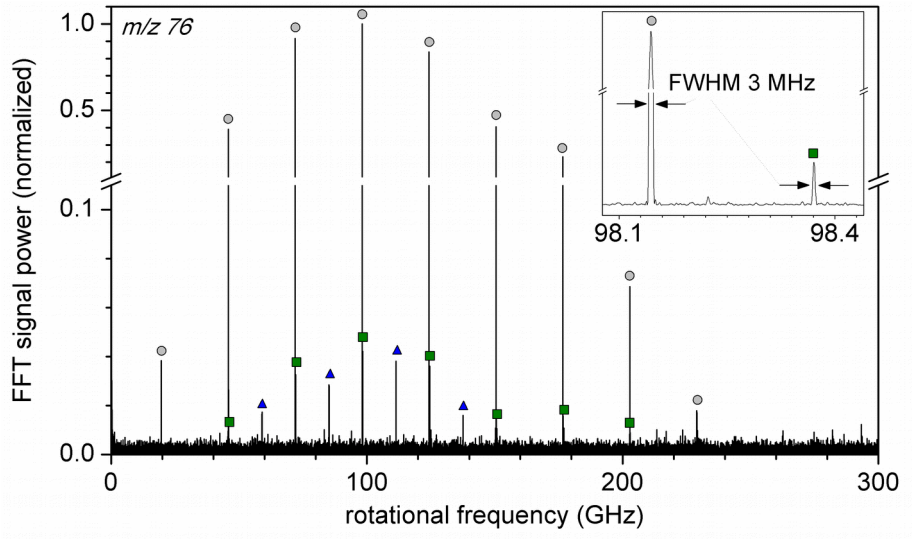

Figure 2: Fourier-transform rotational Raman spectrum for the main isotope of carbon disulfide (mass m/z 76). The vibrational ground state shows a regular progression with frequencies $\omega_J = B \cdot (4J + 6)$ for even J and $\Delta J = 2$ (circles). The lowest vibrational bending mode with angular momentum $l = \pm 1$ gives progressions for even/odd J quantum numbers (marked with squares and triangles, respectively).

Figure 2 shows a mass-CRASY spectrum for the main isotope of carbon disulfide, obtained by the Fourier transformation of a signal trace as shown in Fig. 1. In this mass channel, we resolved progressions for the vibrational ground state of carbon disulfide and the lowest vibrational bending state. A fit of the line positions gave a rotational constant of B = 3271517.2 ± 0.6 kHz and a centrifugal distortion of D = 356 ± 3 Hz for the ground state, and B = 3277905 ± 12 kHz, D = 406 ± 81 Hz for the first bending mode with an l-type splitting of q = 1160 ± 12 kHz.

Our electronic pulse-picking method directly relates the measured rotational frequencies to the laser repetition rate. We monitored the laser repetition rate against a GPS stabilized clock with absolute errors of $\Delta t/t <= 10^{-10}$. Accounting for possible short-term drifts of clock or laser, we can determine absolute frequency values with relative errors $<<10^{-8}$, well below our current measurement accuracy of $2 \cdot 10^{-7}$.

Millimeter-wave spectroscopy of He-HCN and He-DCN: Energy levels near the dissociation limit.

(Kyushu Univ.) Kensuke Harada and Keiichi Tanaka

The He-HCN complex is a weakly bound complex. We have observed the the *j*=1-0 and 2-1 internal rotation and intermolecular stretching bands of He-HCN and He-DCN by millimeter-wave absorption spectroscopy. The upper state of several observed transitions were found to be located above the "dissociation limit" (D_0). These levels are bound due to the parity conservation. The potential energy surface (PES) fitted to the observed transitions has a global minimum in the linear He--HCN configuration with a depth of 29.9 cm^{-1} and has a saddle point at the anti-linear He--NCH configuration. Life times of several quasi-bound levels are predicted for both isotopic species.

The He-HCN complex is a weakly bound complex with binding energy of about 9 cm^{-1}. We have observed the internal rotation band (j = 1←0) of the He-HCN complex by millimeter-wave absorption spectroscopy combined with a pulsed-jet expansion technique and reported the potential energy surface (PES) to reproduce the observed transition frequencies.[1]

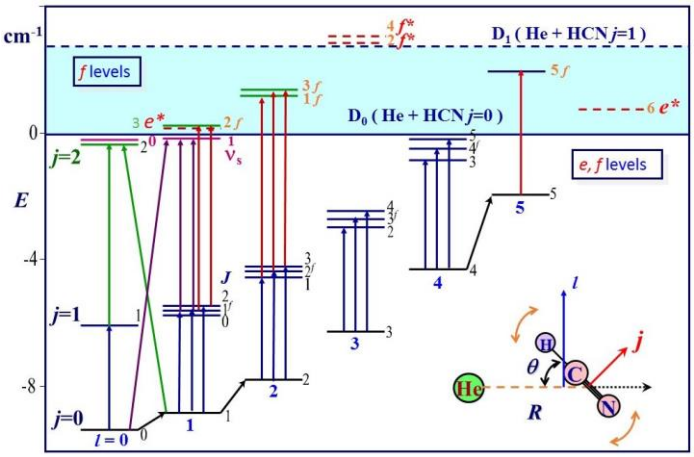

Fig. 1. Energy levels and observed transitions of He-HCN

The measurement was extended to the internal rotation hot band (the j=2-1 band) and the intermolecular stretching band (ν_s). The vdW bands of He-DCN were also observed.

[Energy levels and observed transitions]

The energy levels and observed transitions of He-HCN are illustrated in Fig. 1. The j, l, J are the internal rotation angular momentum of HCN, the angular momentum for the end-over-end rotation of He-HCN, and the total angular momentum of the complex. The intermolecular stretching first excited state (ν_s) and the internal rotation second excited state (j = 2) are determined to be located at 9.140 and 9.053 cm^{-1} above the ground state, very close to the dissociation limit (D_0) of 9.316 cm^{-1}.

The several transitions to the bound states above the ”dissociation limit” (D_0) have been observed for He-HCN. The level of He-HCN has the +/– parity if $j + l$ is even/odd and it is also labeled as *e*/*f* when $J - j - l$ is even/odd. Since the parity and the total angular momentum J are conserved, the *e*/*f* label is conserved even in the dissociation process. If the He-HCN complex dissociates to He and HCN with the j=0 rotational ground state, the He + HCN system has the *e* symmetry, because $J = l$. On the other hand, when the complex dissociates to He and HCN with the j=1 rotational excited state, the system splits into three components; two e ($J = l \pm 1$) and one *f* ($J = l$) state. Due to the conservation of *e*/*f*-symmetry, the *f*-levels of the He-HCN complex dissociate to He + HCN (j=1) because it contains

the lowest *f*-level. The *f*-levels have the other dissociation limit of D_1, located by 2.96 cm^{-1} higher than the dissociation limit D_0 for the *e* levels. The present analysis indicates that four and three *f* levels are bound for He-HCN and He-DCN above the "dissociation limit" (D_0).

In the analysis, we also predicted the quasi-bound energy levels by the method of Hazi and Tayler.[2] The four and three levels (both of *e* and *f* labels) are predicted to be quasi-bound for He-HCN and He-DCN. These levels have finite life times as listed in Table 1 since the centrifugal barriers V_{max} are higher than the energies of these levels.

Table 1. Metastable States of He-HCN

j	*l*	*J*	$E(cm^{-1})$	$V_{max}(0°)$	τ(ns)
He-HCN					
0	6	6^e	0.7509	2.848	1.8
2	1	3^e	0.32	0.453	0.021
2	3	2^f	3.0168	3.118	14
2	3	4^f	3.2538	3.918	16
He-DCN					
0	6	6^e	0.2084	2.849	470
2	3	5^e	1.431	1.752	0.26
2	4	5^f	3.73	4.168	0.053

[Potential energy surface]

The PES fitted to reproduce the observed transition frequencies of He-HCN has a global minimum in the linear He—HCN configuration with a depth of 29.812 cm^{-1} and has a saddle point at the anti-linear He--NCH configuration with a depth of 20.812 cm^{-1}. The potential height on the minimum energy path (MEP) of the PES have been illustrated in Fig. 2. The PES of He-HCN obtained in the analysis is similar to the theoretical PES,[3] although the present PES has by 1 cm^{-1} smaller potential anisotropy ($V_{MEP}(\theta=\pi)-V_{MEP}(\theta=0)$) than the theoretical one.

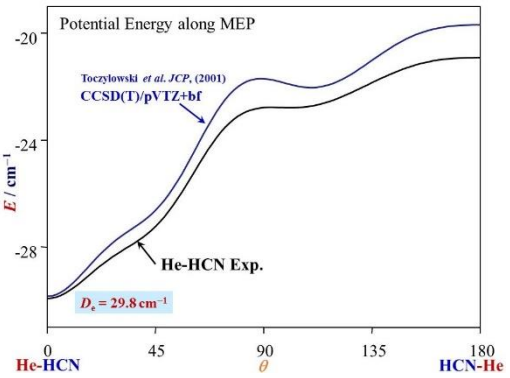

Fig. 2. Potential height on MEP

[Long range potential parameters]

In the present analysis, we have used a coupled potential of a exponential ($e^{-\beta R}$) repulsive potential and a asymptotic long range attractive potential. In total, 8 short range and 8 long range potential parameters have been determined. The long range potential parameters obtained are compared in Table 2. The C_{nl} is the coefficient of the $P_l(\cos\theta) \cdot R^{-n}$ dependence term. The PES reported by CCSD(T)/cc-pVTZ *abinitio* calculation[3] was also fitted by the same potential function and parameters obtained are also compared in Table 2. The long range potential parameters obtained for the normal and deuterated species are similar and also consistent to the parameters fitted to the theoretical PES.

Table 2. Long Range Parameters of He-HCN and He-DCN in au.

	He-HCN	He-DCN	CCSD(T)/cc-pVTZ
C_{60}	16.353(60)	16.924(42)	16.24(15)
C_{80}	280.0(40)	230.4(29)	234.(13)
C_{71}	28.593(98)	29.124(130)	23.8(28)
C_{91}	906.3(134)	822.0(86)	950.(220)
C_{62}	4.480(123)	5.673(96)	5.56(26)
C_{82}	484.2(86)	379.9(75)	332.(22)
C_{73}	26.19(30)	27.244(77)	11.0(24)
C_{93}	---	---	1130.(160)
C_{84}	118.01(52)	115.17(114)	70.2(43)

[1]J. Chem. Phys. **117**, 7041(2002). [2]Phys. Rev. A1, 1109 (1970). [3]J. Chem. Phys. 114, 851 (2001).

A04

Intermolecular Potential Energy Surfaces for HCN-H_2 van der Waals Complex and Their Applications in the Research of HCN-(pH_2)$_N$ Clusters

(Jilin Univ.[a]) Yu Zhai[a], Hui Li[a]
Email:prof_huili@jlu.edu.cn

Morse/Long-Range potential energy model is a spectroscopically accurate model which has been expended to Multi-Dimension Morse/Long-Range (MD-MLR) model to describe the intermolecular interaction. In this work, we adopt the MD-MLR model to fit *ab initio* pointwise energies got from vibrationally averaging over the intramolecular vibrational coordinate, which corresponding to the ground-state HCN-H_2 and excited-state HCN-H_2 interactions, respectively. Furthermore, reduce-dimension PESs, which describe the effective interaction between HCN at different state and *para*-hydrogen (pH_2), are got from adiabatic 'hindered-rotor' average. The obtained 2D PESs are used in Path Integral Monte Carlo (PIMC) quantum simulation of HCN-(pH_2)$_N$. The band origin shifts of HCN in the quantum clusters are calculated based on these PESs. The predicted Infrared spectra of HCN-H_2 and the simulation results for HCN-(pH_2)$_N$ agree well with the experiments.

FTMW spectroscopy of substituted Criegee intermediates

(National Chiao Tung Univ.[a], Institut des Science Chimiques de Rennes[b]) Yasuki Endo[a], Carlos Cabezas, and Jean-Claude Guillemin[b]

Substituted Criegee intermediates (CI's) were investigated by FTMW spectroscopy. In the present study, we were able to identify more than three species through their pure rotational spectra. Among the species observed, the dimethyl CI was found to show internal rotations of two methyl tops. On the other hand, the ethyl and methyl-ethyl CI's are expected to have four conformers. For the ethyl CI, three conformers were identified among the four, while all the four conformers were identified for the methyl-ethyl CI. Both of the species show internal rotation splittings for the methyl part.

Introduction

The Criegee intermediates, R_1R_2COO, are known to be produced by the ozonolysis reaction, the reactions of unsaturated hydrocarbons with ozone, and they are considered to be importance source of the OH radical. Studies of the Criegee intermediates are thus performed very extensively in recent years. So far, we have reported detections of the simplest Criegee intermediate, CH_2OO and its mehyl-substituted species, CH_3CHOO for the *syn* and *anti* forms. In the present study, we were able to detect larger Criegee intermediates, dimethyl-substituted, $(CH_3)_2COO$, ethyl-substituted, and CH_3CH_2CHOO, methyl-ethyl-substituted, $CH_3CH_2C(CH_3)OO$, by FTMW spectroscopy.

Experiments

Pure rotational transitions of all the species were observed by an FTMW spectrometer situated at National Chiao Tung University, Taiwan, which was moved from the University of Tokyo. The three species were produced by discharging a mixture of $CH_3CI_2CH_3$, $CH_3CH_2CHI_2$, and $CH_3CH_2CI_2CH_3$, respecrtively, with O_2 diluted in Ar. The mixture gases were expanded through a pulsed valve with electrodes attached in front of the valve into a vacuum chamber as a supersonic jet. High level *ab initio* calculations at CCSD(T)/aug-cc-pVTZ were performed to predict their structures and rotational constants. Barriers for the methyl internal rotations and relative energies of probable conformers were also calculated.

Spectra of all the species were relatively strong and readily assigned. In addition to the FTMW measurements, FTMW–cm-wave double resonance was used to confirm the assignments.

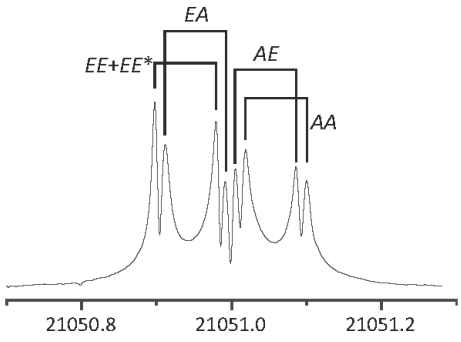

Fig. 1 3_{03}–2_{02} transition of $(CH_3)_2COO$

Results

Lines of $(CH_3)_2COO$ show relatively large splittings due to the methyl-top at the *anti*-position and much smaller splittings due to that at the

syn-position as shown in Fig. 1 (1). Barriers of the internal rotations of methyl-tops were determined for both of the tops, which were compared with those of *syn*- and *anti*-CH_3CHOO.

There are four conformers for the CH_3CH_2CHOO with ethyl part bonded to syn- and *anti*-positions with respect to bent COO. Each conformer has two conformers with Cs symmetry and without symmetry. The potential curves with respect to the ethyl tortional angle are shown in Fig. 2 (2). Among the four possible conformers, only three of them were assigned in our system, where the *anti*2 conformer escaped from the detection. The relative populations for the observed conformers suggest that they are produced at a relatively high temperature, about 1100 K, with a possible relaxation from *anti*2 to *anti*2 and *syn*2 to *syn*1, where the former is fast enough that there is no population for *anti*2, while that of the latter is much slower so that both of them were observed in the present experiment. Internal rotations of the methyl-top were observed only for the two *syn* conformers.

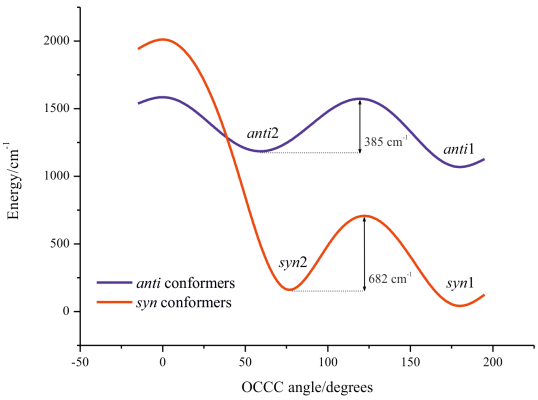

Fig. 2 Potntial energy curves for ethyl-CI

The largest molecules observed in the present study is $CH_3CH_2C(CH_3)OO$, the methyl-ethyl substituted CI. There are three species for the C_4-Criegee intermediates, species containing four carbon atoms; methyl-ethyl, *iso*-propyl, and *n*-propyl substituted CI's. Among the three possible species, pure rotational spectra of methyl-ethyl CI and iso-propyl CI, $(CH_3)_2CHCHOO$, have been observed so far, where analysis of the latter species is still under way. Similar to the case of the ethyl-CI, there are four conformers for the methyl-ethyl CI. All the four conformers were detected for this species, where the methyl internal rotation of the methyl part were more or less resolved for the four species as shown in Fig. 3 (3). Local perturbations were observed for the *syn*2 conformer.

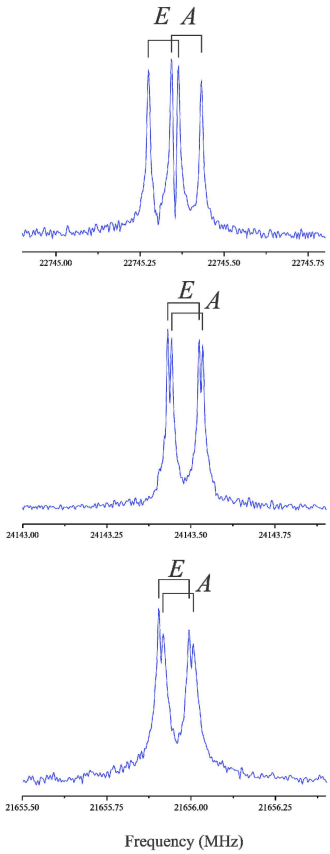

Fig. 3 Observed spectra of methy-ethyl CI for the *syn*1, *anti*1, and *anti*2 conformers

References

(1) M. Nakajima and Y. Endo, *J. Chem. Phys.* **145**, 244307 (2016).
(2) C. Cabezas, J. -C. Guillemin, and Y. Endo, *J. Chem. Phys.* **145**, 224314 (2016).
(3) C. Cabezas, J. -C. Guillemin, and Y. Endo, *J. Chem. Phys., accepted.*

A06

Infrared Absorption Spectrum of Hydroperoxymethyl Formate [$HC(O)OCH_2OOH$] Produced in the Reaction of the Criegee Intermediate CH_2OO with HCOOH

(Department of Applied Chemistry and Institute of Molecular Science, National Chiao Tung University, 1001, Ta-Hsueh Road, Hsinchu 30010, Taiwan [a]
Institute of Atomic and Molecular Sciences, Academia Sinica, Taipei 10617, Taiwan [b])
Jou-Wei Su[a], Chen-An Chung[a], and Yuan-Pern Lee[a,b]

The Criegee intermediates, which are carbonyl oxides produced in ozonolysis of unsaturated hydrocarbons,[1] play important roles in the production of OH, aerosols and organic acids in the atmosphere. Criegee intermediates react readily with other atmospheric species such as NO_2, SO_2, $(H_2O)_2$ and HCOOH. The reaction of CH_2OO with HCOOH was reported to be extremely rapid, with a rate coefficient of 1.1×10^{-10} cm^3 $molecule^{-1}$ s^{-1}.[2] Quantum-chemical calculations indicate that the reaction of CH_2OO + HCOOH proceeds through a barrierless association path to form hydroperoxymethyl formate (HPMF, $HC(O)OCH_2OOH$),[3] in agreement with experimental results by Neeb et al, who observed HPMF and formic acid anhydride (FAN, $(CHO)_2O$) in ozonolysis experiments; FAN and water was proposed to be produced from dissociation of HPMF.[4]

In this work, a step-scan Fourier-transform spectrometer coupled with a multipass absorption cell was employed to record temporally resolved infrared (IR) absorption spectra of the reactants and products during the reaction of CH_2OO with HCOOH in a flow system. CH_2OO were produced from the reaction of CH_2I with O_2, CH_2I was produced from photolysis of CH_2I_2.[5] Observed bands with origins at 887, 925, 1052, 1115, 1169.5, 1341.5, 1391 and 1760 cm^{-1} can be assigned to ν_{16}, ν_{15}, ν_{13}, ν_{12}, ν_{11}, ν_9, ν_7, and ν_5 modes of HPMF, respectively. The observed wavenumbers and relative intensities agree with the anharmonic vibrational wavenumbers and IR intensities predicted with the B3LYP/aug-cc-pVTZ method. Our results also show that the rate coefficient of the reaction CH_2OO + HCOOH is $(7\pm0.3)\times10^{-11}$ cm^3 $molecule^{-1}$ s^{-1}, smaller than the previously reported value.[2]

1. R. Criegee and G. Wenner, J. Liebigs *Ann. Chem.* **564**, 9 (1949).
2. O. Welz et al, *Angew. Chem., Int. Ed.* **53**,4547 (2014).
3. Long et al., *Journal of Molecular Structure: THEOCHEM* **916**, 159 (2009).
4. Neeb et al., *Chemical Physics Letters* **246**,150-156 (1995).
5. O. Welz et al., *Science* **335**, 204 (2012).

Fourier Transform Microwave Spectroscopy of CF_3SF_5

(Kanagawa Inst. Tech.[a], Grad. Univ. Ad. Studies[b])
Yoshiyuki Kawashima[a], Ken Ajiki[a] , Eizi Hirota[b]

We have investigated trifluoromethylsulfur pentafluoride CF_3SF_5 by Fourier transform microwave spectroscopy in order to determine the twelve-fold potential barrier to internal rotation in this molecule and have found the V_{12} value to be close to zero. Relaxation among internal-rotation and overall-rotation levels was found inhomogeneous, resulting in distributions quite different from thermal in low-temperature molecular beam, much affecting thermodynamic properties of the molecule. Spectra of the ^{13}C and ^{34}S species were also observed in natural abundance, leading to the r_s C-S bond length of 1.8808 (7) Å.

1. Introduction

CF_3SF_5 has been attracting much attention because of its unusually large global warming potential. It was subjected by Kisliuk and Silvey to a microwave spectroscopic study to confirm that the molecule was really a symmetric top with the rotational constant B = 1097.6 (4) MHz.[1)] Infrared and Raman spectroscopic investigations and electron diffraction experiments all indicated that the internal rotation was of low barrier, as presumed by the potential function being of as high symmetry as 12-fold. The present study primarily aims at detailed clarification of the internal rotation in CF_3SF_5.

2. Experimental

A sample of CF_3SF_5 was purchased from SynQuest Labs. Inc. and was used without any further purification. CF_3SF_5 was diluted with either Ar or Ne to 0.5% and was introduced in the chamber of a FTMW spectrometer through a pulsed nozzle at the backing pressure of approximately 100 kPa. The relative intensities of the rotational transitions of CF_3SF_5 diluted by Ar were not much different from those recorded using Ne in place of Ar.

3. Observed spectra, assignment, and analysis

We have scanned the frequency regions where we expected to observe $J + 1 \leftarrow J$ rotational transitions of J = 1 to 9, based upon the B rotational constant reported by Kisliuk and Silvey, and have observed a large number of lines centered at multiples of $2B$. Most of them form series, as shown in Fig.1 by the observed frequencies divided by $2(J+1)$ and plotted against J. We have noticed that there are three pairs of prominent lines, two component lines of which are nearly symmetrically displaced each other from the central clusters of lines; the three pairs are identified by A, B, and C.

We have employed a symmetric-top rotational Hamiltonian with some Kivelson's centrifugal terms: Eqs. (1) and (2) and products of free internal-rotation $|m\rangle$ and symmetric-top rotational $|J, k\rangle$ wavefunctions as bases [abbreviated as (m, k)]. We have taken into account interaction Hamiltonians Eqs. (3)-(5), as shown below, and have assigned A series to $(m, k) = (3, 1)_\pm$ [B_1/B_2 symmetry] and B series to $(m, k) = (3, -1)_\pm$ [A_1/A_2 symmetry], and tentatively ascribed C series to $(m, k) = (6, 0)_\pm$ [B_1/B_2 symmetry]. These three series are split in the first order. The C series showed anomalous J dependence of the intensity, which is probably

caused by relaxation inhomogeneously taking place among internal-rotation and overall-rotation energy levels. The Hamiltonians used are

$$H_0 = BJ^2 + (A-B){J_z}^2 + F(p-\rho J_z)^2 + \frac{V_{12}}{2}(1-cos12\alpha) \quad (1)$$

$$H_1 = J^2[G(p-\rho J_z)^2 + L(p-\rho J_z)J_z - D_{JK}{J_z}^2 - D_J J^2 + U_{12}(1-cos12\alpha)] \quad (2)$$

$$H_3 = U_3[e^{3i\alpha}J_{g+} + e^{-3i\alpha}J_{g-}] \quad (3)$$

$$H_6 = e^{6i\alpha}[U_{6A}{J_{g+}}^2 + U_{6B}{J_{g-}}^2] + e^{-6i\alpha}[U_{6B}{J_{g+}}^2 + U_{6A}{J_{g-}}^2] \quad (4)$$

$$H_{12} = i[V_{12a} + U_{12a}J^2](e^{12i\alpha} - e^{-12i\alpha})J_z \quad (5)$$

It is quite difficult to assign the central cluster lines. Most of the "lines" probably consist of several component lines barely resolved one another. We have noticed that the frequencies of the series labeled as c-h, c-ℓ, 3ℓ1, 3ℓ2, and 2ℓ1 in Fig.1 are closely fit to the expression: $f_0 + f_1 n^2$, where n = 0, 1, 2, 3, and 4, respectively, and the running number n may be identified as either k or m., k being more reasonable than m.

We have also searched and assigned spectra of ^{13}C and ^{34}S isotopic species in natural abundance. The rotational constants thus determined for the two isotopic species are 1093.6564 (37) and 1095.4166 (9) MHz, which lead to the r_s value of C-S: 1.8808 (7) Å. This value may be compared with the r_a 1.887 (8) Å reported by Marsden *et al.*[2)]

The present study determined the internal-rotation potential barrier V_{12} to be small: -0.211 (97) cm^{-1}; the internal rotation in CF_3SF_5 is essentially free, as expected. The negative sign of V_{12} means that the equilibrium conformation is staggered. The DFT molecular parameters obtained by present quantum chemical calculations, agreed with those reported previously.[3)] Molecular constants calculated were compared with the present results. The V_{12} obtained by MP2/6-311++G(d, p) was in much closer agreement with the observed than those by DFT.

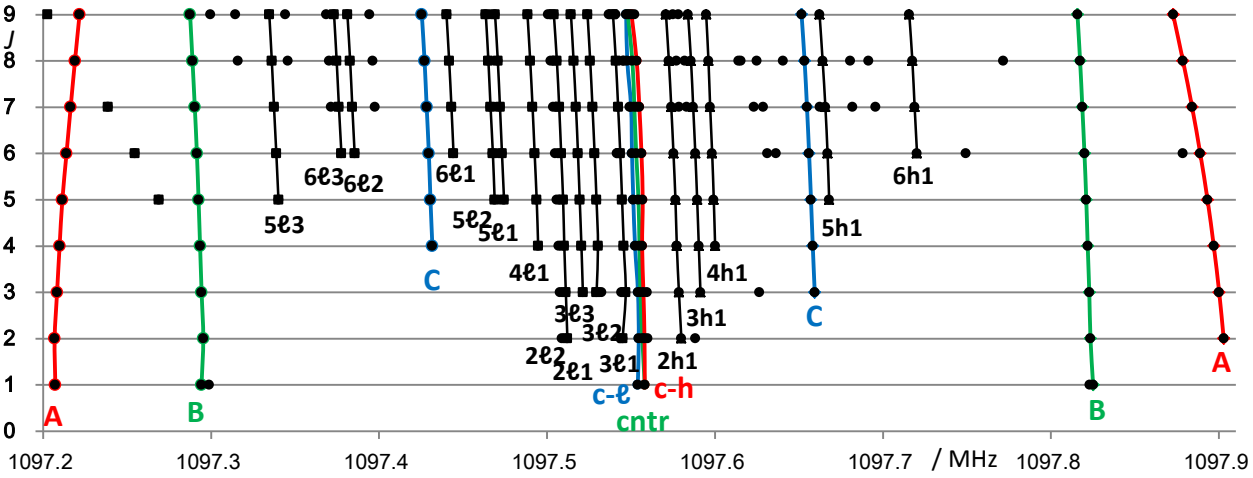

Fig. 1 Observed frequencies of the transitions from J = 2←1 up to 10←9, divided by 2(J+1)

References [1)] P. Kisliuk and G. A. Silvey, *J. Chem. Phys*. 20 (1952) 517. [2)] C. J. Marsden, *et al. J. Mol.Struct*. 131 (1985) 299. [3)] W. Xu, *et al. Mol. Phys*. 102 (2004) 1415.

Some Theoretical Considerations on the Microwave Three-wave Mixing Experiments

Takayoshi Amano
Jet Propulsion Laboratory, California Institute of Technology, Pasadena, CA 91109, USA

Patterson and Doyle demonstrated that optical isomers could be discriminated by using microwave three-wave mixing experiments [1]. Apparently their work was carried out, being stimulated by a theoretical work on microwave triple resonance by Hirota [2]. Subsequently their work was followed by several investigations performed by using similar techniques [3–8]. Grabow presented theoretical background on this microwave three-wave mixing experiments [9]. Also Lobsiger *et al.* gave similar theoretical explanations [8].

For C_1 enantiomers, all the dipole moment components along the principal moment of inertia axes are nonzero. The sign of the product of the three components should be different for the different enantiomers. This is the reason why the experiments are designed to observe the phenomena that depend on it; triple resonance or microwave three-wave mixing. In this investigation, we present some theoretical background of those experiments which is similar to that given by Grabow [9]. However, in the end, we will see a different factor which might evoke a different perspective on the experiments.

Consider a three level system depicted in Fig. 1. Assume, for simplicity, that a system is similar to that used in Patterson and Doyle; the transition between the levels 1 and 2 is a c-type transition and between the levels 2 and 3 an a-type, and between the levels 1 and 3 a b-type. The time evolution of the wave functions is generally described as a linear combination of the three eigenstates with time dependent coefficients such as

$$\Psi(t) = \sum_i a_i(t)\phi(i). \tag{1}$$

The density matrix ρ is defined to be $\rho_{ij} = a_i a_j^*$ as its matrix element. The time dependent density matrix equation is given by

$$i\hbar\frac{d\rho}{dt} = [\mathcal{H}, \rho], \tag{2}$$

where the Hamiltonian $\mathcal{H}$ consists of the zero-th order molecular Hamiltonian and the interaction with the applied external radiation field,

$$\mathcal{H} = \mathcal{H}_0 + \mathcal{H}'. \tag{3}$$

We assume two resonant microwave radiations are applied to excite the transitions between the levels 1 and 2 and the levels 2 and 3. Therefore

$$\mathcal{H}' = -\mu\mathcal{E}(t) \tag{4}$$

$$\mathcal{E}(t) = \mathcal{E}_0\cos\,\omega t + \mathcal{E}_0'\cos\,\omega' t \tag{5}$$

where $\omega = (E_2 - E_1)/\hbar$ and $\omega' = (E_3 - E_2)/\hbar$. As the transition between the levels 1 and 2 is a c-type transition, the Rabi frequency $\Omega_{12}(=\mu_{12}\mathcal{E}_0/\hbar)$ can be written as $i\Omega$, and accordingly $\Omega_{21} = -i\Omega$ with Ω being a real quantity by adapting the phase convention used in microwave spectroscopy (see, for example, Townes and Schawlow). For the transition between the levels 2 and 3, $\Omega_{23} = \Omega_{32} = \Omega'$, and Ω' is real.

By using the rotating wave approximation,

$$\rho_{12} = \tilde{\rho}_{12}e^{i\omega t},\ \rho_{23} = \tilde{\rho}_{23}e^{i\omega' t},\ \rho_{13} = \tilde{\rho}_{13}e^{i\omega t}e^{i\omega' t},$$

and by defining three Bloch vector components for each of the three transitions,

$$\begin{aligned} u^c &= \tilde{\rho}_{12} + \tilde{\rho}_{21},\ v^c = i(\tilde{\rho}_{21} - \tilde{\rho}_{12}),\ w^c = \rho_{11} - \rho_{22} \\ u^a &= \tilde{\rho}_{23} + \tilde{\rho}_{32},\ v^a = i(\tilde{\rho}_{32} - \tilde{\rho}_{23}),\ w^a = \rho_{22} - \rho_{33} \\ u^b &= \tilde{\rho}_{13} + \tilde{\rho}_{31},\ v^b = i(\tilde{\rho}_{31} - \tilde{\rho}_{13}),\ w^b = \rho_{11} - \rho_{33} \end{aligned}$$

the equations of motion can be written as

$$\begin{aligned} \dot{u^c} &= \Omega w^c + \frac{\Omega'}{2}v^b,\ \dot{v^c} = -\frac{\Omega'}{2}u^b,\ \dot{w^c} = -\Omega u^c - \frac{\Omega'}{2}v^a \\ \dot{u^a} &= \frac{\Omega}{2}u^b,\ \dot{v^a} = -\Omega' w^a + \frac{\Omega}{2}v^b,\ \dot{w^a} = \frac{\Omega}{2}u^c + \Omega' v^a \\ \dot{u^b} &= \frac{\Omega'}{2}v^c - \frac{\Omega}{2}u^a,\ \dot{v^b} = -\frac{\Omega'}{2}u^c - \frac{\Omega}{2}v^a,\ \dot{w^b} = -\frac{\Omega}{2}u^c + \frac{\Omega'}{2}v^a. \end{aligned}$$

Suppose first we apply a pulse radiation field which is resonant to the c-type transition of the time duration of Δt to excite the transition between the levels 1 and 2. Then we obtain,

$$\begin{aligned} u^c(\Delta t) &= w^c(0)\sin(\Omega\Delta t) \\ v^c(\Delta t) &= w^c(0)\cos(\Omega\Delta t) \\ w^a(\Delta t) &= \frac{1}{2}w^c(0)[1 - \cos(\Omega\Delta t)] + w^a(0) \\ w^b(\Delta t) &= -\frac{1}{2}w^c(0)[1 - \cos(\Omega\Delta t)] + w^b(0), \end{aligned}$$

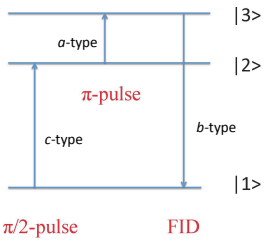

FIG. 1: First shine a pulse radiation which is resonant to the transition between the levels 1 and 2. Immediately after this pulse, we apply the second pulse to excite the transition between the levels 2 and 3. Following these preparation processes, observe free induction decay from the level 3 to 1.

with all other components to be zero. Following this pulse, we apply a resonant radiation to excite the a-type transition between the levels 2 and 3.

$$
\begin{aligned}
u^a(t) &= 0 \\
v^a(t) &= -(\frac{1}{2}w^c(0)[1-\cos(\Omega\Delta t)]+w^a(0))\sin\Omega'(t-\Delta t) \\
w^a(t) &= (\frac{1}{2}w^c(0)[1-\cos(\Omega\Delta t)]+w^a(0))\cos\Omega'(t-\Delta t) \\
u^b(t) &= 0 \\
v^b(t) &= w^c(0)\sin(\Omega\Delta t)\sin\frac{\Omega'}{2}(t-\Delta t) \\
w^b(t) &= -\frac{1}{2}(w^a(0))(1-\cos\Omega'(t-\Delta t))+w^b(0) \\
u^c(t) &= w^c(\Delta t)\sin(\Omega\Delta t)\cos\frac{\Omega'}{2}(t-\Delta t) \\
v^c(t) &= 0 \\
w^c(t) &= \frac{1}{2}w^c(0)\cos(\Omega\Delta t)(1-\cos\Omega'(t-\Delta t)) \\
&+ w^c(0)\cos(\Omega\Delta t).
\end{aligned}
$$

Now we see that the polarization of the b-type transition is induced through this "double resonance" process. The induced polarization is expressed for this transition as

$$\mathbf{P} = N\mathrm{Tr}(\mu\rho) \tag{6}$$

It can be written explicitly as

$$
\begin{aligned}
\mathbf{P} &= N(\mu_{13}\rho_{31}+\mu_{31}\rho_{13}) \\
&= N\bar{\mu}[(\tilde{\rho}_{31}+\tilde{\rho}_{13})\cos\omega''t - i(\tilde{\rho}_{31}-\tilde{\rho}_{13})\sin\omega''t]
\end{aligned} \tag{7}
$$

where $\omega''=\omega+\omega'$. Here we assume the matrix elements of the dipole moment, μ_{13} and μ_{31}, are real and equal, and designated as $\bar{\mu}$, but the sign can be either positive or negative. This induced polarization generates the electric field and the relationship between the two is given by

$$\mathbf{P} = \frac{1}{2}\chi\mathcal{E}_0 e^{i\omega''t} + c.c. \tag{8}$$

where χ is complex susceptibility, $\chi=\chi'-i\chi''$. The susceptibility is related to the density matrix elements as follows;

$$\chi'\mathcal{E}_0 = N\bar{\mu}(\tilde{\rho}_{31}+\tilde{\rho}_{13}) = N\bar{\mu}u^b \tag{9}$$

$$\chi''\mathcal{E}_0 = iN\bar{\mu}(\tilde{\rho}_{31}-\tilde{\rho}_{13}) = N\bar{\mu}v^b \tag{10}$$

Power emitted (or absorbed) is given by

$$W = \overline{\mathbf{E}\frac{\partial\mathbf{P}}{\partial t}} = \frac{\omega''}{2}\mathcal{E}_0^2\chi''$$

Therefore we obtain

$$
\begin{aligned}
W &= N\frac{\omega''}{2}\mathcal{E}_0\bar{\mu}w^c(0)\sin(\Omega\Delta t)\sin\frac{\Omega'}{2}(t-\Delta t) \\
&= (N_1(0)-N_2(0))\frac{\omega''}{2}\mathcal{E}_0\bar{\mu}\sin(\Omega\Delta t)\sin\frac{\Omega'}{2}(t-\Delta t)
\end{aligned} \tag{11}
$$

The emitted power is maximized by applying sequentially $\pi/2$- and π-pulses. As formulated above, the induced polarization from the two-step pumping process appears to depend on the product of the matrix elements of the three dipole moment components, μ_a, μ_b, and μ_c. In the treatment presented above, the Rabi frequencies are implicitly assumed to be the signed quantities. This assumption should be examined carefully. In all cases for two level systems, the sign of the dipole moment does not matter, and we automatically use the absolute value of the dipole moment in calculating the Rabi frequency. In general, the oscillation frequency of the polarization is given by $\bar{\Omega}=\pm\sqrt{(\omega-\omega_0)^2+\Omega^2}$, as the radiation frequency may not be in exact resonance. The sign of $\bar{\Omega}$ can be either positive or negative, but the sign has nothing to do with the sign of the dipole moment. It should be noted that, in the microwave three-wave mixing experiments done so far, the process was the three-step sequential two-level processes. If the sign of the product of the three dipole moment components really plays a role, the power given in eq.(11) indicates emission for one enantiomer, on the other hand the signal corresponds to absorption for the other enantiomer. This is not reasonable.

[1] D. Patterson and J. M. Doyle. *Phys. Rev. Lett.*, **111**,023008(2013).
[2] E. Hirota. *Proc. Jpn. Acad. B*, **88**,120-128(2012).
[3] D. Patterson, M. Schnell, and J. M. Doyle. *Nature*, **497**,475-478(2013).
[4] D. Patterson and M. Schnell. *Phys. Chem. Chem. Phys.*, **16**,11114-11123(2014).
[5] V. A. Shubert, D. Schmitz, D. Patterson, J. M. Doyle, and M. Schnell. *Angew. Chem. Int. Ed.*, **53**,1152-1155(2014).
[6] V. A. Shubert, D. Schmitz, and M. Schnell. *J. Mol. Spectrosc.*, **300**,31-36(2014).
[7] V. A. Shubert, D. Schmitz, C. Medcraft, A. Krin, D. Patterson, J. M. Doyle, and M. Schnell. *J. Chem. Phys.*, **142**,214201(2015).
[8] S. Lobsiger, C. Perez, L. Evangelisti, K. K. Lehmann, and B. H. Pate. *J. Phys. Chem. Lett.*, **6**,196-200(2015).
[9] J. Grabow. *Angew. Chem. Int. Ed.*, **52**,11698-11700(2013).

Infrared Spectrum of Hydrogen Fluoride Anion Isolated in Solid Argon

(NSRRC) Yu-Jong Wu, Meng-Chen Liu, Chih-Hao Chin, Tzu-Ping Huang
E-mail: yjwu@nsrrc.org.tw

Hypervalent molecules are one of the exceptions to the octet rule. Bonding in most hypervalent molecules is well rationalized by the Rundle-Pimentel model (three-center four-electron bond), and high ionic bonding between the ligands and the central atom is essential for stabilizing hypervalent molecules. Here, we produced one of the simplest hypervalent anions, HF^-, which is known to deviate from the Rundle-Pimentel model, and identified its ro-vibrational features shown in Fig. 1. High-level ab inito calculations reveal that its bond dissociation energy is comparable to that of dihalides, as supported by secondary photolysis experiments with irradiation at various wavelengths. The charge distribution analysis suggested that the F atom of HF^- is negative and hypervalent and the bonding is more covalent than ionic.

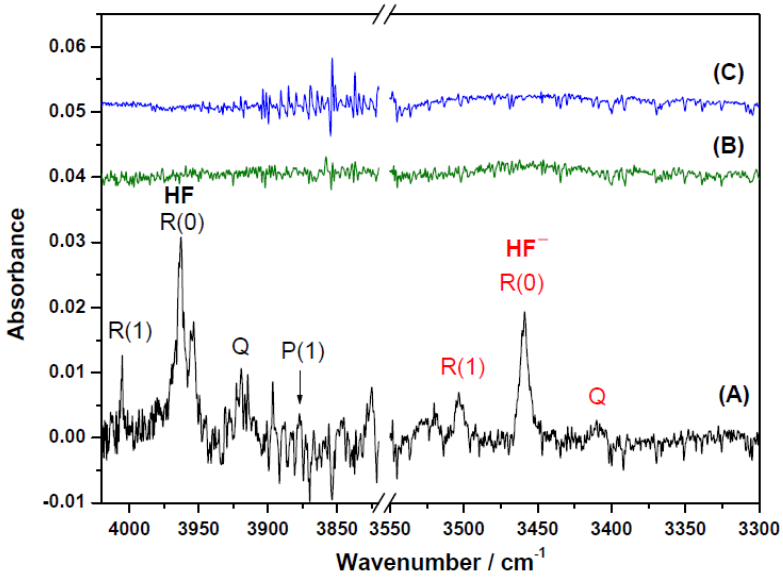

Fig. 1 Partial IR spectra of electron-bombarded (2000 eV, 0.3 mA) matrix samples at 10 K. (A) CH_3F/Ar (1/500), (B) CH_4/Ar (1/500), and (C) Ar. The ro-vibrational transitions of the observed bands are assigned.

A10

Variation of H-bond properties with density in astrophysical ice structures

(Instituto de Estructura de la Materia, IEM-CSIC, Madrid, Spain[a], Universidad Complutense de Madrid, Madrid, Spain[b], Institute of Low Temperature Science, Hokkaido University, Sapporo, Japan[c])

Rafael Escribano[a], Pedro C. Gómez[b], Víctor J. Herrero[a], Naoki Watanabe[c]

(rafael.escribano@csic.es, pgomez@ucm.es, v.herrero@csic.es, watanabe@lowtem.hokudai.ac.jp)

The interpretation of infrared measurements of remote sources, like in astronomical missions, often relies on the knowledge of the density of the sample measured by other means. For icy samples containing water, the analysis of the infrared spectra may reveal the presence of different kinds of O-H bonding types, from free or nearly free O-H bonds to O-H…O hydrogen bonds of diverse strength. Each bonding type has a different signature, but also this signature may vary with the density of the sample.

We have chosen for this investigation a mixture of water and methane, plus a relevant amount of nitrogen, frozen at 50 K, to simulate the possible content of a spot at the surface of Pluto, the Pulfrich crater [1], recently observed by the New Horizons mission. By varying the size of the cell containing this mixture of molecules, we can study the effect of the corresponding density of the sample on the predicted IR spectra.

We have covered a large density range, from a very low value that simulates a gas-phase mixture, to values corresponding to solids under fairly high internal stress, with a middle range that could be expected to cover the values of mixtures at astronomical conditions.

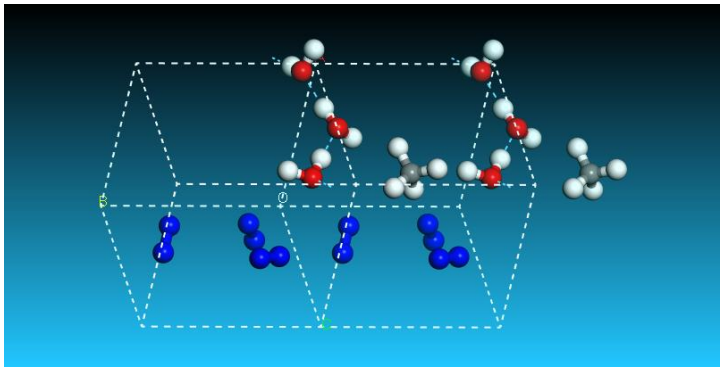

Fig. 1. Sample with density 0.75 g cm^{-3}. Two unit cells are shown to better appreciate the optimized structure. Note the apparent porosity of the sample.

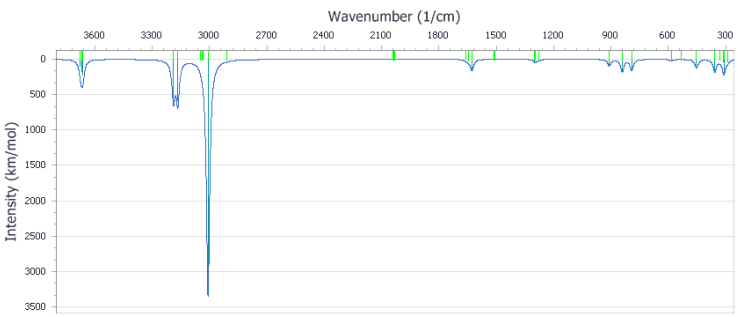

Fig. 2. Predicted IR spectrum of the sample in Fig. 1.

References

[1] W.M. Grundy et al, Science 351, aad9189, 2016.

A11

Infrared spectra of protonated aniline in solid *para*-hydrogen

Yu-Syuan Chen[a], Masashi Tsuge[a] and Yuan-Pern Lee[a,b]

[a]*Department of Applied Chemistry and Institute of Molecular Science, National Chiao-Tung University, Hsinchu 30010, Taiwan*

[b]*Institute of Atomic and Molecular Sciences, Academia Sinica, Taipei 10617, Taiwan*

Aniline is a prototypical aromatic amine. It contains two types of basic centers that can accept an approaching proton, namely the amino group and the aromatic ring. The alkaline properties of aniline in solution result from the stabilization of the nitrogen-protonated form when solvated. However, the site of protonation in gaseous aniline is unclear [1]. Previously, the studies on protonated aniline in the gas phase are mainly based on mass spectrometry and thus provide only indirect, and sometimes ambiguous, information about the preferred protonation site of aniline [2]. Therefore, understanding the protonation site of aniline without solvent is desirable.

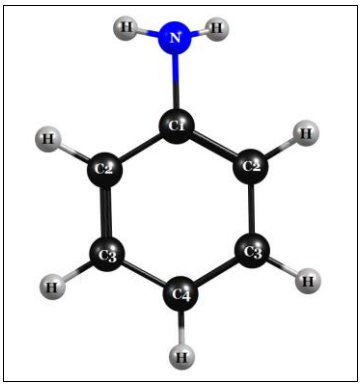

A new method for investigating the IR spectra of protonated species and their neutral counterparts was developed in our laboratory using electron bombardment during deposition of a gaseous mixture of *para*-hydrogen (p-H_2) matrix host containing a small proportion of guest molecules. This method produces mainly protonated parent molecules and corresponding neutrals without fragmentation; the IR spectra show true absorption intensity with small linewidths, excellent signal-to-noise ratio, and wide spectral coverage [3].

We applied this technique to investigate the IR spectrum of protonated aniline in a solid p-H_2 matrix. We grouped spectral lines into various species according to their behaviors after maintaining in darkness and upon secondary photolysis; the assignments were derived on comparison with quantum-chemical calculations using the B3LYP/CC-pVTZ method. The results indicate that three protonated isomers are observed: protonation on carbon 2 (absorption lines at 3479.0, 3391.8, 1666.7, 1503.9, 1451.8, 1418.9, 1341.5, 1188.1, 776.7 and 736.3 cm^{-1}), on carbon 4 (absorption lines at 3482.5, 3395.2, 1669.0, 1523.1, 1337.1, 1197.5, 886.4, 884.1 and 816.8 cm^{-1}), and on the nitrogen atom (absorption lines at 3302.8, 3278.8 and 3236.0 cm^{-1}); the numbering of the carbon atoms is shown in the Figure.

[1] F. M. Pasker, N. Solcà and O. Dopfer, J. Phys. Chem. A. 110, 12793 (2006).
[2] M. J. Nold and C. Wesdemiotis, J. Mass. Spectrom. 31, 1169 (1996).

[3] M. Bahou, P. Das, Y. -F. Lee, Y. -J. Wu and Y. -P. Lee, Phys. Chem. Chem. Phys. 16, 2200 (2014).

A12

Phonon-mediated nuclear spin relaxation of H_2O trapped in Ar matrix

(Gakushuin Univ.) Koichiro Yamakawa, Shinya Azami, Ichiro Arakawa
koichiro.yamakawa@gakushuin.ac.jp

Water molecules are classified into two kinds of nuclear spin isomers, i.e., ortho and para, just like hydrogen molecules. The abundance ratio of ortho to para, so called ortho-to-para ratio (OPR), has attracted much attention in the fields of astronomy and interstellar physics [1,2]. Since the nuclear spin conversion (NSC) of gaseous H_2O through radiation is extremely slow [3], one assumed that OPR provides information of the temperature where an interstellar medium was formed [1]. However, recent investigations have revealed that NSC of H_2O proceeds much faster in condensed systems [4,5]. Thus, interest in the NSC mechanism and channels is getting greater. In the present work, we devised a theoretical model of the phonon-mediated nuclear spin relaxation of H_2O trapped in cryomatrices to correctly describe the temperature dependence of the NSC rate [6]. For the purpose of testing the validity of this model, we also monitored the rotational relaxation of H_2O in solid Ar associated with the nuclear spin flip to experimentally obtain the NSC rates in the temperature range of 5-15 K.

After baking at 373 K for 24 hours, the interior of a vacuum chamber went below 1×10^{-8} Pa. An oxygen-free copper block was screwed in the bottom of a helium continuous-flow cryostat, which was mounted on the vacuum chamber. A $15 \times 15 \times 5$ mm^3 gold plate mechanically fixed on the copper block was used for the substrate. Temperature of the substrate was measured with a silicon diode sensor and was raised with a heater wrapped around the bottom part of the cryostat. The substrate and block were covered with a radiation shield attached to the cryostat, so that the helium flow made the substrate temperature as low as 5.2 K. The gases of H_2O and Ar were mixed in the gas handling system equipped with a quartz oscillator gage; distilled water was preliminarily degassed by multiple freeze-pump-thaw cycles whereas the Ar gas (99.9999% purity) was used without further purification. The molar ratio of Ar to H_2O was set to be 1.0×10^4 using the standard manometric technique. The mixed gas was dosed through a variable leak valve onto the substrate kept at 13 K. Infrared spectra were recorded with a Fourier transform infrared spectrometer and a HgCdTe detector at the resolution of 2 cm^{-1}. We used the reflection configuration, where the incident angle of infrared light was 80 degrees. The whole optical path was evacuated in order to eliminate infrared absorption by atmospheric CO_2 and H_2O.

In Fig. 1, time evolution of the infrared spectrum of H_2O in solid Ar is shown. The time when the substrate temperature settled at 7.0 K was set to be 0 s. Sharp absorption peaks at 1608 (O1), 1624 (P1), and 1636 cm^{-1} (O2) are assigned to the $1_{10} \leftarrow 1_{01}$, $1_{11} \leftarrow 0_{00}$, and $2_{12} \leftarrow 1_{01}$ rovibrational transitions of H_2O, respectively [7,8]. In the notation of $J_{kk'}$, the quantum number of the rotational angular momentum is denoted by J, and that of its projection on the a (c) axis of H_2O is expressed by k (k'). While P1 corresponds to the transition of para H_2O, O1 and O2 originate from the ortho species. P1 grew with increasing time whereas O1 and O2 decayed. This time evolution

means NSC of H_2O. We obtained the integrated intensity of P, which is proportional to the number of para H_2O, by Gaussian fitting. The time dependence of the integrated intensity was well-described by an exponential function with the relaxation rate of 0.36 h^{-1}. We also measured the rate at other temperatures in the range of 5-15 K. Figure 2 shows the temperature dependence of the measured relaxation rate. The solid line, which was derived from the phonon-mediated relaxation model we devised, is found to reproduce the experimental data well. This result supports the validity of our model and suggests that the rotational relaxation from 1_{01} to 0_{00} associated with the nuclear spin flip proceeds not only directly but also indirectly, i.e., via 1_{11} [6].

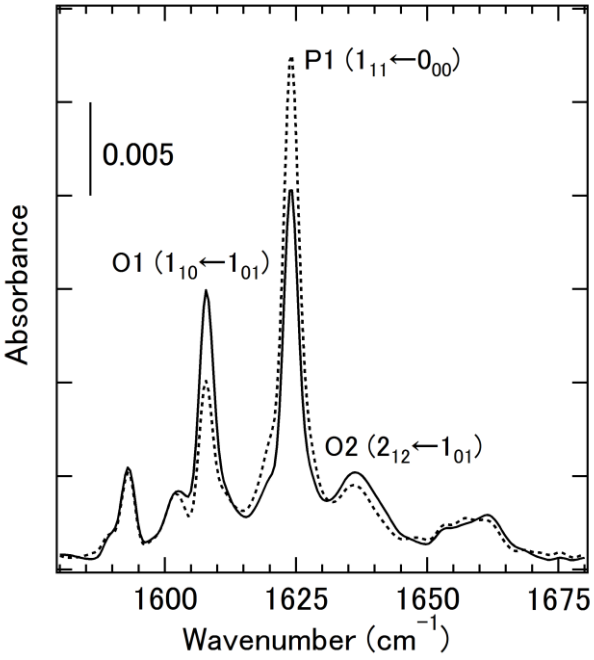

Fig. 2 Infrared spectra of H_2O in solid Ar at 50 (solid line) and 11730 (dotted line) s. The substrate temperature was 7.0 K.

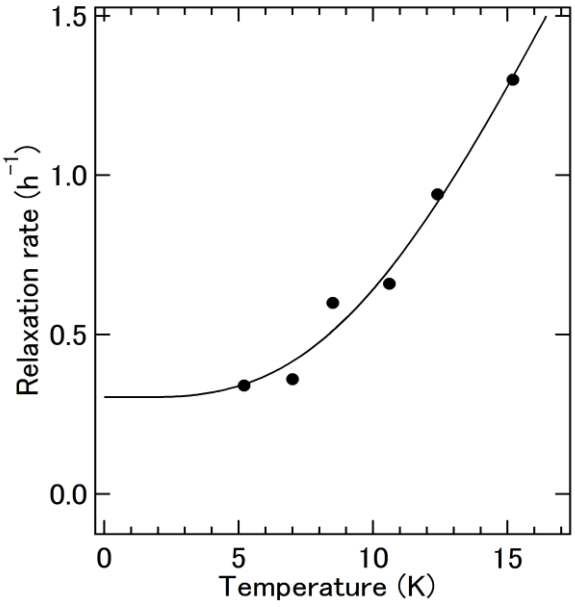

Fig. 1 Temperature dependence of the NSC rate of H_2O in solid Ar. The solid curve was derived from the phonon-mediated relaxation model.

References

[1] M. J. Mumma et al., Science **232**, 1523 (1986).
[2] M. Emprechtinger et al., A&A **521**, L28 (2010).
[3] A. Miani and J. Tennyson, J. Chem. Phys. **120**, 2732 (2004).
[4] L. Abouaf-Marguin et al., Chem. Phys. Lett. **447**, 232 (2007).
[5] R. Sliter et al., J. Phys. Chem. A **115**, 9682 (2011).
[6] K. Yamakawa et al., Eur. Phys. J. D **71**, 70 (2017).
[7] X. Michaut et al., Vib. Spectrosc. **34**, 83 (2004).
[8] J. P. Perchard, Chem. Phys. **273**, 217 (2001).

A13

Cross-Contamination of the Fitting Parameters in Multidimensional Tunneling Treatments

(Kanazawa University, Kanazawa, Japan[a], NIST, Gaithersburg, MD, USA[b]) Nobukimi Ohashi[a], Jon T. Hougen[b]

In this talk we examine the two-dimensional tunneling formalism used previously to fit the hydrogen-transfer and internal-rotation splittings in the microwave spectrum of 2-methylmalonaldehyde in an effort to determine the origin of various counterintuitive results concerning the isotopic dependence of the internal-rotation splittings in that molecule. We find that the cause of the problem lies in a "parameter contamination" phenomenon, where some of the numerical magnitude of splitting parameters from modes with large tunneling splittings "leaks into" the parameters of modes with smaller tunneling splittings. We find that such parameter contamination, which greatly complicates the determination of barrier heights from the least-squares-fitted splitting parameters, will be a general problem in spectral fits using the multi-dimensional tunneling formalism, since it arises from subtle mathematical features of the non-orthogonal framework functions used to set up the tunneling Hamiltonian. Transforming to a physically less intuitive orthonormal set of basis functions allows us to give an approximate numerical estimate of the contamination of tunneling parameters for 2-methylmalonaldehyde by combining a dominant tunneling path hypothesis with results recently given for the hydrogen-transfer--internal-rotation potential function for this molecule.

A14

Conformational Structures of Indole-3-acetic Acid by UV-UV hole-burning and IR-dip spectroscopy

(Gyeongsang Nat. Univ.) Yeon Guk Seong, Cheol Joo Moon, Ahreum Min, Ahreum Ahn, Myong Yong Choi (mychoi@gnu.ac.kr)

Indole-3-acetic acid (IAA) is the most common plant hormone that plays an essential role in the regulation of plant growth and fruit development. The special role in nature has led us to investigate the intrinsic properties of IAA in the gas phase. We have measured the electronic spectra of IAA by employing a resonant two-photon ionization (R2PI) and UV-UV hole-burning (UV-UV HB) technique in the free jet conditions. As a result, we identified three different conformers of IAA. A combination of infrared-dip, R2PI, UV-UV HB spectroscopy is used to characterize the IAA conformers. Further investigation with ab initio and density functional theory calculations of IAA is carried out for the study of potential energy landscapes of IAA.

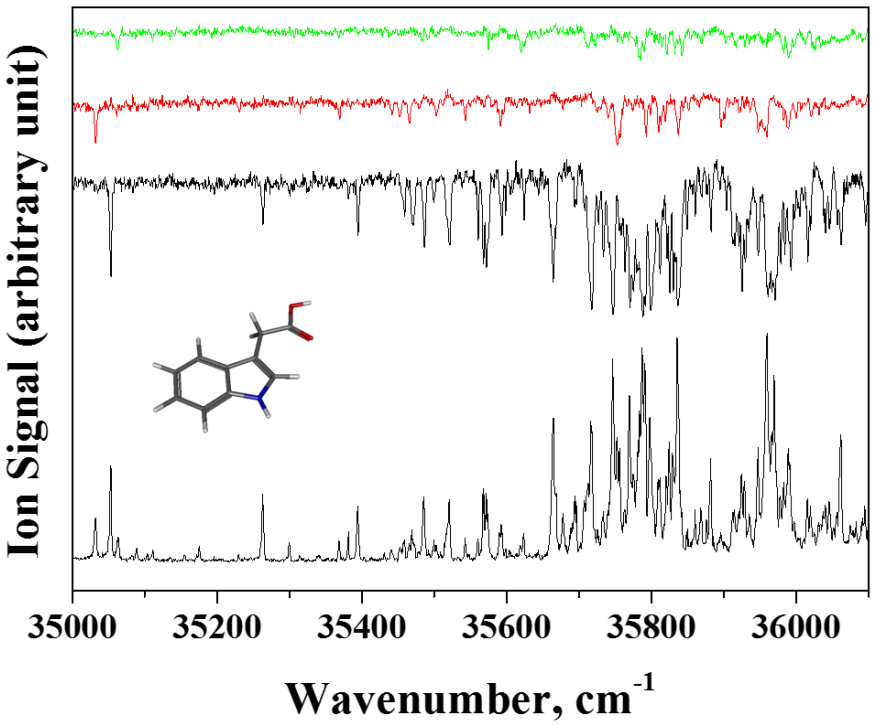

A15

Rapid Non-radiative Decay of Jet-cooled 2-hydroxyformanilide: IR-dip Spectroscopy and Computational Studies

(Gyeongsang Nat. Univ.) Cheol Joo Moon, Yeon Guk Seong, Ahreum Min, Ahreum Ahn, Myong Yong Choi (mychoi@gnu.ac.kr)

In this study, we present the conformational investigations and excited state dynamics of jet-cooled 2-hydroxyformanilide (2-HFA). The number of conformers and their structures of 2-HFA are assigned on the basis of resonance enhanced multiphoton ionization (REMPI), ultraviolet-ultraviolet hole burning (UV-UV HB), infrared-dip (IR-dip) spectroscopy. From comparison between REMPI and UV-UV HB spectra, three species coexist in the supersonic jet. Two species among them are 2-HFA-AC (Anti and Cis) and the other is 2-HFA-AT (Anti and Trans). The similar UV-UV HB spectra are due to the anharmonic coupling between the peptide group and some ring deformations in the excited state. We speculate that the observance of IR upstream in the IR-dip spectrum might come from the contribution of 2-HFA-ST (Syn and Trans). The structures of these conformers are determined by the IR-dip spectroscopy and Franck-Condon simulations. Also, the observed spectra are compared with the predictions of ab initio and density functional theory calculations.

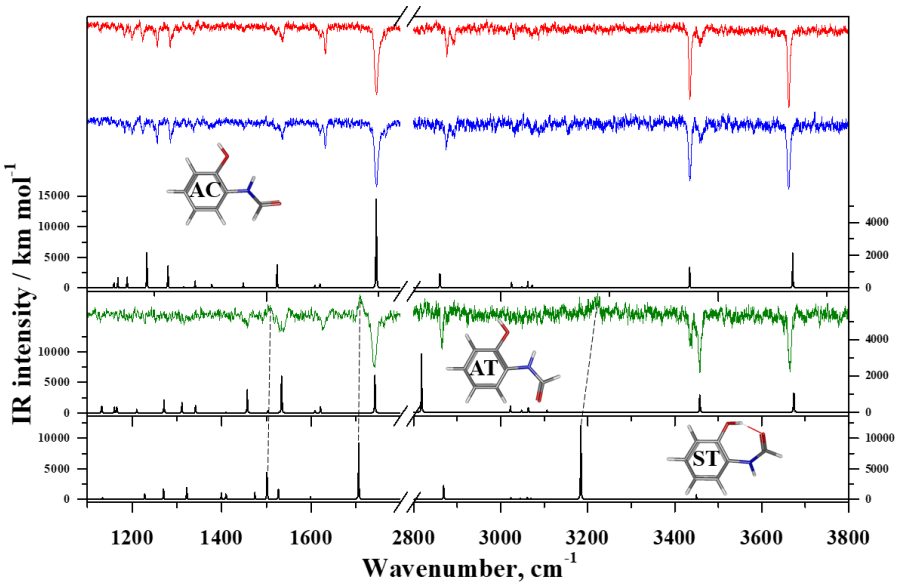

High-resolution Fourier transform emission spectroscopy of the $A^2\Pi_i$ - $X^2\Pi_i$ band of the OCS^+ ion

Yoshihiro Nakashima, Kensuke Harada, ○Keiichi Tanaka and Takehiko Tanaka
Department of Chemistry, Faculty of Sciences, Kyushu University,
Motooka, Nishiku, Fukuoka 819-0395, Japan

High resolution Fourier transform (FT) emission spectroscopy of the $A^2\Pi_i$ - $X^2\Pi_i$ band of OCS^+ generated by Penning ionization with metastable He* atom was performed in the 370 - 490 nm UV region at a resolution of 0.03 cm^{-1}. The ν_1 (CO stretching) progression bands from the ground vibrational state of $A^2\Pi_i$ to the ν_1 excited states of $X^2\Pi_i$ were observed for the $\nu_1 = 0 \leftarrow 2$ - 5 bands of the $\Omega = 3/2$ and 1/2 components. The parity doubling were resolved for the *P*- and *R*-branch lines for $\Omega = 1/2$.

Observed ν_1 progression bands were analyzed together with the origin bands reported by LIF study to give the accurate molecular constants of OCS^+. The spin-orbit interaction constants A_0 determined are -381.0(56) and -126.5(56) cm^{-1}, respectively, for the $X^2\Pi_i$ and $A^2\Pi_i$ states to agree with the previously reported ones. The CO bond length for the $A^2\Pi_i$ state is longer by 0.1756 Å than that for the $X^2\Pi_i$ state, while the CS bond length shorter by 0.0905 Å, as determined by the observed rotational constants B_0 and Franck-Condon factors, implying the excited state has much weaker CO bond than that of the ground state. The large change in the molecular structure between $A^2\Pi_i$ and $X^2\Pi_i$ causes the prominent ν_1 progression bands observed in the present FT emission spectrum.

＜Introduction＞ For the OCS^+ ion, observation of the $A^2\Pi_i$ - $X^2\Pi_i$ emission band is limited only from the vibrational ground state of $A^2\Pi_i$ to the ν_1 (CO stretch) vibrational excited states of the $X^2\Pi_i$ state (**Fig. 1**). It is because the internal conversion (IC) occurs from the $A^2\Pi_i$ state to the highly excited vibrational levels of $X^2\Pi_i$ state and the OCS^+ ion rapidly predissociates to $S^+(^4S_u)$ + $CO(X^1\Sigma^+)$ due to the crossing of a repulsive $^4\Sigma^-$ state. In the present study[1], we report a Fourier transform (FT) emission spectroscopy of the $A^2\Pi_i$ - $X^2\Pi_i$ band of OCS^+ for both the Ω=3/2 and 1/2 spin components to give the accurate molecular constants in the $X^2\Pi_i$ state.

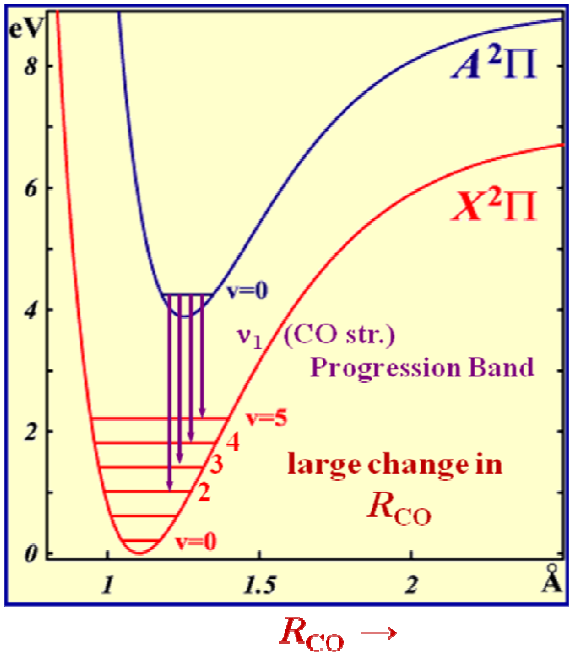

Fig.1 A-X Emission Bands of OCS^+

＜Experiment＞ The OCS^+ ion was generated by Penning ionization of OCS with metastable helium atoms, He*+OCS → He+ (OCS^+)*. Emitted UV light was introduced to a FT spectrometer (Brucker IFS-120 HR) to be recorded with a resolution of 0.03 cm^{-1} accumulating for 60 hours in total. Four CO-stretch progression bands (ν_1= 0→2-5) were observed in the frequency range of 21,000-27,000 cm^{-1}

which were split into two spin components (Ω = 3/2 and 1/2). The $v_1 = 0 \rightarrow 3$ band (Ω = 3/2) has a strong *R*-branch head together with the well resolved *P*- and *R*-branch lines and a weak *Q*-branch in the *R* and *P* branch gap (**Fig. 2**). The *R* and *P*-branch lines for Ω = 1/2 split into the Λ-type doubling, but no *Q*-branch lines were recorded. Accuracy of the line position is estimated to be 0.005 cm^{-1}.

＜Results＞ The progression bands (v_1=0→2-5) for both Ω = 3/2 and 1/2 were analyzed together with the origin band (v_1=0→0) observed by LIF study[2] accounting for the spin-orbit interaction explicitly. Eighteen molecular constants were fitted as listed in **Table 1** including the spin-orbit interaction constants A_0 and A_{D0} and the Λ-type doubling constant $(q+p/2)_0$. The standard deviation of the fit was 0.0034cm^{-1} consistent with the estimated accuracy of 0.005cm^{-1}.

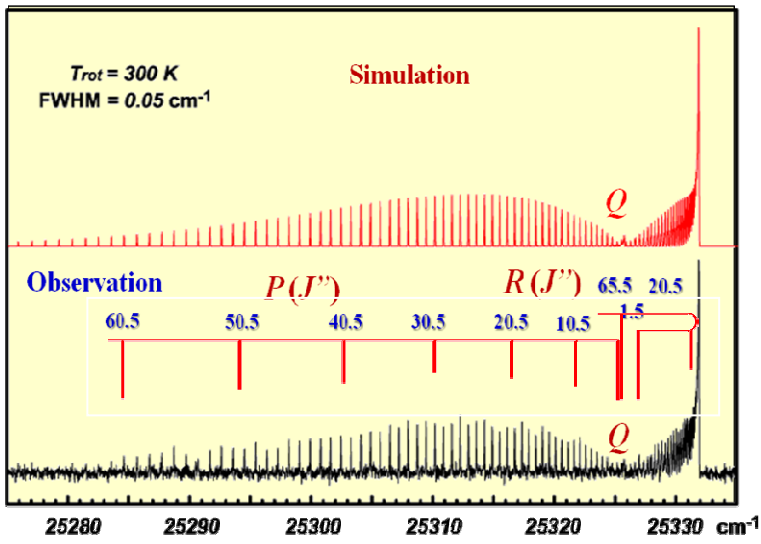

Fig. 2　$A^2\Pi_i$-$X^2\Pi_i$　v=0→3 (Ω=3/2) band of OCS^+

The rotational constants B_0 determined for the ground $X^2\Pi_i$ state is by 0.007659(18) cm^{-1} (~4%) larger than that for the excited $A^2\Pi_i$ state. The spin-orbit interaction constant A_0 = -381.0(56) cm^{-1} for the $X^2\Pi_i$ state is three times larger in magnitude than that -126.5 (56) cm^{-1} for the $A^2\Pi$ state, which are consistent with those (-367.2 and -111.8 cm^{-1}) reported by laser induced fragmentation study[3].

The CO bond length for the $X^2\Pi_i$ state was determined to be 1.10543 Å from the rotational constant B_0 assuming that for CS to be 1.6570 Å as given by the MRSD-CI calculation[4]. The CO and CS bond lengths for the $A^2\Pi_i$ state were determined to be 1.2810 and 1.5665 Å, respectively, from Franck-Condon factors given by emission band intensities and the observed rotational constant B_0. The CO bond length for the $A^2\Pi_i$ sate is longer by 0.1756 Å than that for the $X^2\Pi_i$ state, but the CS bond length is shorter by 0.0905 Å to accord with the prominent ν_1 progression bands observed in the wide range of UV region.

Excitation of one electron from the 2π orbital to the 3π orbital gives the $A^2\Pi_i$ excited state with the electronic configuration of $(8\sigma)^2\,(9\sigma)^2\,(2\pi)^3\,(3\pi)^4$, where the 2π orbital consists of the π_{CO} bonding orbital and the 3π orbital mainly of a π bonding orbital between C and S to weaken the CO bond and to strengthen CS bond for $A^2\Pi_i$ than those for $X^2\Pi_i$.

Table 1.　Molecular Constants of OCS+

	$X^2\Pi$		$A^2\Pi$	cm^{-1}
T_0	0.0		31276.826	Term Value
A_0	-381.0	>	-126.5	S-O Int.
ω_1	2088.97		(2039.50)	Vib. Freq.
$\omega_1 x$	19.975		(9.78)	
B_0	0.19477	>	0.18711	Rot. Con.
$\alpha_1 * 10^4$	6.435		---	
$D_0 * 10^8$	6.43		4.23	Cent. Dist.

<文献>

1) *JCP* **146**, 144302 (2017).　2) *CPL* **115**, 373 (1987).　3) *CPL* **119**, 467 (1985).　4) *TCA* **107**, 33 (2001).

Quantum Zeno effect in field-free methanol gas

(Shandong Univ.[a], Kashigar Univ.[b]),

Zhen-Dong Sun[a,b]

The quantum Zeno effect has been observed for the ultra-cold $^{9}Be^{+}$ ions in a magnetic field[1] and at room temperature for $^{13}CH_3F$ gas in an external electric field[2]. Now we demonstrate the observation of the quantum Zeno effect at room temperature in field-free methanol (CH_3OH) gas.

The CH_3OH molecule has the torsion of the CH_3 group and of the OH group with respect to each other[3]. The molecules of CH_3OH gas are mixed by different species of nuclear-spin isomers (NSIs) whose nuclear spins of identical nuclei in the CH_3 group are entangled with each other. It is from the three spin–1/2 hydrogen nuclei of this CH_3 group that the ortho-CH_3OH and para-CH_3OH are modified, which has a total nuclear spin quantum number I = 3/2 and 1/2, respectively. We show in this study that the ortho-para conversion of CH_3OH isomers can be induced by non-magnetic molecular collisions in a quantum relaxation process from a non-equilibrium concentration of them prepared by a technique of Light-induced drift[4] towards the zero equilibrium level of their populations. The ortho-para conversion rates have been obtained by using a least-square method to fit an exponential function to the observed curves of the population variations of the ortho and para isomers at low pressures from 0.3 to 2 Torr. The pressure dependence of the obtained conversion rates clearly show the inhibition of the interconversion between the ortho-CH_3OH and para-CH_3OH isomers by frequent collisions of the re-population molecules with increasing pressures. We attribute this interesting quantum phenomenon to the NSIs-torsion-specific states-mixing systems of CH_3OH. The torsion mediates the intermodes couplings for the strongly mixing near-degenerate ortho–para level pairs and providing doorway channels for population and intramolecular energy re-distribution[5]. Usually the energy gaps between two states of molecular ions and molecules can be narrowed via splitting of the levels by the applied external electric and/or magnetic field. Here, the observation of the quantum Zeno effect at room temperature is the first time for a field-free gas induced by non-magnetic molecular collisions.

I express sincere thanks to Profs. Kojiro Takagi, Yoshiki Moriwaki, Fusakazu Matsushima, and R. M. Lees for very helpful discussions. I acknowledge financial support from the National Natural Science Foundation of China (Grants No. 91536105 and 11174186).

References

[1] W. M. Itano, D. J. Heinzen, J. J. Bollinger, and D. J. Wineland, *Phys. Rev. A* **41**, 2295 (1990).

[2] B. Nagels, L. J. F. Hermans, and P. L. Chapovsky, *Phys. Rev. Lett.* **79**, 3097 (1997).

[3] G. Moruzzi, B. P. Winnewiser, M. Winnewiser, I. Mukhopadhyay, and F. Strumia, *Microwave, Infrared and Laser Transitions of Methanol: Atlas of Assigned Lines from 0 to 1258 cm^{-1}* (CRC Press, Boca Raton, FL, 1995).

[4] F. Kh. Gel'mukhanov and A. M. Shalagin, *JETP Lett.* **29**, 711(1979).

[5] R. M. Lees, L.-H. Xu, J. W. C. Johns, B. P. Winnewisser, and M. Lock, *J. Mol. Spectrosc.* **243**, 168 (2007).

A18

Ab Initio Calculations of Torsionally Mediated Hyperfine Splittings in E States of Acetaldehyde

Li-Hong Xu[1], E.M. Reid[1], B. Guislain[1], J.T. Hougen[2], E.A. Alekseev[3,4], I. Krapivin[3]
(lxu@unb.ca)

[1] Department of Physics and Centre for Laser, Atomic, and Molecular Sciences, University of New Brunswick, Saint John, NB, E2L 4L5, Canada

[2] Sensor Science Division, National Institute of Standards and Technology, Gaithersburg, MD 20899-8441, USA.

[3] Institute of Radioastronomy of National Academy of Sciences of Ukraine, Chervonopraporna 4, 61002 Kharkov, Ukraine.

[4] Quantum Radiophysics Department of V.N. Karazin Kharkiv National University, Svobody Square 4, 61022, Kharkov, Ukraine

Hyperfine splittings in methanol (CH_3OH) have been revisited in three recent publications.
[i] Coudert et al. [JCP 143 (2015) 044304] published an analysis of splittings observed in the low-*J* range. They calculated 32 spin-rotation, 32 spin-spin, and 16 spin-torsion hyperfine constants using the ACES2 package. Three of these constants (c_{zz}^{0}, $c_{zz}^{0,h}$ and $s_z^{0,h}$) were adjusted to fit hyperfine patterns for 12 transitions.
[ii] Three present authors and collaborators [JCP 145 (2016) 024307] analyzed medium to high-*J* experimental Lamb-dip measurements in methanol and presented a theoretical spin-rotation explanation that was based on torsionally mediated spin-rotation hyperfine operators. These contain, in addition to the usual nuclear spin and overall rotational operators, factors in the torsional angle α of the form $e^{\pm in\alpha}$. Such operators have non-zero matrix elements between the two components of a torsion-rotation ^{tr}E state, but have zero matrix elements within a ^{tr}A state. More than 55 hyperfine splittings were successfully fitted using three parameters (c_{xx}^{2}, c_{yy}^{2}, and c_{xy}^{2}) and the fitted values agree well with ab initio values obtained in [i]. [iii] Lankhaar et al. [JCP **145** (2016) 244301] published a reanalysis of the data set from [i], using CFOUR recalculated hyperfine constants based on their rederivation of the relevant expressions. They explain why their choice of fixed and floated parameters leads to numerical values for all parameters that seem to be more physical than those in [i]. The results in (ii) raise the question of whether large torsionally-mediated spin-rotation splittings will occur in other methyl-rotor-containing molecules. This abstract presents ab initio calculations of torsionally mediated hyperfine splittings in the E states of acetaldehyde using the same three operators as in [ii], and spin-rotation constants computed by Gaussian09. We explore the first 13 *K* states for *J* from 10 to 40 and v_t = 0, 1, and 2. Our calculations indicate that hyperfine splittings in CH_3CHO are just below current measurement capability. This conclusion is confirmed by available experimental measurements.

Keywords by relevance: Large amplitude motions, internal rotation – (Hyper)fine structure, tunneling – Microwave and THz – Theory and Computation

A19

Molecular Vibronic Spectra in Solution Simulated by Damped Franck-Condon Factors

Chen-Wen Wang, Chaoyuan Zhu and Sheng-Hsien Lin

Department of Applied Chemistry, National Chiao-Tung University,

1001, Ta-Hsueh Rd., Hsinchu 300, Taiwan

E-mail address: cyzhu@mail.nctu.edu.tw

Abstract

Franck-Condon factors bridge the gap between theoretical modeling and experimental observations for molecular electronic spectroscopy and electron transfer. Under the displaced harmonic oscillator approximation, multidimensional Franck-Condon factors are decomposed into a product of many one-dimensional (1D) Franck-Condon (FC) factors, which are successfully applied to simulate molecular vibronic spectra in gases phase. For dealing with simulation of the spectra in solution, various ab. initio methods, such as polarizable continuum model (PCM) and explicit solvent model, added correction in static interactions between solute and solvent molecules. However, how to treat dynamic correction to the spectra is not well-studied. We have recently developed the dynamic correction method leading to direct modification of Franck-Condon factors by damped oscillators. This method was applied to simulate absorption and fluorescence spectra of perylene, isoquinoline, rubrene molecule in solutions. The present simulation presents nice physical insights for dynamic correction to solvent-enhanced vibronic spectra.

References

[1] C.-W. Wang, L. Yang, C. Zhu, J.-G. Yu and S. H. Lin, *J. Chem. Phys. 141, 2014,* 084106.

[2] Y. H. Liu, S. M. Wang, C.-W. Wang, C. Zhu, K.-L. Han and S. H. Lin, *J. Chem. Phys. 145, 2016,* 164314.

[3] Y. Hu, C.-W. Wang, C. Zhu, F. L. Gu and S. H. Lin, *RSC Adv., 2017,7,* 12407.

Unravelling of Baird's Rule via Spectroscopic Analysis: Reversal of Hückel Aromaticity in the Excited Singlet and Triplet States of Hexaphyrins

Dongho Kim*

Department of Chemistry, Yonsei University, Seoul, South Korea, 03722
**dongho@yonsei.ac.kr*

Attention on the aromaticity in the ground state has been shifted to that in the excited state and its application because the determination of excited state aromaticity not only rationalizes the photostability and photoreactivity but also provides crucial insight into photosynthetic mechanisms and designing photoactive materials such as saturable absorbers. The excited state aromaticity was first described by Baird, where he proposed that Hückel aromatic and antiaromatic characters are reversed in the lowest excited triplet state into antiaromatic and aromatic ones, respectively (known as aromaticity reversal; Baird's rule).[1]

Here, we discuss the aromaticity reversal in the excited state of a comparable set of Hückel aromatic/antiaromatic hexaphyrin congeners by time-resolved infrared (TRIR) spectroscopy. Aromaticity is deeply related with molecular conformations;[2-6] electronically unstable antiaromatic molecules tend to become stable via structural distortions while aromatic ones exhibit planar and rigid geometries for more effective π-conjugation.[7-9] Judging from this aromaticity-dependent conformational differences, we investigate the aromaticity reversal in the excited state with the IR-activity of C=C stretching modes, which are sensitive to conformational distortions due to the vibrational selection rule for a change of the dipole moment.[5] The aromatic/antiaromatic hexaphyrin congeners showed the interconvertible IR spectral features between the ground and excited states arise from aromaticity-driven structural changes, which clearly demonstrates the

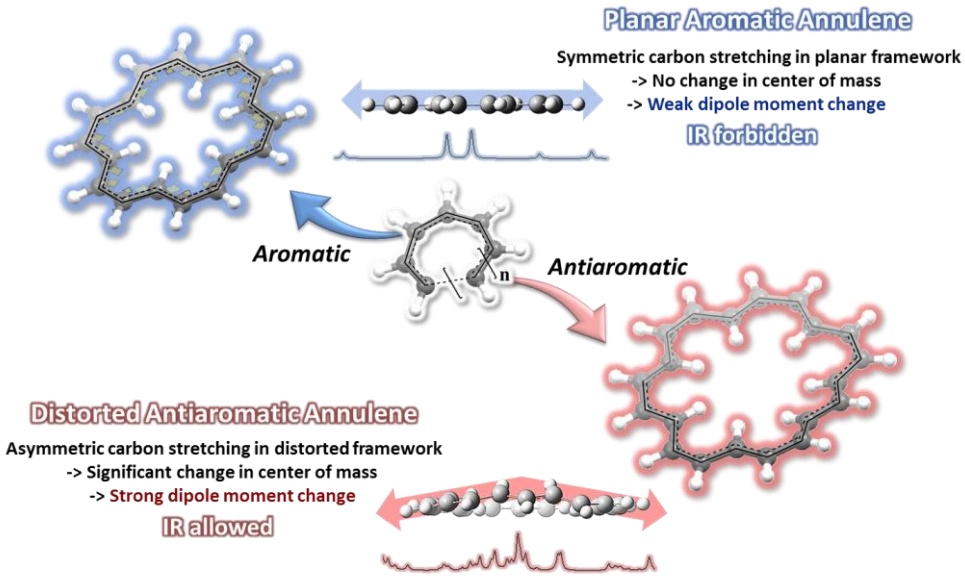

Figure 1. Aromaticity-dependence of molecular structures and IR-activities.

aromaticity reversal in the excited state. Our unconventional findings by the IR spectroscopy will provide deeper insight into the effect of aromaticity reversal on the photochemical synthesis as well as the photostability and photoreactivity for photoactive materials.

[1] Baird, N. C. *J. Am. Chem. Soc.* **1972**, *94*, 4941–4948.
[2] Sung, Y. M.; Yoon, M. C.; Lim, J. M.; Rath, H.; Naoda, K.; Osuka, A.; Kim, D. *Nat. Chem.* **2015**, *7*, 418–422.
[3] Sung, Y. M.; Oh, J.; Kim, W.; Mori, H.; Osuka, A.; Kim, D. *J. Am. Chem. Soc.* **2015**, *137*, 11856–11859.
[4] Oh, J.; Sung, Y. M.; Kim, W.; Mori, S.; Osuka, A.; Kim, D. *Angew. Chem. Int. Ed.* **2016**, *55*, 6487-6491.
[5] Sung, Y. M.; Oh, J.; Naoda, K.; Lee, T.; Kim, W.; Lim, M.; Osuka, A.; Kim, D. *Angew. Chem. Int. Ed.* **2016**, *55*, 11930–11934.
[6] Hong, Y.; Oh, J.; Sung, Y. M.; Tanaka, Y.; Osuka, A.; Kim, D. *Angew. Chem. Int. Ed.* **2017**, *56*, 2932-2936.
[7] Sung, Y. M.; Oh, J.; Cha, W.; Kim, W.; Lim, J. M.; Yoon, M. C.; Kim, D. *Chem. Rev.* **2017**, *117*, 2257-2312.
[8] Cha, W.; Kim, T.; Ghosh, A.; Zhang, Z.; Ke, X.; Ail, R.; Lynch, V. M.; Jung, J.; Kim, W.; Lee, S.; Fukuzumi, S.; Park, J. S.; Sessler, J.; Chandrashekar, T. K.; Kim, D. *Nat. Chem.* Under revision.
[9] Ueda, M.; Jorner, K.; Sung, Y. M.; Mori, T.; Kim, D.; Ottosson, H.; Aida, T.; Itoh, Y. *Nat. Commun.* Under revision.

Theoretical Study on Geometrical Isotope Effect and Rotational Constants of Polyatomic Molecules

(Hiroshima Univ.[a], Kyoto Univ.[b], Conflex Corp.[c], FOCUS[d]) Takayoshi Ishimoto[a], Masaaki Baba[b], Naofumi Nakayama[c], Umpei Nagashima[d]
e-mail: tishimo@hiroshima-u.ac.jp

It is of great importance to determine the geometrical structure of an isolated polyatomic molecule. Recently, it has been shown the possibility of the direct comparison in the experimental spectroscopic observations and *ab initio* theoretical calculation due to the achievements of both accurate measurements and calculations.

However, in the usual *ab initio* calculations, the equilibrium structures are obtained, although the determine structures by the experiment mean the averaged structures. This difference becomes larger when the mass of atom becomes smaller, i.e., hydrogen case. In addition, due to the anharmonicity of the potential, it is well known that the X-D distance in D-compounds are shorter than the X-H one in H-compounds. But, it is difficult to discuss the difference of X-H/X-D distances under the conventional *ab initio* calculations.

To take into account the geometrical changes by the H/D isotope effect, we developed the multi-component molecular orbital (MC_MO) approach [1]. The MC_MO method enables one to analyze the quantum effects of a proton (deuteron) because the MC_MO method determines both the electronic and the protonic (deuteronic) wavefunctions simultaneously and directly. We have already found that the MC_MO method can be used to analyze the geometrical isotope effect and kinetic isotope effect induced the difference in quantum behavior between protons and deuterons. Before the analysis of spectroscopic properties, we first optimized the H/D-compounds for polyatomic molecules, such as, acetaldehyde, acetone, benzene, and methoxy radical. The rotational constants based on the optimized structures including H/D geometrical isotope effect showed good agreement with the experimental value. We clearly found that the geometrical changes induced by the H/D isotope effect influence the spectroscopic properties, such as rotational constants[2-4].

Acknowledgements
Activities of Advanced Automotive Research Collaborative Laboratory in Hiroshima University are supported by MAZDA Corporation.

References

[1] T. Ishimoto, M. Tachikawa, and U. Nagashima, *Int. J. Quantum Chem.*, **109**, 2677 (2009).
[2] T. Ishimoto, Y. Ishihara, H. Teramae, M. Baba, and U. Nagashima, *J. Chem. Phys.*, **128**, 184309 (2008).
[3] T. Ishimoto, Y. Ishihara, H. Teramae, M. Baba, and U. Nagashima, *J. Chem. Phys.*, **129**, 214116 (2008).
[4] T. Ishimoto, M. Baba, U. Nagashima, N. Nakayama, and M. Koyama, *J. Comput. Chem. Jpn.*, **15**, 199 (2016).

A22

Conformational Structures of Jet-cooled Acetaminophen-water Clusters: A Gas Phase Spectroscopic and Computational Study

(Gyeongsang National Univ.[a], Chungbuk National Univ.[b]) Ahreum Min[a,b], Ahreum Ahn[a], Cheol Joo Moon[a], Yeon Guk Seong[a], Nam Joon Kim[b], Myong Yong Choi[a]

Acetaminophen (AAP) is a widely used over-the-counter antipyretic and analgesic, a major ingredient in various cold and flu drugs, Tylenol®. On the basis of the results with AAP monomer, we would like to step further on the study of AAP-water clusters. For the acetaminophen (AAP)-water clusters (AAP-$(H_2O)_1$) have been investigated by mass-selected resonant two-photon ionization (R2PI), ultraviolet-ultraviolet hole-burning (UV-UV HB), infrared-dip (IR-dip), and infrared-ultraviolet hole-burning (IR-UV HB) spectroscopy. Each *syn*- and *anti*-AAP rotamer has three distinctive binding sites (-OH, >CO, and >NH) for a water molecule, thus 6 different AAP-$(H_2O)_1$ conformers are expected to exist in the molecular beam. The origin bands of the AAP(OH)-$(H_2O)_1$ and AAP(CO)-$(H_2O)_1$ conformers (including its *syn*- and *anti*-conformers) in the R2PI spectrum are shifted to red and blue compared to those of the AAP monomer, respectively. The spectral assignments of the origin bands in the R2PI spectrum and the IR vibrational bands in the IR-dip spectra for the four lowest-energy conformers of AAP-$(H_2O)_1$, [*syn*- and *anti*-AAP(OH)-$(H_2O)_1$ and *syn*- and *anti*-AAP(CO)-$(H_2O)_1$], are aided by *ab initio* and time-dependent density functional theory (TDDFT) calculations. Further investigation on the IR-dip spectra has revealed a hydrogen-bonded NH stretching mode, supporting the presence of the *syn*-AAP(NH)-$(H_2O)_1$ conformer. Moreover, by employing IR-UV HB spectroscopy, we have reconfirmed the existence of the *syn*-AAP(NH)-$(H_2O)_1$ conformer, which happened to be buried underneath the broad background attributed from the AAP(OH)-$(H_2O)_1$ conformers

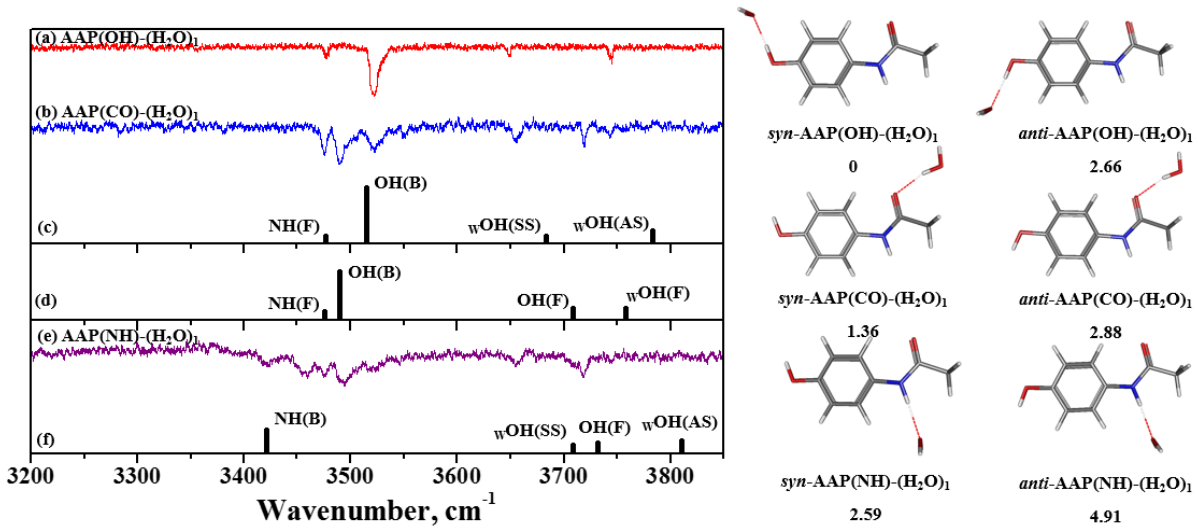

Figure 1. IR-dip and calculated IR bar spectra of three major *syn*- AAP-$(H_2O)_1$ conformers. The optimized structures of 6 different conformers of AAP-$(H_2O)_1$ in the ground state. The relative energies are shown below the corresponding structure (kJ/mol, zero-point energy corrected).

A23

Vibrational Predissociation of the Ã state of the C_3Ar complex in the excitation energy region of 25410-25535 cm^{-1}

（Institute of Atomic and Molecular Sciences） Yi-Jen Wang, Yen-Chu Hsu

About 11 C_3Ar bands near the $0\ 4^-\ 0-\ 000$ and $0\ 2^+\ 0-\ 000$ transitions of the $\tilde{A}\ ^1\Pi_u - \tilde{X}\ ^1\Sigma^+_g$ system of C_3 have been studied by both laser-induced fluorescence and wavelength-resolved emission(WRE) techniques. Two prominent pairs of C_3Ar features were observed to the red of each of these two C_3 transitions. Each pair consists of a type A band and a type C band, with the type C band lying about 3 cm^{-1} above the type A band. Rotational analysis showed that three of the bands are comparatively sharp, with line widths of 0.035 cm^{-1}, but the pair at 25504 and 25507 cm^{-1} shows clear evidence of diffuseness. The spectral widths of the rotational lines do not depend on the excitation energies in any simple way. Most of the spectral features in the WRE spectra can be assigned as emission from vibrationally excited levels of the Ã state of the C_3 fragments down to the ground electronic state. Two different types of vibrational excitation of the C_3 fragments have been found: pure C_3-bending and antisymmetric C-C stretching. The branching ratios of the C_3 product states, the C_3Ar vdW binding energy, and propensity rules for vibrational predissociation processes will be presented.

A24

Variations in the electron detachment spectra of $F^-\cdots H_2O$ Anion induced by proton motion

(Institute of Atomic and Molecular Sciences, Academia Sinica Taiwan[a])
Kaito Takahashi[a] kt@gate.sincia.edu.tw

For the understanding of the solvation structure of ions in the aqueous phase, one has to define observables that change with solvation structure. In the condensed phase due to complex thermal fluctuation, the definition of the structure becomes very unambiguous. Therefore, the researchers in the gas phase community have studied size selected gas phase charged clusters to help decode the complexity. Through the comparison with theoretical simulations, vibrational spectra of anion clusters have given information toward the geometrical structure of these clusters. On the other hand, photodetachment and X-ray absorption spectra are used to probe the electronic structure of anions in the aqueous phase. In most previous studies on the photodetachment spectra, the simulation of the spectra was performed by calculating the vertical detachment energies at equilibrium geometries, at cluster cut out from classical trajectories or at zero-point vibration distributions. Here, we aim to provide new insight from the simulation of vibrational state dependent photodetachment spectra for $X^-\cdots(H_2O)_n$ anion, where X= F, Cl, Br. Utilizing the reflection principle, we simulated the photodetachment spectra from different vibrational excited states for F^-H_2O, Cl^-H_2O and Br^-H_2O.[1] From these spectra, we can observe changes in the electron distribution between the anion and neutral $X\cdots H_2O$ system that are induced by vibrational excitation. Notably, for F^-H_2O, the excitation of the ionic hydrogen bonded (IHB) OH stretching vibration causes a large tail on the low energy side of the photodetachment spectra compared to the detachment from the zero-point vibration state. This low tail shows that IHB OH stretching vibration of F^-H_2O causes charge delocalization from F^- to the oxygen atom in H_2O and the photodetachment from $FH\cdots OH^-$ occurs at lower energies.

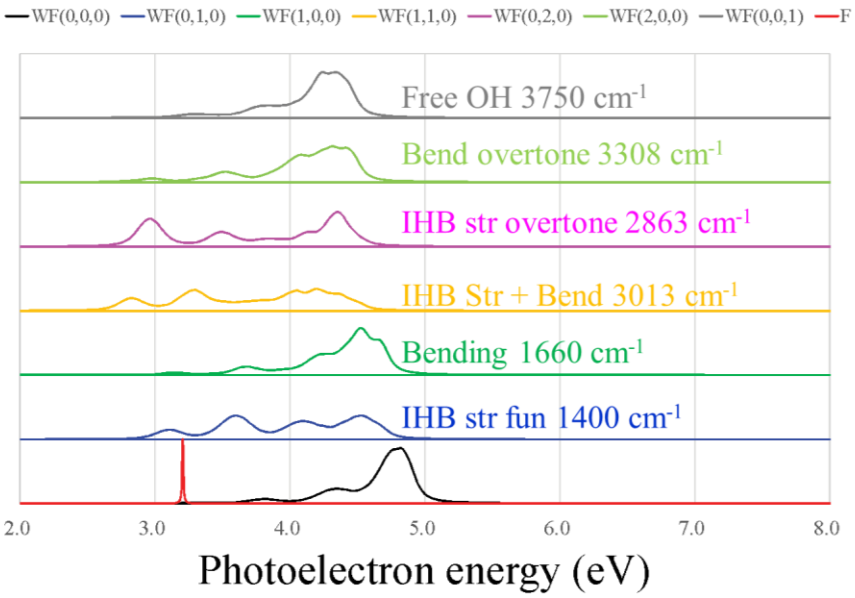

A25

Photoinduced Proton Transfer of N-Methyl-Hydroxyquinolinium to Small Water Clusters

(Department of Chemistry, Ulsan National Institute of Science and Technology (UNIST)[a], Center for Soft and Living Matter, Institute for Basic Science (IBS)[b]) Taewan Kim[a], Won-Woo Park[a], and Oh-Hoon Kwon[a,b*] (ohkwon@unist.ac.kr)

The excited-state proton transfer (ESPT) to water was studied in the presence of a series of strong photoacids, N-methyl-n-hydroxyquinolinium ions, with a hydroxyl group at 3(NM3HQ$^+$), 5(NM5HQ$^+$), 6(NM6HQ$^+$), 7(NM7HQ$^+$) and 8(NM8HQ$^+$) positions, in an aprotic solvent of acetonitrile.

We measured excited-state lifetimes of the prototropic species of NMnHQ$^+$ using picosecond-resolved fluorescence spectroscopy and analyzed their chemical kinetics to reveal the ESPT mechanism. The results show that water, as a base, forms small clusters during the ESPT process, the sizes of which have are: three for NM7HQ$^+$, two for NM3HQ$^+$ and NM6HQ$^+$, and one for NM5HQ$^+$ and NM8HQ$^+$.

From the Förster analysis modified from its original version [1], acid dissociation constants in excited state (pKa*) of the photoacids were evaluated and found to correlate with the size of the water clusters as base; the number of molecules constituting the water clusters tend to decrease as the photoacid becomes acidic, i.e., with lower pKa* values. From the comparison with our previous results reporting the size of alcohol clusters as Brønsted base in the ESPT of the same photoacids [2-4], it is found that water is less reactive in acid-base reactions than alcohol when hydrogen-bond network is limited to form small clusters.

References

[1] Tolbert, L. M.; Solntsev, K. M. *Acc. Che. Res.* **2002** *35*, 19-27

[2] Park, S. Y.; Lee, Y. M.; Kwac, K.; Jung, Y.; Kwon, O.-H. *Chem. Eur. J.* **2016**, 22, 4340-4344

[3] Lee, Y, M.; Park, S. Y.; Kim, H.; Kim, T. G.; Kwon, O.-H. *Methods Appl. Fluoresc.* **2016**, 4, 024004

[4] Park, S. Y.; Kim, T. G.; Ajitha, M. J.; Kwac, K., Lee, Y. M.; Kim, H.; Jung, Y.; Kwon, O.-H. *Phy. Chem. Chem. Phys.* **2016**, 18, 24880-24889

High-resolution spectroscopy of deuterated benzenes

(Kyoto Univ.[a], Institute of Molecular Science[b], The Univ. of Tokyo[c], Tokyo Inst. of Tech.[d])
Sachi Kunishige[a], Takaya Yamanaka[b], Masaaki Baba[a],
Masakazu Nakajima[c], Yasuki Endo[c] and Yasuhiro Ohshima[d]

We performed spectroscopic experiments to elucidate the properties of the 13 deuterated benzenes in the S_0 and S_1 states. The molecular structure of benzene was determined by microwave spectroscopy and geometric calculation. The deuterium effects on the normal coordinates and rotational structures were seen in the high-resolution mass-selective REMPI spectra.

【Introduction】

Deuteration changes nuclear motions such as vibration or rotation. Especially, partly deuterium substitution in benzene could reduce the molecular symmetry from D_{6h} symmetry into D_{3h}, C_{2v} and so on (Figure 1). These changes would make the vibrational or rotational structure quite different. The objective of the present study is to clarify the change of spectra of benzenes by deuteration.

【Experiments】

The supersonic jet method was used in all the experiments. For the sample we synthesized a mixture of 13 deuterated benzenes by maintaining the mixture of C_6H_6 and C_6D_6 at 800 K for 7 h with alumina powder.

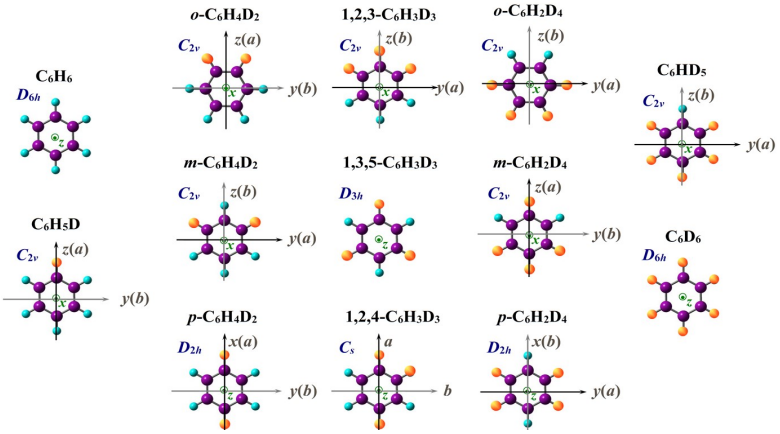

Figure 1: All the deuterated benzenes.

【Results】

For elucidating the molecular structure of benzene in the electronic ground state, we determined the rotational constants of some deuterated benzenes by microwave spectra. Then the least-squared fit was performed using the observed and calculated rotational constants, assuming that all bond angles are 120°. The result suggests that the molecular structure at the zero-vibrational level in the S_0 state is the almost same for all the deuterated benzenes. This is different from other molecules or radicals such as CH_4 in which r_0(C-H) – r_0(C-D) = 5 mÅ.

Then we observed the rotationally-resolved high-resolution spectra of the 6^1 band for all the partly deuterated benzenes to clarify the property of deuterated benzenes in the S_1 state. The ν_6 (e_{2g}) vibration splits into two components, 6a and 6b, in the lower molecular symmetry than D_{3h}. Furthermore, the Coriolis interaction exists between 6a and 6b which shifts the energy of rotational levels. We clarified the mass dependence of this interaction through observation and theory.

【Reference】

[1] S. Kunishige et al., J. Chem. Phys. **143**, 244302(2015)
[2] S. Kunishige et al., J. Chem. Phys. **143**, 244303(2015)
[3] S. Kunishige et al., J. Chem. Phys. **143**, 244304(2015)

PRECISION SATURATED ABSORPTION SPECTROSCOPY OF H_3^+

Yu-Chan Guan[1], Yung-Hsiang Chang[1], Yi-Chieh Liao[1] and Jow-Tsong Shy[1, 2]

[1]*Institute of Photonics Technologies, National Tsing Hua University, 101, Section 2, Kuang-Fu Rd., Hsinchu 30013, Taiwan*

[2]*Department of Physics, National Tsing Hua University, 101, Section 2, Kuang-Fu Rd., Hsinchu 30013, Taiwan*

Abstract:

In our previous work on the Lamb dips of the ν_2 fundamental band of H_3^+, the saturated absorption spectrum was obtained by the third-derivative spectroscopy using frequency modulation [1]. However, the frequency modulation also causes error in absolute frequency determination. To solve this problem, we have built an offset-locking system to lock he OPO pump frequency to an iodine-stabilized Nd:YAG laser. With this modification, we are able to scan the OPO idler frequency precisely and obtain the profile of the Lamb dips. Double modulation (amplitude modulation of the idler power and concentration modulation of the ion) is employed to subtract the interference fringes of the signal and increase the signal-to-noise ratio effectively. To Determine the absolute frequency of the idler wave, the pump wave is offset locked on the R(56) 32-0 a_{10} hyperfine component of $^{127}I_2$, and the signal wave is locked on a GPS disciplined fiber optical frequency comb (OFC). All references and lock systems have absolute frequency accuracy better than 10 kHz. Here, we demonstrate its performance by measuring one transition of methane and sixteen transitions of H_3^+. This instrument could pave the way for the high-resolution spectroscopy of a variety of molecular ions.

[1] H.-C. Chen, C.-Y. Hsiao, J.-L. Peng, T. Amano, and J.-T. Shy, Phys. Rev. Lett. 109, 263002 (2012).

Doppler-free two-photon absorption spectroscopy of vibronic excited states of naphthalene with reference to an optical frequency comb

(UEC[a], Fukuoka Univ.[b], Kyoto Univ.[c]) A. Nishiyama[a], K. Nakashima[b], M. Misono[b], M. Baba[c]

1. INTRODUCTION

In the excited states of polyatomic molecules, there are some interesting phenomena such as, internal conversion (IC), intersystem crossing (ISC), and intramolecular vibrational energy redistribution (IVR). In the first electronic excited state of naphthalene, it was reported that IVR become dominant for the excess energy (E_x) larger than about 2000 cm^{-1}.

In this study, we observed Doppler-free two-photon absorption (DFTPA) spectra of three transitions, A^1B_{1u} ($v_4 = 1$, $E_x = 1560$ cm^{-1}) <- X^1A_g ($v = 0$), A^1B_{1u} ($v_4 = 1$, $v_8 = 1$, $E_x = 2260$ cm^{-1}) <- X^1A_g ($v = 0$) , and A^1B_{1u} ($v_4 = 1$, $v_7 = 1$, $E_x = 2545$ cm^{-1}) <- X^1A_g ($v = 0$), in the following, we call "orange band," "yellow band," and "lemon band," respectively. Then, we analyze the linewidth of rovibronic lines in each band.

2. EXPERIMENT

Figure 1 shows our experimental setup. This system consists of DFTPA system for naphthalene and frequency measurement system [1]. The light source for DFTPA system is a single mode CW dye laser. Its output power is about 1.8W, and the linewidth is about 130 kHz. Most part of the dye laser output is used to observe DFTPA spectra of naphthalene. The resonance frequency of the Fabry-Perot interferometer is locked to the dye laser frequency by Pound-Drever-Hall method. The frequency of the dye laser is scanned and the fluorescence intensity is observed by the photon counting system.

We use a GPS-disciplined Ti:Sapphire optical frequency comb as a frequency measure. The spectral range of the Ti:Sapphire comb is broadened by a photonic crystal fiber. A part of the dye laser output is split to measure its frequency. An acousto-optic frequency shifter in double pass configuration shifts the dye laser frequency to realize wide range continuous frequency measurements [2].

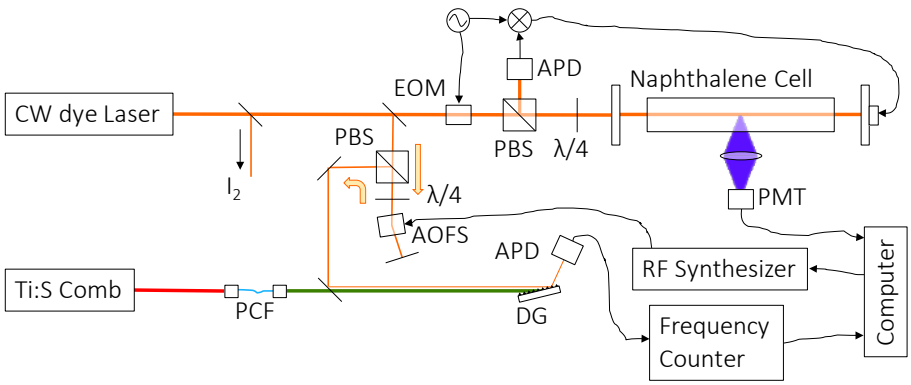

Figure 1. Experimental setup. PCF, photonic crystal fiber; PBS, polarizing beam splitter; EOM, electro-optic modulator; AOFS, acousto-optic frequency shifter; APD, avalanche photodiode; DG, diffraction grating; PMT, photomultiplier tube.

3. RESULTS AND DISCUSSION

The observed spectra are shown in the figure 2. They are a part of spectra of the lemon band, the yellow band, and the orange band from top to bottom. For the orange and yellow bands, linewidths are about 2.5 MHz, and they show small dependences on the rotational quantum numbers. On the other hand, the linewidths in the lemon band spectra become broad, and depend on the rotational quantum numbers. This means that the IVR become dominant in the upper state of the lemon band transition.

[1] A. Nishiyama, K. Nakashima, A. Matsuba, and M. Misono, J. Mol. Spectrosc., 318, 40 (2015).
[2] A. Nishiyama, A. Matsuba, and M. Misono, Opt. Lett., 39, 4923 (2014).

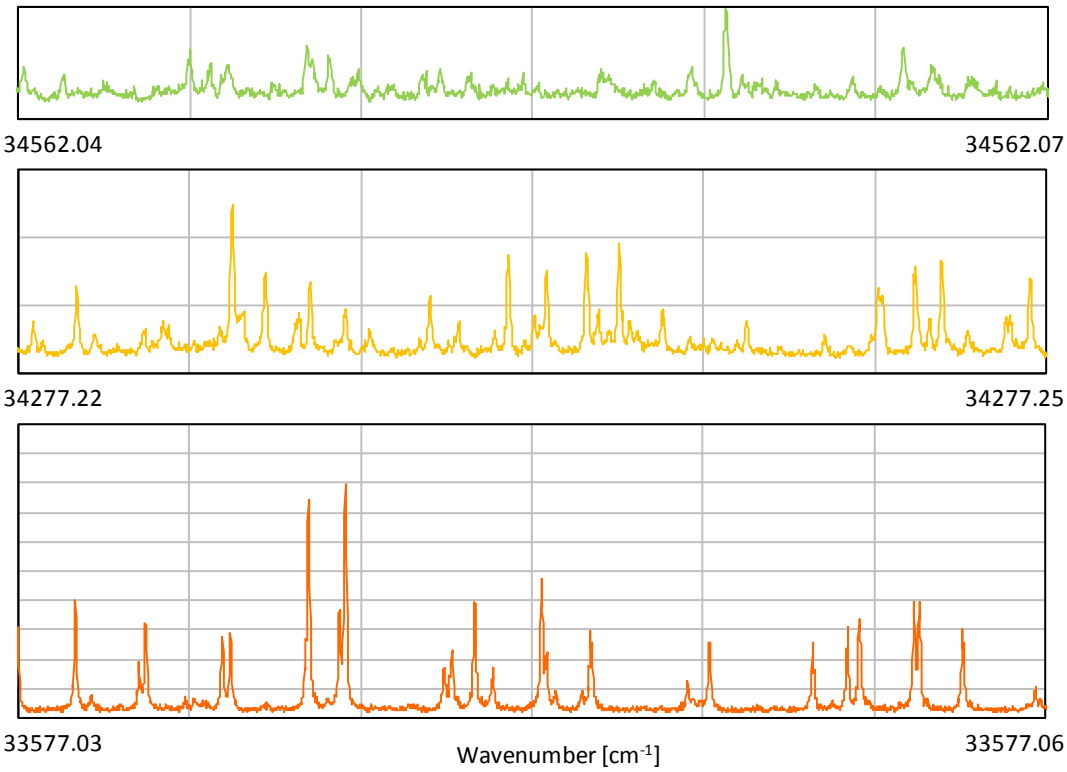

Figure 2. Observed spectra.

High-sensitive and precise measurement of Doppler-free two-photon absorption spectra of Rb using dual-comb spectroscopy

([a]Univ. Electro-Communications, [b]JST, ERATO MINOSHIMA IOS Project, [c]JSPS)
Akiko Nishiyama[a,b,c], Satoru Yoshida[a,b], Takuya Hariki[a], Yoshiaki Nakajima[a,b], Kaoru Minoshima[a,b]

Introduction

Dual-comb techniques are applicable to high-resolution and precise spectroscopies [1,2]. In this work, we demonstrated Doppler-free two-photon absorption dual-comb spectroscopy of Rb. We obtained high signal-to-noise ratio spectra of the $5S_{1/2} - 5D_{5/2}$ transition and precisely determined absolute frequencies of the hyperfine spectra.

Experiment

Figure 1(a) depicts the principle of the two-photon absorption spectroscopy using the dual-comb technique [3]. In spite of the weak comb mode power, two-photon transitions which are nonlinear processes are observable due to the contribution of many comb mode pairs with the same sum frequency. We observe the fluorescence from the excited states, and obtain the spectra by taking the fast Fourier-transform of the fluorescence signals. The sensitivity of the dual-comb measurement is significantly improved by the fluorescence detection scheme.

The experimental setup is illustrated in Fig. 1(b). We used second-harmonic generations (SHG) of mode-locked Er-doped fiber lasers. The center wavelength of the SHG spectra were adjusted near 778 nm by temperature control of PPLN crystals

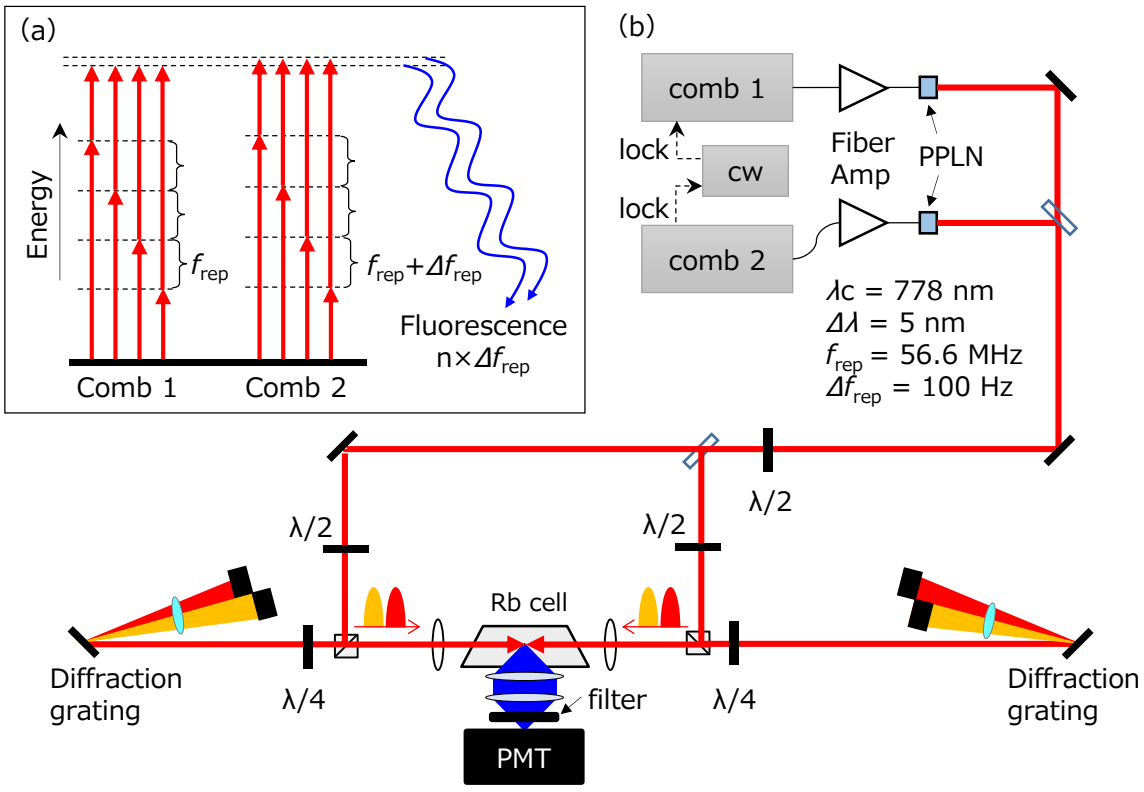

Fig. 1 (a) Principle of the two-photon dual-comb spectroscopy. (b) Experimental setup. PPLN: periodically-poled lithium niobate, PMT: photomultiplier tube.

to observe the $5S_{1/2}$ – $5D_{5/2}$ transition at 778.1 nm. The two outputs were overlapped and split into two arms. In each arm, two color parts (>778 nm, <778 nm) of the spectra were separated using a diffraction grating and two mirrors with an adjustable delay. The delay of the two color pulse was used to eliminate Doppler-broadening background, then we can observe background-free spectra which were caused by only counter-propagating pulses. The counter-propagating pulses were overlapped in the center of a Rb vapor cell, and the fluorescence interferogram was detected by a photomultiplier tube (PMT).

Results

Figures 2 (a) shows Doppler-broadened spectrum of the $5S_{1/2}$ – $5D_{5/2}$ transition observed with only unidirectional incident beam without the delay. The spectral width of transitions from a hyperfine level of the ground state of ^{87}Rb was about 1.3 GHz. Figure 2 (b) shows the Doppler-free and background-free spectrum observed with counter-propagating pulses with the delay of 1 cm, and magnified view of the $5S_{1/2}$ (F''=1) – $5D_{5/2}$ (F'=1, 2, 3) transitions of ^{87}Rb is shown in Fig. 2(c). The observed spectra had a flat baseline and showed fully-resolved hyperfine structure of the excited state. Center frequencies of the background-free spectra were precisely determined with the uncertainty of less than 100 kHz.

The spectral widths of the hyperfine spectra were approximately 5 MHz which was broader than the natural linewidth of the transition. As shown in Fig. 2(c), the observed sub-Doppler spectra were fitted to Gaussian profiles, because the main contribution to the broadening was residual Doppler shifts. In the dual-comb two-photon absorption scheme, many pairs of modes introduce a transition, and frequency differences of the mode pairs cause the residual Doppler shift. The broadband comb spectrum increases the variety of mode pairs, then the observed sub-Doppler spectral widths are broadened.

This work was supported by JST through the ERATO MINOSHIMA Intelligent Optical Synthesizer Project (IOS) and Grant-in-Aid for JSPS Fellows (16J02345).

[1] S. Okubo, et. al., Opt. Express 23(26), 33184 (2015).
[2] A. Nishiyama, et. al., Opt. Express 24 (22), 25894 (2016).
[3] A. Hipke, et. al., Phys. Rev. A 90, 011805(R) (2014).

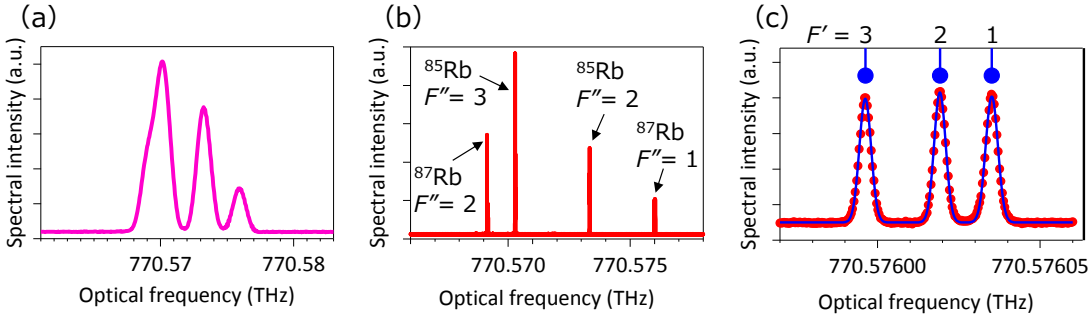

Fig.2. (a) Doppler-limited spectrum of $5S_{1/2}$ – $5D_{5/2}$ transition of Rb. (b) Doppler-free spectrum observed with counter-propagating beams. (c) Magnified view of the Doppler-free spectra of $5S_{1/2}$ (F'' = 1) – $5D_{5/2}$ (F' = 3, 2, 1) of ^{87}Rb.

Absolute frequency measurement of the molecular iodine hyperfine transition at 647 nm

(National Tsing Hua Univ.[a]) Yao-Chin Huang[a], Yu-Chan Guan[a], Jow-Tsong Shy[a], Li-Bang Wang[a]

Molecular iodine (I_2) has played an important role in optical frequency standards for many applications. The most striking element of the iodine absorption spectrum is the long series of the B-X system in the range from the green to near-IR and has very strong strength and narrow linewidth in the region close to the dissociation limit. Molecular iodine is commonly used for frequency stabilization of laser.

Iodine absorption lines at 647 nm are very close to the doubling wavelength (2×323 nm) of the 2S-3P transition of atomic lithium (Li). Therefore, these iodine lines can be frequency references for Li atom research, e.g., the development of laser cooling and the measurement of hyperfine intervals. The frequency references at 647 nm using a simple iodine cell are particularly helpful for atomic physics laboratories where no optical frequency combs are available.

In this work, we perform Doppler-free saturation spectroscopy in an iodine vapor cell using modulation transfer spectroscopy. The effect of pressure shift is investigated by changing the cold finger temperature and extrapolating the absolute transition frequency at zero pressure. The saturated absorption signal is used to lock the laser frequency, and the absolute frequency of the transition lines are measured by an optical frequency comb. A frequency stability of 5×10^{-12} at a 200 s integration time is achieved when the light source is stabilized to the P(46) 5-4 a_{15} line. To our knowledge, there are no precision measurements around this wavelength, and our results provide useful input for the theoretical predictions.

CO_2 line intensities near 1.6μm by cavity ring-down spectroscopy

（Univ Sci & Technol China）P Kang, J Wang, L-G Tao, Y R Sun, A-W Liu, T-P Hua, S-M Hu

Accurate parameters of the CO_2 transitions in the 1.6 μm region are needed for monitoring global CO_2 concentration in the atmosphere. Line intensities with relative uncertainty lower than 0.5% are required. However, discrepancies up to 3-10% have been reported between experimental data and calculated results [1-4]. We present measurements of the CO_2 lines in this region using frequency-locked cavity ring-down spectroscopy. Ro-vibrational transitions of the 30011-00001 band with line intensities in the order of 10^{-25} to 10^{-24} cm/molecule have been studied. We have been able to determine the line intensities with an accuracy of 0.5%, which fulfills the requirements for remote sensing applications. We also present a comparison among present results, HITRAN data, and recent calculations.

Reference:

[1] R. A. Toth *et al*., J. Mol. Spectrosc. **239**, 221-242 (2006).

[2] E. Zak *et al*., J. Quant. Spectrosc. Radiat. Transf. **177**, 31-42 (2016).

[3] O. L. Polyansky *et al.*, Phys. Rev. Lett. **114**, 243001 (2015).

[4] S. A. Tashkun *et al*., J. Quant. Spectrosc. Radiat. Transf. **152**, 45-73 (2015).

B07

Mid-infrared saturated absorption spectroscopy inside the hollow fiber using difference frequency generation source

D.N. Patel[1], Tzu-Han Su[2], Hsiang-Chen Chui[2] and Jow-Tsong Shy[1, 3]

[1]*Department of Physics, National Tsing Hua University, 101, Section 2, Kuang-Fu Rd., Hsinchu 30013, Taiwan*
[2]*Department of Photonics, National Cheng Kung University, No.1, University Road, Tainan City 70101, Taiwan*
[3]*Institute of Photonics Technologies, National Tsing Hua University, 101, Section 2, Kuang-Fu Rd., Hsinchu 30013, Taiwan*

Email: dnp.iitk@gmail.com

Abstract:

Saturation spectroscopy is recognized as a powerful tool to observe the frequency precession far below the Doppler limit [1]. We have performed the mid-infrared Doppler-free spectroscopy inside the hollow fiber using a difference frequency generation (DFG) source. We have established a widely tunable mid-infrared DFG source using a 1 W tapered amplifier boosted external cavity diode laser (ECDL) system and a 10 W YDFA (ytterbium-doped fiber amplifier) boosted Nd:YAG laser system. The two laser beams from ECDL and Nd:YAG laser systems are mixed in a 50 mm long MgO doped periodically poled lithium niobate (MgO:PPLN) crystal to generate the DFG radiation over the tuning range of 3.97 to 4.71 μm. The maximum power of DFG source is about 3 mW. The iodine stabilization scheme is used to stabilize the Nd:YAG laser frequency and saturated absorption spectroscopy is performed on R(60) transition of CO_2 fundamental ($00^01 \leftarrow 00^00$) band at 4.193 μm inside a hollow fiber of diameter 300 μm and length 100 cm while keeping the CO_2 pressure at 100 mTorr. The hollow fiber is manufactured by Opto-Knowledge Systems Inc. having the attenuation of 3dB over 100 cm length. The observed spectrum is fitted with a combination of Gaussian and Lorentzian profile and the full width half maximum (FWHM) of the Lamb dip is reported to 4.56±0.23 MHz. We have also determined the line width (4.40±0.15 MHz) of Lamb dip in well agreement with the measured dip using the dependence of peak amplitude of the third derivative signal with respect to the modulation width [2]. The comparison of width with free space measurements will be discussed [3]. The third derivative locking method is used to lock the ECDL frequency to a hyperfine transition of CO_2. This study may potentially be used in the generation of compact mid-IR frequency standard source.

[1] T. W. Hansch, I. S. Shahin, and A. L. Schawlow, Nature-Phys. Sci. **235**, 63 (1972).

[2] H.-M. Fang, S.-C. Wang and J.-T. Shy, Opt. Commun. **257**, 76 (2006).

[3] C.-C. Liao, K.-Y. Wu, Y.-H. Lien, J.-T. Shy, High precision mid-IR spectroscopy of $^{12}C^{16}O_2$: $00^01 \leftarrow 00^00$ band near 4.3 μm, *Proceedings of the 63rd Ohio State University International Symposium on Molecular Spectroscopy*, Columbus, Ohio, 2008.

Electronic transitions of tungsten monosulfide

L. F. Tsang[1], Man-Chor Chan[1], Wenli Zou[2], and Allan S-C. Cheung[3*]

[1]Department of Chemistry, The Chinese University of Hong Kong, Shatin, NT, Hong Kong
[2]Institute of Modern Physics, Northwest University, Xi'an, Shaanxi, China and Shaanxi Key Laboratory for Theoretical Physics Frontiers, Xi'an, Shaanxi, China.
[3]Department of Chemistry, The University of Hong Kong, Pokfulam Road, Hong Kong

*Email: hrsccsc@hku.hk

Abstract

Electronic transition spectrum of the tungsten monosulfide (WS) molecule in the near infrared region between 725 nm and 885 nm has been recorded using laser ablation/reaction free-jet expansion and laser induced fluorescence spectroscopy. The WS molecule was produced by reacting laser - ablated tungsten atoms with 1% CS_2 seeded in argon. Fifteen vibrational bands with resolved rotational structure have been recorded and analyzed, which were organized into seven electronic transition systems. The ground state has been identified to be the $X^3\Sigma^-(0^+)$ state with bond length, r_o, and vibrational frequency, $\Delta G_{1/2}$, determined to be 2.0676 Å and 556.7 cm^{-1} respectively. In addition, vibrational bands with $\Omega = 1$ component in lower state have also been analyzed. Least-squares fit of the measured line positions yielded molecular constants for the electronic states involved.

Spectroscopic constants and potential energy curves of 30 low-lying Λ-S states and Ω sub-states of the WS molecule have been calculated using state-averaged complete active space self-consistent field (SA-CASSCF) and followed by MRCISD+Q (internally contracted multi-reference configuration interaction with singles and doubles plus Davidson's cluster correction). The active space consists of 10 electrons in 9 orbitals corresponding to the W 5*d*6*s* and S 3*p* shells. The lower molecular orbitals from W 5*s*5*p* and S 3*s* are inactive but are also correlated, and relativistic effective core potential (RECPs) are adopted to replace the core orbitals with 60 (W) and 10 (S) core electrons, respectively. The spin-orbit coupling (SOC) is calculated via the state-interaction (SI) approach with RECP spin-orbit operators using SA-CASSCF wavefunctions, where the diagonal elements in the SOC matrix are replaced by the corresponding MRCISD+Q energies calculated above. The calculated spectroscopic properties of the ground and low-lying electronic states are generally in good agreement with our experimental determinations. This work represents the first experimental investigation of the electronic and molecular structure of the WS molecule.

B09

The low-lying electronic states of scandium monocarbide, ScC

(Institute of Atomic and Molecular Sciences) Chiao-Wei Chen, Anthony J. Merer , Yen-Chu Hsu

Extensive wavelength-resolved fluorescence studies have been carried out for the electronic bands of ScC and $Sc^{13}C$ lying in the range 14000 - 16000 cm^{-1}. Taken together with detailed rotational analyses of these bands, they have clarified the natures of the low-lying electronic states. The ground state is an Ω = 3/2 state, with a vibrational frequency of 648 cm^{-1}, and the first excited electronic state is an Ω = 5/2 state, with a frequency of 712 cm^{-1}, lying 155.57 cm^{-1} higher. These states are assigned as the lowest spin-orbit components of $X^2\Pi_i$ and $a^4\Pi_i$, respectively. The quartet nature of the a state is confirmed by the observation of the $^4\Pi_{3/2}$ component 18.69 cm^{-1} above the $^4\Pi_{5/2}$ component. The strongest bands in the region studied go to two $^4\Delta_{7/2}$ excited states, lying 14355 and 15445 cm^{-1} above $X^2\Pi_{3/2}$. Extensive doublet-quartet mixing occurs, which results in some complicated emission patterns. The energy order, $a^4\Pi$ above $X^2\Pi$, is consistent with the ab initio calculations of Mavridis et al,.[a] but differs from that found by Simard et al.[b] in the isoelectronic YC molecule.

[a] A. Kalemos, A. Mavridis and J.F. Harrison, J. Phys. Chem. **A155**, 755 (2001).
[b] B. Simard, P.A. Hackett and W.J. Balfour, Chem. Phys. Lett., **230**, 103 (1994).

B10

Laser spectroscopic study of the B/B' $^2\sum^+$ v=9, 10, 11 and 18 levels of CaH

(Univ. of Toyama[a], Univ. New Brunswick[a])
Kyohei Watanabe[a], Kaori Kobayashi[a], Fusakazu Matsushima[a],
Yoshiki Moriwaki[a], Stephen C. Ross[b]

Spectroscopic studies on Calcium monohydride (CaH) have been carried out for long time. It was 1908 that electric transitions of CaH were observed for the first time through solar observations [1]. The first laboratory spectroscopy is the $C^2\Sigma^+$ - $X^2\Sigma^+$ transitions in near-UV region in 1925 [2]. Despite the long history of study of this molecule, the discrepancy exists between the experimental and theoretical analysis in higher vibrational levels of the second excited the B/B'$^2\sum^+$ state. The B/B'$^2\sum^+$ state is formed by the avoided crossing with the D state, resulting in a double minimum potential energy function[3]. Then there are strong perturbations between the B/B'$^2\sum^+$ and the $D^2\Sigma^+$ states. We have observed electric rotationa-vibrational transition of the B/B'$^2\Sigma^+$ - $X^2\Sigma^+$ above the double-minimum potential energy for experimentally elucidating the perturbation between the B/B'$^2\sum^+$ and the $D^2\Sigma^+$, for the general knowledge of molecule structure.

We observed four vibrational levels and attributed them to the B/B' $^2\Sigma^+$ (v=12, 13, 14 and 16) - $X^2\Sigma^+$ transitions, and five levels which had been previously miss assigned to the D state reassigned to the B/B' state [4]. In additional to this, we recently observed the B/B' (v=9, 10, 11, 18) levels. Then we observed unusual behaviors of vibrational structure, rotational structure and line intensity as follows;

- The vibrational spacing energy have oscillation pattern for higher vibraional levels.
- O－C value for some rotational line are much larger than RMS value
- Line intensity: Low J rotational transition lines even vibrational states in the B/B' state is weak and especially the J=0→1 transition lines are completely missing

We consider that there should be perturbation with some other electric states. In this talk, we report assignments of new four vibrational levels and discuss the perturbation.

[1] C. M. Olmsted, Astrophys. J. **27**, 66(1908).
[2] R. S. Mulliken, Phys. Rev. **25**, 509 (1925).
[3] H. Martin, J. Chem. Phys. **88** (1988) 1797.
[4] K. Watanabe et al., Chem. Phys. Lett. **657**, 1 (2016).

Vibronic Emission Spectroscopy of Jet-Cooled Benzyl-type Radicals Generated from Corona Discharge of Chloro-Substituted o-Xylenes

(Department of Chemistry, Pusan National University, Pusan 46241, Korea)
Sang Kuk Lee (sklee@pusan.ac.kr)

Abstract: Jet-cooled but vibronically excited chloro-substituted methylbenzyl radicals were generated from corona discharge of precursors, chloro-substituted *o*-xylenes with a large amount of carrier gas helium in a technique of corona excited supersonic expansion. From the analysis of the spectra observed, we can identify each benzyl-type radical formed by comparing the observation with the ab initio calculation, from which the red-shift of the origin band of the chloro-substituted methylbenzyl radicals was explained in terms of the lowest occupied molecular orbital (LUMO).

Introduction: Whereas benzyl radical, a prototypic aromatic free radical, has been the subject of numerous spectroscopic studies, chloro-substituted benzyl radicals have received less attention, due to the difficulties associated with production of radicals from precursors. The weak C-Cl bond can be easily dissociated in corona discharge of high voltage, leading to the formation of other benzyl-type radicals. During past years, we have concentrated the spectroscopy of chloro-substituted methylbenzyl radicals produced from corona discharge of precursor seeded in a large amount of helium carrier gas using a pinhole-type glass nozzle in a technique of corona excited supersonic expansion.

Experiment: For the production of jet-cooled but vibronically excited benzyl-type radicals, we have employed a technique of corona excited supersonic expansion coupled with a pinhole-type glass nozzle which has been well developed in this laboratory. The precursors were vaporized in a glass vessel of 2 atom helium gas and undergone corona discharge of less than 2 kV during supersonic jet expansion. The weak green-blue emission was recorded to obtain the vibronic emission spectra shown in Fig. 1 using a long path monochromator (Jobin Yvon U1000).

Results and Discussion: From the analysis of the spectra observed, we obtained the spectroscopic data listed in Table 1 from the assignment of the origin band of each benzyl-type radical using the substituent effect on electronic transition energy, especially of orientation effect of substituents. The large and small red shifts were confirmed for the 5-chloro- and 3-chloro-o-methylbenzyl radicals, respectively. The elliptic shape of the molecular orbitals at the lowest unoccupied state agrees well

Table1 1. Red-shifts of chloro-substituted-o-methylbenzyl radicals in the $D_1 \rightarrow D_0$ transition[a]

Molecules	Origin band	Shift[b]	Difference[c]
3-chloro-*o*-methylbenzyl	20680	1322	143
4-chloro-*o*-methylbenzyl	21376	626	31
5-chloro-*o*-methylbenzyl	20270	1732	-267
6-chloro-*o*-methylbenzyl	20418	1584	35

[a]Measured in vacuum (cm^{-1}).

with the observation, leading to the understanding the orbital shape of delocalized π electrons shown in Fig. 2. We believe this is the first attempt to describe the orbital motion of delocalized π electrons on the benzene ring perturbed by substituents.

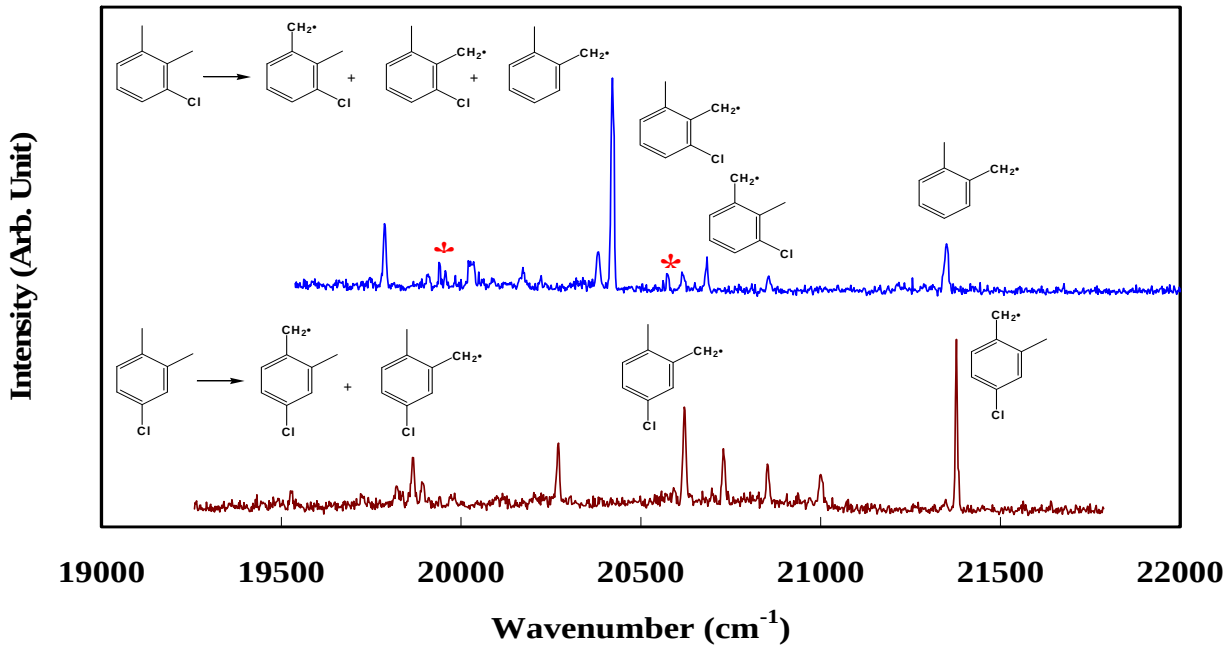

Figure 1. The vibronic emission spectra observed from the corona discharge of chloro-substituted o-xylene precursors seeded in a large amount of carrier gas helium. The top and bottom spectra were observed from 3-chloro-o-xylene and 4-chloro-o-xylene, respectively.

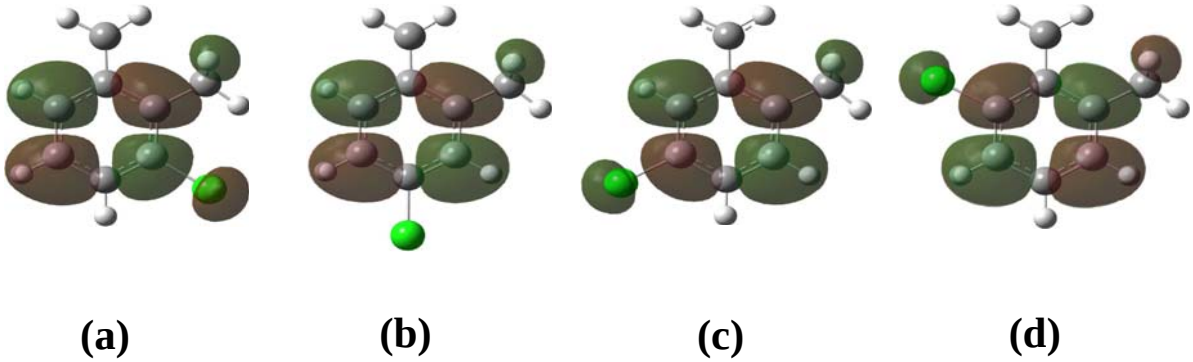

Figure 2. The 2-dimensional shape of lowest unoccupied molecular orbital of the chloro-substituted methylbenzyl radicals. The (a), (b), (c), and (d) represent the 3-chloro-, 4-chloro-, 5-chloro-, and 6-chloro-methylbenzyl radicals, respectively. The elliptic shape of molecular orbitals is believed to attribute to the size of red-shift of the origin band of the benzyl-type radical in the $D_1 \rightarrow D_0$ transition.

High-resolution laser spectroscopy and Zeeman effect of nitrate radical

(Kyoto Univ.[a], Kobe Univ.[b], Hiroshima City Univ.[c], The Grad. Univ. for Adv. Stds.[d])
Kohei Tada [a], Michihiro Hirata [b], Shunji Kasahara [b], Takashi Ishiwata [c], and Eizi Hirota [d]

1. Introduction

The nitrate radical (NO_3) is one of the important intermediate species in various chemical reactions involving nitrogen oxides and ozone [1]. In the ancient time the NO_3 was identified by a significant visible absorption, and this absorption system is now well known to correspond to an optically allowed $B\ ^2E' \leftarrow X\ ^2A_2'$ electronic transition. The 0 – 0 band of the $B – X$ transition is the strongest band in intensity, which is located at 15100 cm^{-1}, and some bands corresponding to the transitions to the vibrationally excited states lie in 15850 – 16100 cm^{-1} region.

The NO_3 is regarded as one of the important models for understanding the intra-molecular interactions in polyatomic radicals; thus, we have investigated the $B – X$ transition of the NO_3 by applying rotationally-resolved high-resolution laser spectroscopic methods [2-4]. In this talk, we summarize our studies of the 0 – 0 bands of the $^{14}NO_3$ and $^{15}NO_3$, and also we report the progress of the analysis of the transitions to the vibrationally excited states.

2. Experimental

Dinitrogen pentoxide (N_2O_5) was employed as a precursor of the NO_3, and the NO_3 was generated by the pyrolysis reaction of the N_2O_5: $N_2O_5 \rightarrow NO_3 + NO_2$ after jet-expanding the mixture of N_2O_5 vapor and helium gas into a high-vacuum chamber through a pulsed nozzle. The sample gas was shaped into a molecular beam with mechanical apertures. A single-mode ring dye laser (Coherent, CR699-29) pumped by a Nd: YVO_4 laser (Coherent, Verdi V-10) was used as a light source. The molecular beam was crossed with the dye laser beam at the right angles to reduce the Doppler width, and we observed rotationally-resolved laser-induced fluorescence (LIF) spectra. The linewidth of the rotational lines was typically 25 MHz, which is mainly the residual Doppler width. The absolute wavenumbers of the signals were calibrated to the accuracy of 0.0001 cm^{-1} by the simultaneous measurements of the fringe patterns of a cavity-length-stabilized etalon and Doppler-free saturation spectra of molecular iodine. The contamination of the NO_2 to the NO_3 spectrum was unavoidable in our experimental setup; thus, we observed the LIF spectra of the NO_2 to distinguish the NO_3 signals from the NO_2 signals.

3. The 0 – 0 band of the $^{14}NO_3$ isotopologue [2,4]

More than 3000 rotational lines with less rotational regularity were found in the observed 15070 – 15145 cm^{-1} region. Based on the NO_2 experiment the contamination of the NO_2 signals was confirmed to be negligible in this energy region. In the observed spectrum remarkable strong line pairs with energy spacing of 0.0248 cm^{-1} were found. This spacing is the same in magnitude with the spin-rotation splitting of the $X\ ^2A_2'$ ($\upsilon'' = 0$, $k'' = 0$, $N'' = 1$) level, where N is the quantum number of the total angular momentum excluding the electronic spin, and k is that of the projection of $\boldsymbol{N}$ along the molecular-fixed z axis. Then we found that the $B\ ^2E'$ state is described well in Hund's case (a) and the spin-orbit interaction splits this state into the $^2E'_{3/2}$ and the $^2E'_{1/2}$, because if this state is described in Hund's case (b) this 0.0248 cm^{-1} spacing is not detected directly due to the selection rule $F_1 \leftrightarrow F_1$ and $F_2 \leftrightarrow F_2$. Based on the selection rules $\Delta k = +1$, $\Delta J = 0, \pm 1$, the line pairs with the 0.0248 cm^{-1} spacing

should be assigned as the transitions to the $^2E'_{3/2}$ ($P' = 1.5$, $J' = 1.5$), $^2E'_{1/2}$ ($P' = 0.5$, $J' = 0.5$) or $^2E'_{1/2}$ ($P' = 0.5$, $J' = 1.5$) level, where J is the quantum number of the total angular momentum and P is that of the projection of $\boldsymbol{J}$ along the z axis. We observed the three types of Zeeman splitting up to 360 G with a pair of solenoid to distinguish these three types of transitions from each other. Finally, we identified seven transitions to the $^2E'_{3/2}$ ($P' = 1.5$, $J' = 1.5$) and 15 transitions to the $^2E'_{1/2}$ ($P' = 0.5$, $J' = 0.5$). From the density of the excited states we concluded that the $B\ ^2E'$ state interacts vibronically with the dark $A\ ^2E''$ state via the e′ type (asymmetric stretching and in-plane bending) vibrational modes. The effective spin-orbit interaction constant was estimated to be –21 cm^{-1}, based on the energy spacing of the averaged transition energies to the $^2E'_{3/2}$ (15100 cm^{-1}) and the $^2E'_{1/2}$ (15121 cm^{-1}).

In order to extend the assignment of rovibronic transitions to larger quantum numbers, we re-analyzed our high-resolution spectrum mainly based on the ground state combination differences. Owing to the selection rules $\Delta k = +1$, $\Delta J = 0, \pm 1$, the set of six rotational lines ${}^rP_{|k''|}(J' + 1)_{F'2}$, ${}^rP_{|k''|}(J' + 1)_{F'1}$, ${}^rQ_{|k''|}(J')_{F'2}$, ${}^rQ_{|k''|}(J')_{F'1}$, ${}^rR_{|k''|}(J' - 1)_{F'2}$, and ${}^rR_{|k''|}(J' - 1)_{F'1}$, which share an upper ($k'$, J') level, should be identified. We made rotational assignments for 162 lines (27 six-line sets) up to $|k''| = 15$, $J' = 18.5$. The molecular constants of the $B\ ^2E'_{3/2}$ state were roughly estimated as $B = 0.49(4)$ cm^{-1}, $C = 0.22(3)$ cm^{-1}, and $T_0 = 15099(8)$ cm^{-1}. On the other hand, those of the $B\ ^2E'_{1/2}$ state were roughly estimated as $B = 0.49(3)$ cm^{-1}, $C = 0.28(2)$ cm^{-1}, and $T_0 = 15110(5)$ cm^{-1}.

4. The 0 – 0 band of the $^{15}NO_3$ isotopologue [3]

We observed the rotationally-resolved LIF spectrum of the $^{15}NO_3$ in 15080 – 15103 cm^{-1} region, where about 200 strong lines and several thousand weak lines were found. We assumed that the $^{15}NO_2$ contamination is negligible, and the excited $B\ ^2E'$ state can be described in Hund's case (a). We identified two transitions to the $^2E'_{3/2}$ spin-orbit component, whereas six transitions to the $^2E'_{1/2}$. For the intrinsic $B\ ^2E'_{1/2}$ state we successfully made the rotational assignments of the $k = 1 \leftarrow 0$ stack up to $J' = 10.5$, and the molecular constants of this upper state were determined as $T_0 = 15098.20(4)$ cm^{-1}, $B = 0.4282(7)$ cm^{-1}, and $D_J = 4 \times 10^{-4}$ cm^{-1}. The spin-orbit interaction constant of the $B\ ^2E'$ state was estimated to be –12 cm^{-1} as the lower limit in magnitude.

5. The vibrationally excited $B\ ^2E'$ states of the $^{14}NO_3$ isotopologue

The vibronic band located at around 15900 cm^{-1} was assigned as the 4^2_0 band of the $B – X$ transition [5]. The high-resolution spectrum in 15860 – 15920 cm^{-1} has been observed, and we are in the progress of analyzing this spectrum. We identified many strong line pairs with the 0.0248 cm^{-1} spacing corresponding to the transitions to the levels with the smallest quantum numbers of both the $^2E'_{3/2}$ and $^2E'_{1/2}$ spin-orbit components. These line pairs are not random in distribution but consisting of band groups, and we found that these $^2E'_{3/2}$ and $^2E'_{1/2}$ groups appear alternately.

[1] R. P. Wayne, I. Barnes, P. Biggs, J. P. Burrows, C. E. Canosa-Mas, J. Hjorth, G. Le Bras, G. K. Woortgat, D. Perner, G. Poulet, G. Restelli, H. Sidebottom, Atmos. Environ. **25A**, 1 (1991).
[2] K. Tada, W. Kashihara, M. Baba, T. Ishiwata, E. Hirota, and S. Kasahara, J. Chem. Phys. **141**, 184307 (2014).
[3] K. Tada, K. Teramoto, T. Ishiwata, E. Hirota, and S. Kasahara, J. Chem. Phys. **142**, 114302 (2015).
[4] K. Tada, T. Ishiwata, E. Hirota, and S. Kasahara, J. Mol. Spectrosc. **321**, 23 (2016).
[5] M. Fukushima, and T. Ishiwata, 67th Int. Symp. Mol. Spectrsc. TI06 (2012).

Vibronic Coupling in the $\tilde{X}\ ^2A_2'$ state of NO_3

Masaru Fukushima and Takashi Ishiwata

Faculty of Information Sciences, *Hiroshima City University*
Asa-Minami, *Hiroshima 731-3194*, *Japan*

For the vibrational structure of the $\tilde{X}\ ^1A_1'$ state of NO_3, two assignments are proposed; a traditional assignment and one proposed by Stanton [1]. The major difference is the position of the ν_3 fundamental, at 1492 and ~1000 cm^{-1}, respectively. To solve this problem, we have measured dispersed fluorescence (DF) spectrum from the single vibronic levels (SVL's) of the $\tilde{B}$ state of jet cooled NO_3, for both isotopomers, $^{14}NO_3$ and $^{15}NO_3$ [2]. The spectrum from the vibration-less level consists of three regions; (I) regions around 1050 and 1500 cm^{-1}, (II) the region below 1850 cm^{-1} except (I), and (III) the region above 1850 cm^{-1}. Region II displays relatively regular vibrational structure including ν_1 fundamental and ν_4 progressions, 4^0_n, n = 0, 1, 2, 3, and $1^0_1 4^0_n$, n = 0, 1, 2. Region III possesses congested structure with levels thought to be heavily mixed difficult to vibrationally characterize. In this paper, we will focus the vibrational structure of the region I and the 2nd over-tone region of ν_1, ~2000 cm^{-1}, in region III, and discuss vibronic coupling in the $\tilde{X}\ ^1A_1'$ state.

First of all, three important findings are described. (1) We have found a new vibronic band very close to the ν_1 fundamental in region I [2], and thus two relatively intense vibronic bands are observed in the ν_1 fundamental region, ~1050 cm^{-1}, on the DF spectrum. In contrast, no bands have been detected in this region of the IR spectrum [3]. (2) In the 1500 cm^{-1} region of (I), only one intense band at 1500 cm^{-1} is observed on DF, while two bands at 1492 and 1499 cm^{-1}, which are *e*' and a_1' bands, respectively, are identified on IR hot bands [3]. (3) In the 2 ν_1 region, two bands, at 2010 and 2118 cm^{-1}, are observed on DF, and both are attributed to be a_1', because they have not been observed on IR [4]. The two bands show regular isotope shift [2]. Assuming Stanton's assignment, the levels at 1055 cm^{-1} (observed only on DF) and 1492 cm^{-1} (observed only on IR) will be attributed to the *e*' bands of the ν_3 fundamental and $\nu_3 + \nu_4$ combination levels, respectively, and his calculated DF spectrum quite nicely reproduces the observed [1]. However, this calculated DF spectrum does not match the observed DF spectrum. If the new band at 1055 cm^{-1} is labeled an *e*' band of the ν_3 fundamental, then the *e*' band of the combination, i.e. the 1492 cm^{-1} band, should be observed even in DF, but it isn't, while the a_1' band at 1500 cm^{-1} was remarkably observed in both DF and IR. In addition to this mismatch at ~1500 cm^{-1}, it is unusual for IR that no *e'* bands in region I have been observed; e.g. the ν_3 fundamental, expected to lie at 1055 cm^{-1}, should be observed in the IR spectrum, because the *e'* band of the combination at 1492 cm^{-1} is observed as the strongest band. Generally, a_1' bands are preferentially observed in DF. Thus we think that the two intense bands at 1055 and

1499 cm^{-1} on DF are both attributed to a_1'. The inverse isotope shift of the ν_1 fundamental lying close to the former [2] is easily understandable, and the major component of the latter is thought to be the 2nd over-tone of ν_2 (this is an out-of-plane umbrella mode, and the fundamental is at 762 cm^{-1} [3]), in which a favorable Franck-Condon factor is expected. This raises the question, what is the 1055 cm^{-1} a_1' band ?

We assign the 1055 cm^{-1} band to the 3rd over-tone of the ν_4 asymmetric (e') mode, 3 ν_4 (a_1'). We also assigned a weaker band at about 160 cm^{-1} above the new band to one with a final vibrational level of 3 ν_4 (a_2'). The 3 ν_4 (a_1') and (a_2') levels are ones with l = ±3. On the basis of experimental evidence of the strong correlation of the spin-orbit constant upon the ν_4 vibrational level, Hirota proposed a new vibronic coupling mechanism which suggests degenerate vibrational modes induce electronic orbital angular momentum even in non-degenerate electronic states and $K = \Lambda + l$ (this is written as $\overline{\Lambda} = \Lambda + l$ in [5]) should be conserved, where Λ is the induced Λ [5]. According to this, one of the components of the 3rd over-tone level,$|\, K = +3\,;\, \Lambda = 0\,;\, v_4 = 3\,,\, l = +3\,\rangle$, can have contributions of three components, $|\, +3\,;\, +1\,;\, 3\,,\, +2\,\rangle$, $|\, +3\,;\, +2\,;\, 3\,,\, +1\,\rangle$, and $|\, +3\,;\, +3\,;\, 3\,,\, 0\,\rangle$. The counter pair of the state, $|\, -3\,;\, 0\,;\, 3,\, -3\,\rangle$, has contributions of $|\, -3\,;\, -1\,;\, 3,\, -2\,\rangle$, $|\, -3\,;\, -2\,;\, 3\,,\, -1\,\rangle$, and $|\, -3\,;\, -3\,;\, 3\,,\, 0\,\rangle$. Accordingly, it is expected that there are sixth-order vibronic couplings, $(\, {q_+}^2\, {Q_+}^4 + {q_-}^2\, {Q_-}^4\,)$ and $(\, {q_+}^4\, {Q_+}^2 + {q_-}^4\, {Q_-}^2\,)$, for the 1st and 2nd components, respectively, among the three between the two 3 ν_4 components with l = ±3, $|\, +3\,;\, 0\,;\, 3,+3\,\rangle$ and $|\, -3\,;\, 0\,;\, 3,\, -3\,\rangle$. The two 6th order couplings above can be interpreted as 2nd order coupling of the 3rd order couplings, $(\, q_+\, Q_+^2 + q_-\, Q_-^2\,)^2$: Hirota-type [6] and $(\, {q_+}^2\, Q_+ + {q_-}^2\, Q_-\,)^2$: dynamical-Jahn-Teller-type, respectively. In the case of Renner-Teller interaction which is a typical of vibronic interactions, the 6th order couplings are weaker than the Renner-Teller term (the 4th order term, $(\, {q_+}^2\, {Q_-}^2 + {q_-}^2\, {Q_+}^2\,)$), but stronger than the 8th order term, $(\, {q_+}^4\, {Q_-}^4 + {q_-}^4\, {Q_+}^4\,)$. It is well known in linear molecules that the former, the 4th order term, shows huge splitting, comparable with vibrational frequency, among the vibronic levels of Π electronic states, and the latter, the 8th order term, shows considerable separation, ~10 cm^{-1}, for Δ electronic states. Consequently, the ~160 cm^{-1} splitting at v_4 = 3 is attributed to the 6th order interaction. The relatively strong intensity for the band to 3 ν_4 (a_1') can be interpreted as part of the huge 0-0 band intensity, because the 3 ν_4 (a_1') level, $|\, \pm 3\,;\, 0\,;\, 3\,,\, \pm 3\,\rangle$, can connect with the vibration-less level, $|\, 0\,;\, 0\,;\, 0\,,0\,\rangle$, through the Hirota- and dynamical-Jahn-Teller-types coupling above. 3 ν_4 (a_1') has two-fold intensity because of the vibrational wavefunction, $|\, +3;\, 0\,;\, 3,+3\,\rangle + |\, -3;\, 0\,;\, 3,-3\,\rangle$, while negligible intensity is expected for 3 ν_4 (a_2') with $|\, +3;\, 0\,;\, 3,+3\,\rangle - |\, -3;\, 0\,;\, 3,-3\,\rangle$ due to cancellation.

[1] J. F. Stanton, *J. Chem. Phys.* 126, 134309 (2007) and 69th ISMS, paper MI16.
[2] M. Fukushima and T. Ishiwata, 68th ISMS, paper WJ03.
[3] K. Kawaguchi *et al*., *J. Phys. Chem. A* 117, 13732 (2013).
[4] T. Ishiwata *et al*., *J. Phys. Chem. A* 82, 980 (2010). [5] E. Hirota, *J. Mol. Spectrosco.* 310, 99 (2015).
[6] E. Hirota, K. Kawaguchi, T. Ishiwata, and I. Tanaka, *J. Chem. Phys.* 95, 771 (1991).

B14

The Microwave Spectroscopy of Ground State CD_3SH

(Univ. of Toyama[a], Kanazawa Univ.[b]) Kaori Kobayashi[a], Wataru Nakamura[a], Tatsuro Matsushima[a], Shozo Tsunekawa[a] and Nobukimi Ohashi[b]

Methyl mercaptan (methanethiol, CH_3SH) is an interstellar organic molecule containing sulfur. We have studied an isotopologue, CD_3SH by using microwave spectroscopy. In this study, 484 A-species transitions up to $J = 46$ and $K_a = 10$ and 581 E-species transitions up to $J = 46$ and $K_a = 10$ in the ground state were least-squares-analyzed by using the pseudo-principal axis method (PAM) Hamiltonian with 22 parameters consisting of rotational, centrifugal distortion, and internal-rotational constants.

The methyl mercaptan molecule has similar molecular structure to methanol and its rotational spectra has also similar characteristics including torsional-rotational interaction. This molecule was also identified in interstellar Sgr B2 in 1979 [1]. The triply-deuterated methanol, CD_3OH was found in IRAS 16293-2422 [2] encouraged us to study this CD_3SH molecule. Previous microwave studies on this molecule are limited [3-5].

We also introduced pseudo-principal axis method (pseudo-PAM) [6], which was successfully applied to the analysis of the $HCOOCH_3$ in the second torsional excited state. The internal-rotation parameter ρ of methyl formate is about 0.08, which is fairly small, while CD_3SH has much larger ρ of about 0.8.

The spectra was taken by the conventional Stark/source-modulation microwave spectrometer. The enriched sample was purchased from the manufacturer (MSD isotopes) and used without further purification. The 12-240 GHz frequency region was observed at room temperature without gap. Fig. 1 shows an example spectrum.

Based on the preceding studies, we were able to make predictions and to extend the assignments. In total, we analyzed 1065 transitions by using the pseudo-PAM method. The comparison with the rho-axis method (RAM) will be shown.

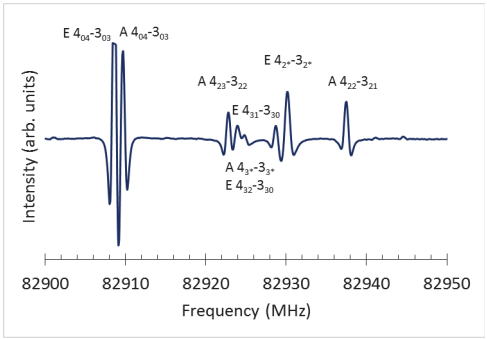

Fig. 1 Spectrum of CD3SH in the ground state. The asterisk denotes the unresolved K doublets.

References

[1] R. A. Linke, M. A. Frerking, and P. Thaddeus, 234 (1979) Astrophys. J., L139-L142.
[2] B. Parise, A. Castets, E.Herbst, E.Caux, C. Ceccarelli, I. Mukhopadhyay, and A. G. G. M. Tielens, 416 (2004) Astron. Astrophys., 159.
[3] T. Kojima, J. Phys. Soc. Jpn., 15 (1960) 1284-1291.
[4] Akihiro Kimura, University of Toyama, Master's Thesis (1983).
[5] Tomoaki Hayashi, University of Toyama, Master's Thesis (1990).
[6] K. Kobayashi, K. Takamura, Y. Sakai, S. Tsunekawa, H. Odashima, N. Ohashi, Astrophys. J. Suppl. Ser. 205 (2013) 9-15.

B15

Mass-analyzed threshold ionization spectroscopy of some sandwich molecules.

(IAMS, Academia Sinica, Taiwan[a], G. A. Razuvaev Institute of Organometallic Chemistry, Russian Academy of Sciences[b]) Sheng-Yuan Tzeng[a](flyswimcamel@hotmail.com), Pei-Ying Wu[a](d01223104@ntu.edu.tw), Sergey Yulievich Ketkov[b](sketkov@iomc.ras.ru), and Wen-Bih Tzeng[a](wbt@sinica.edu.tw)

We applied the photo ionization efficiency and mass-analyzed threshold ionization (MATI) techniques to record the cation spectra of (η^6-benzene)(η^6-biphenyl)chromium and bis(η6-biphenyl)chromium. The adiabatic ionization energies (IEs) of these two sandwich molecules are determined to be 43374 and 42874 ± 10 cm^{-1}, respectively. The prominent features appeared at 63, 150, 209, and 270 cm^{-1} with respect to the 0^+ band in the MATI spectrum of (η^6-benzene)(η^6-biphenyl)chromium result from the ring bending vibrations of the cation. We also performed the density functional theory (DFT) calculations at the B3PW91/6-311++G(d,p) level to predict the optimized molecular structure, transition energy, and vibrational frequency for these species. These calculations underestimates the IEs of these species by no more than 2%. The 0^+ band in the MATI spectrum of bis(η^6-biphenyl)chromium has a full width at half maximum of about 200 cm^{-1}, which is much broader than a typical value of 10-20 cm^{-1}. This broad spectral feature likely results from overlap of the 0^+ bands of six conformational isomer. Our DFT calculations support the present experimental findings.

B16

Study of 2-Chloro-4-fluoroanisole by two-color resonant two-photon mass-analyzed threshold ionization spectroscopy

(IAMS, Academia Sinica, Taiwan[a]) Yu-Che Sun[a](sirjackmatt@gmail.com), Wen-Bih Tzeng[a](wbt@sinica.edu.tw)

We applied the resonant two-photon ionization (R2PI) and mass-analyzed threshold ionization (MATI) spectroscopic techniques to record the vibronic and cation spectra of 2-chloro-4-fluoroanisole (2C4FAN). The band origin of the $S_1 \leftarrow S_0$ electronic transition of 2C4FAN was found at 34 621 ± 2 cm^{-1} and the adiabatic ionization energy was determined to be 67 204 ± 5 cm^{-1}. These spectra provide information about the active vibrations of this molecule in the electronically excited S_1 state and cationic ground D_0 state. Comparing these experimental data of 2C4FAN with those of o-chloroanisole, p-fluoroanisole, and anisole, we can learn the effect of the nature and the location on the ring of substituents on transition energy and molecular vibration.

B17

One-photon mass-analyzed threshold ionization (MATI) spectroscopy of thietane cation

(Kangwon National Univ.) Yu Ran Lee, Hong Lae Kim, and Chan Ho Kwon*
E-mail:chkwon@kangwon.ac.kr

Thietane as a four-membered heterocyclic ring compound is prototypical molecule for studying on equilibrium configuration of the neutral and the cation. We have measured the high-resolution vibrational spectrum of theitane (trimethylene sulfide) cation in the gas phase by employing the vacuum ultraviolet mass-analyzed threshold ionization (VUV-MATI) technique. The measured VUV-MATI spectrum featured complicatedly in the low frequency region, which demonstrated notably the twin peaks separated by 17 cm^{-1} with the FWHM of ~8 cm^{-1} as the lowest frequency bands. Peaks in the low frequency region of the observed spectrum of thietane cation could be successfully reproduced by solving the Schrodinger equation with one-dimensional (1D) symmetric double-well potentials along the ring puckering coordinates on both the S_0 and D_0 states of thietane, respectively, which revealed as a progression of the ring puckering vibrational mode. The values of the interconversion barrier and the ring puckering angle on the S_0 state, the parameters used for the quantum chemical calculations, were assumed to be 274 cm^{-1} and 26°. The barrier and the angle on the D_0 state, however, are found to be 48.0 cm^{-1} and 18.2°, respectively, where such small barrier height and puckering angle for the cation suggest that the conformation of thietane cation on the D_0 state should be more planar than that of the thietane neutral. Then, the accurate ionization energy of thietane was determined to be 69,762 ± 3 cm^{-1} (8.6493 ± 0.0004 eV) under the zero field limit.

B18

One-photon vacuum ultraviolet mass-analyzed threshold ionization (VUV-MATI) spectroscopy of crotonaldehyde

(Kangwon National Univ.) Sung Man Park, Hong Lae Kim, and Chan Ho Kwon*

E-mail:chkwon@kangwon.ac.kr

We measured the cationic vibrational spectrum of crotonaldehyde (2-butenal) using one-photon vacuum ultraviolet mass-analyzed threshold ionization (VUV-MATI) spectroscopy. The VUV radiation was generated by four-wave difference frequency mixing in Kr gas. From the origin band in the MATI spectrum, the adiabatic ionization energy of crotonaldehyde determined to be 9.7501 ± 0.0005 eV (78642 ± 0.0004 cm^{-1}). This value is in agreement with the previous one. To analyze the cationic vibrational spectrum, we performed the Franck-Condon simulation at M062x/aug-cc-pVDZ level, which revealed to be four stereo isomers of trans-*s-trans*, trans-*s-cis*, cis-*s-trans*, and cis-*s-cis* crotonaldehyde. Most of vibrational peaks observed in the spectrum were assigned to that of trans-*s-trans* crotonaldehyde and the remained peaks were assigned to the vibrational peaks of trans-*s-cis,* cis-*s-trans,* or cis-*s-cis* crotonaldehyde. The adiabatic ionization energies of trans-*s-cis,* cis-*s-trans,* and cis-*s-cis* crotonaldehyde were determined to be 9.7619 ± 0.0005 eV (78737 ± 4 cm^{-1}), 9.7121 ± 0.0005 eV (78335 ± 4 cm^{-1}), and 9.6481 ± 0.0005 eV (77819 ± 4 cm^{-1}), respectively.

B19

Conformer-specific ion spectroscopy of isobutanal

(Kangwon National Univ.) Yu Ran Lee, Hong Lae Kim, and Chan Ho Kwon*

E-mail:chkwon@kangwon.ac.kr

Isobutanal is an aliphatic aldehyde which has been extensively considered as one of important intermediates in isomerization reaction as well as astrochemical relevant models in the interstellar medium. We report conformer-specific ionization dynamics and cationic vibrational spectra of the isobutanal utilizing one-photon mass-analyzed threshold ionization (MATI) spectroscopy using the vacuum ultraviolet (VUV) laser pulse for the first time. The conformational preference of isobutanal in the various supersonic expansion conditions was explored to identify the conformers, from which the intrinsic ionization dynamics were elucidated by directly measuring the VUV-MATI spectrum corresponding to each conformer. The observed conformer-specific vibrational spectra of isobutanal cations could be definitely analyzed through the Franck-Condon simulations at the B3LYP/cc-pVTZ level for isobutanal conformers, trans and gauche. Most of all, we confirm that there exist two stable conformers as gauche and trans in the lowest ionic state as well as the neutral ground state, producing by accurate adiabatic ionization energies of 78,557 ± 3 cm^{-1} (9.7398 ± 0.0004 eV) and 78,136 ± 3 cm^{-1} (9.6878 ± 0.0004 eV), respectively. Notably, only gauche conformer undergoes the unique geometrical change upon ionization, resulting in the progression of the CHO torsional mode.

B20

Vacuum ultraviolet mass-analyzed threshold ionization spectroscopy of hydrazoic acid (HN_3)

(Kangwon National Univ.) Do Won Kang, Hong Lae Kim, and Chan Ho Kwon*

E-mail:chkwon@kangwon.ac.kr

We obtained the vibrational spectrum of hydrazoic acid (HN_3) cation in the electronic ground state by utilizing the vacuum ultraviolet mass-analyzed threshold ionization (VUV-MATI) spectroscopy for the first time. For the one-photon ionization of hydrazoic acid, the tunable and coherent vacuum ultraviolet (VUV) radiation in the 86200-88100 cm^{-1} (10.687-10.923 eV) range was generated by non-resonant four-wave sum frequency mixing ($\omega_{VUV} = 2\omega_{UV}+\omega_{Vis}$) in Xe and Ar mixture. The accurate ionization energy of HN_3 was determined to be 86,591 $\pm$ 5 cm^{-1} from the 0-0 band position in the MATI spectrum. To assign the peaks observed in the MATI spectrum, we carried out the Franck-Condon simulations employing various methods and levels, from which the precise structure of HN_3 could be determined. It revealed that the observed spectrum displayed mainly totally symmetric vibrational modes of A' for the linear HN_3.

Vacuum Ultraviolet Mass-Analyzed Threshold Ionization Spectroscopy of Tetrahydrofuran

(Kangwon National Univ.) Sung Man Park, Chan Ho Kwon*, Hong Lae Kim*

E-mail:hlkim@kangwon.ac.kr

A vibrational spectrum of tetrahydrofuran (THF) cation in the gas phase was measured by one-photon vacuum ultraviolet mass analyzed threshold ionization (MATI) spectroscopy. The cation of a designated mass was detected with a time-of-flight mass spectrometer by pulsed field ionization of the molecule in the high Rydberg states delayed by a laser pulse scanning across the region of the vibrational spectrum. From the position of the 0-0 band in the zero field limit and the photoionization efficiency curve, the accurate first adiabatic ionization energy was measured, which is 9.4256 eV. The observed ionization energy was assigned as a result of the transition of the molecule with C_2 symmetries on both the ground S_0 and cationic ground D_0 states. Quantum chemical calculations for the molecule in the S_0 and D_0 states were performed and the peaks in the spectrum were successfully assigned employing the dipole selection rules between the S_0-D_0 transition and Franck-Condon factors calculated by varying structural parameters, which determines the accurate molecular structure of the tetrahydrofuran cation.

Temperature effect on the microscopic hydration structures of phenol cation

(Kitasato Univ.) Itaru Kurusu, Reona Yagi, Ryota Kato, Yashutoshi Kasahara, Haruki Ishikawa
E-mail: harukisc@kitasato-u.ac.jp

Temperature effects on the hydration structure is very important to understand microscopic nature of the hydrogen bond network. One of the temperature effects on the hydration structure in the cluster is a change in relative populations among the isomers. In the present study, we have carried out ultraviolet photodissociation spectroscopy of hydrated phenol cation trapped in the temperature-variable ion trap. We have succeeded in observing a clear change in the relative populations between the isomers having distinct hydration structures. The temperature-dependence observed is well interpreted by flexibility of the hydration structures of the isomers obtained by theoretical calculations.

Introduction

Hydrogen bond plays an important role in various chemical and biological process. To investigate the microscopic nature of hydrogen bond, a large number of spectroscopic studies of the gas-phase molecular clusters have been carried out and hydration structures of various systems have been determined so far. Since hydration structures are flexible in nature, temperature effect is very important. One of the temperature effects on the microscopic hydration structure is a change in relative populations among the isomers. In the present study, we have carried out ultraviolet (UV) photodissociation (PD) spectroscopy of hydrated phenol cation, $[PhOH(H_2O)_5]^+$, trapped in our temperature-variable 22-pole ion trap. We have succeeded in observing a clear temperature dependence of the relative populations of the isomers having distinct hydration structures. Possible hydration structures of the clusters are obtained by density functional theory (DFT) calculations. The relative populations of the isomers are also estimated by statistical mechanically based on the results of the DFT calculation. In the present paper, we would like to discuss the temperature effect on the hydration structure of $[PhOH(H_2O)_5]^+$ based on the experimental and theoretical results.

Experimental and computational details

In the present study, we used our temperature-variable 22-pole ion trap apparatus [1]. The hydrated phenol cation clusters were generated by the combination of laser ionization and supersonic expansion techniques. The clusters produced were mass-separated by the first quadrupole mass filter and then introduced into the 22-pole ion trap. The ions in the trap were temperature-controlled by the He buffer gas cooling method. After the achievement of the thermal equilibrium condition, UV laser light was irradiated to the clusters. The photofragment ions were mass-analyzed and detected by the second quadrupole mass analyzer. Possible hydration structures of isomers of $[PhOH(H_2O)_5]^+$ were obtained by the DFT calculation at ωB97X-D/6-311++G(3df,3pd) level. We also estimated Gibbs energy of the isomers at various temperatures based on statistical mechanics. Then relative populations of the isomers were obtained assuming the Boltzmann distribution.

Results and Discussion

In the present study, we evaluated the vibrational temperatures of the ions in the trap based on the relative intensities of hot bands in the electronic spectra of phenol-trimethylamine cation, $[PhOH\text{-}TMA]^+$. Since a proton of the phenol moiety is transferred to trimethylamine side, the chromophore of the UV transition is a phenoxy radical in the cluster. The UV transition observed in the present study corresponds to the D_3-D_0 transition of the phenoxy radical. As a result, vibrational temperatures of the $[PhOH\text{-}TMA]^+$ are almost the same as the temperature of the trap except for the case when the temperature of the trap is set below 30 K. The vibrational temperature of 30 K is the lowest one achieved in our trap.

Then, we measured the UV photodissociation spectrum of $[PhOH(H_2O)_5]^+$ at vibrational temperatures from 30 to 150 K. In Figure 1, the spectra observed at 30 K and 150 K are shown. In the spectra measured at 30 K, only one isomers are observed. Hereafter, this isomer is referred to as isomer A. As the temperature elevates, another isomer is observed in the spectra. In Figure 1(b), the 0-0 band of a newly appeared species (isomer B) is denoted as B. The intensity of the 0-0 band of the isomer B is larger than that of the isomer A. This indicates an inversion of the relative populations between the isomers A and B occurs around at 150 K. Anyway, these spectra clearly indicates the change in the relative population between the two isomers along the temperature elevation.

Possible structures of the isomers A and B are also shown in Figure 1. They have distinct hydration structures and are expected to exhibit different temperature dependence in the relative populations. The isomer B has a flexible chain type hydration structure, which indicates a large entropic contribution in the temperature dependence. On the other hand, the hydration structure of the isomer A involves ring type structure. It should be less flexible than the chain type structures. Thus, the inversion of the relative population experimentally observed around 150 K is qualitatively interpreted by the difference in the flexibility of the hydration structures of the isomers A and B.

Details of the discussion will be presented in the paper.

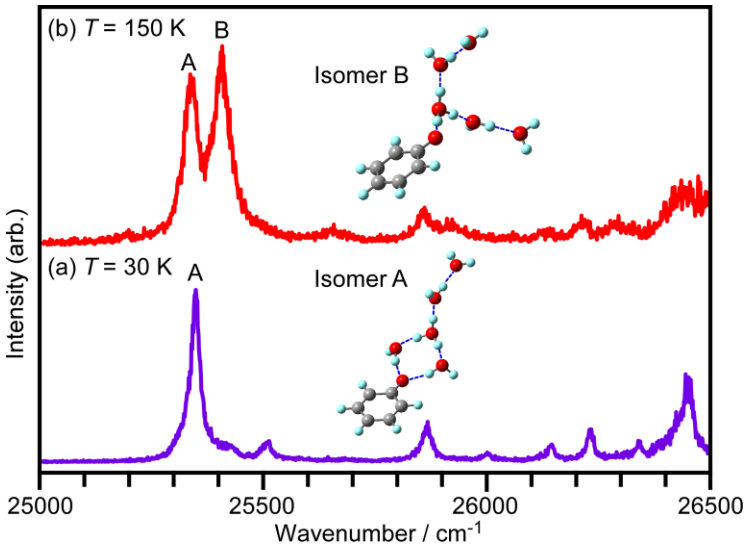

Figure 1. Photodissociation spectra of $[PhOH(H_2O)_5]^+$ measured at (a) T = 30 K and (b) T = 150 K. Possible hydration structures of the isomers A and B are inserted.

[1] H. Ishikawa et al. *Chem. Phys. Lett.* **514**, 234 (2011).

B23

Proton diffusion dynamics along a diol as a proton-conducting wire in a photo-amphiprotic model system

(Center for Soft and Living Matter, Institute for Basic Science (IBS)[a], Department of Chemistry, School of Natural Science, Ulsan National Institute of Science and Technology (UNIST)[b])

Ye-Jin Kim[a, b] (gne1019@unist.ac.kr), Kyeong Eun Mun(mke3321@unist.ac.kr), and Oh-Hoon Kwon[a, b] (ohkwon@unist.ac.kr)

We investigated the dynamics of excited-state proton transfer (ESPT) of photo-amphiprotic 7-hydroxyquinoline (7HQ) in the presence of a hydrogen (H)-bond bridging diol in a polar aprotic medium. The formation of 1 : 1 H-bonded complexes of 7HQ with various diols of different alkane chain lengths was revealed using steady-state electronic spectroscopy. With femtosecond-resolved fluorescence spectroscopy, cyclic H-bonded 1 : 1 complexes were found to undergo facile ESPT from the acidic enol to the basic imine group of 7HQ *via* the H-bond bridge. Through quantum chemical calculations, we found that the proton-transfer rate of the well-configured H-bonded complex correlated with the intramolecular H-bond length of a H-bond wiring diol molecule. Noncyclic, singly H-bonded 7HQ with a diol molecule was observed to undergo ESPT once another diol molecule diffuses to the noncyclic complex and accomplishes the formation of a reactive cyclic H-bonded 7HQ-$(diol)_2$ complex, which was evidenced by the observation that the overall proton-transfer rate constant decreases when a longer-chain diol was used as the bridging wire part. The kinetic isotope effect on the proton relay was investigated to confirm that the nature of the activation barrier for the proton diffusion along the wire is isotope-sensitive proton tunnelling, while for the non-cyclic configuration, the isotope-insensitive H-bond bridge formation is a prerequisite for ESPT.

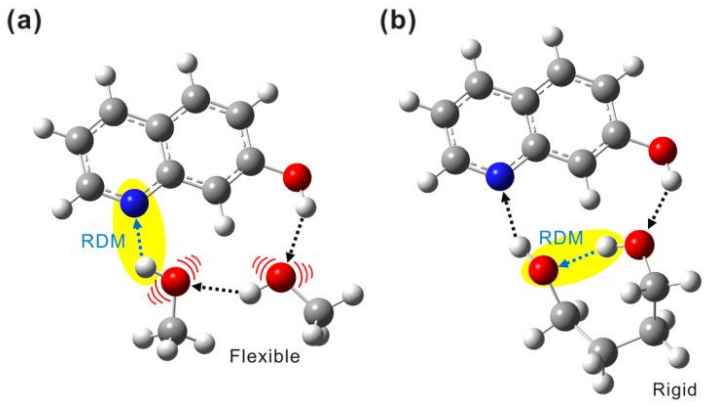

Figure Transition of the reaction coordinate for the ESPT of cyclic H-bond bridged complexes of 7HQ. (a) H-bonded complex with two alcohol molecules as a H-bond bridge. (b) H-bond complex with one diol molecule as the bridge. RDM denotes the rate-determining step.

B24

Orientation change and structure according to the various pH conditions of 4-amino-4'-cyanobiphenyl on silver surfaces: SERS and DFT study

(Kangwon National Univ.) So Young Eom, Hong Lae Kim*, and Chan Ho Kwon*
E-mail: chkwon@kangwon.ac.kr

Surface-enhanced Raman Scattering (SERS) spectra of 4-amino-4'-cyanobiphenyl (44ACBP) adsorbed on Ag colloidal nanoparticles were measured in various pH conditions. In neutral and alkaline solutions, the molecule should be adsorbed flat on the surface whereas in acidic solution, the molecule should vertically be adsorbed through the CN-metal bonding due to protonation in the amine group. The peaks observed in the spectra were assigned in comparison to those in the normal Raman spectra taking advantage of quantum chemical density functional theory (DFT) calculations. The adsorption behavior could be identified from spectral analyses of relative enhancement of the in-plane against the out-of-plane vibrational modes observed in the SERS spectra. The orientation of 44ACBP adsorbed on the Ag surface could be reversibly controlled to flat or vertical orientation by changing pH in solution.

B25

Study of Hydrogen-Bonding Energetics and Dynamics of Biological Water Using Ultrafast Electronic Spectroscopy

(Center for Soft and Living Matter, Institute for Basic Science (IBS)[a], Department of Chemistry, School of Natural Science, Ulsan National Institute of Science and Technology (UNIST)[b], Department of Molecular Science and Technology, Ajou University[c])
Young Jae Kim[a,b], Byeong Sung Lee[c], Tae Hyeon Yoo[c], Oh-Hoon Kwon[a,b*] (ohkwon@unist.ac.kr)

When water molecules locate near a biological macromolecule such as protein, their properties are known to deviate from those of water molecules in bulk. Those water molecules in the vicinity of protein surfaces are called biological water. Biological water plays crucial roles in the structure, dynamics and function of biological entities including protein-protein and protein-substrate interactions [1]. Therefore, the study of the energetics and dynamics of biological water is an essential step towards better understanding the characteristics of biological phenomena.

At a biological surface, the hydrogen bond of a water molecule among them can be either replaced by that to a hydrophilic protein surface or limited depending on the topology, hydrophobicity, and/or the charged state of the protein surface (and pocket). The hydration dynamics of biological water has been intensively explored, experimentally and theoretically, to show its deceleration compared to the dynamics of bulk water [1-3]. On the other hand, its energetics has been overlooked, which is a key to understand the molecular interactions at biological surfaces.

Here we report the analysis of the hydrogen-bond energy of biological water through chemical kinetics analysis of excited-state proton transfer (ESPT) mediated by a water hydrogen-bond bridge. The fluorescent, non-canonical amino acid, 7-azatryptophan (AW), was used in this study as a probe. The chromophore of AW, 7-azaindole, is well-known for undergoing ESPT catalyzed by a water molecule, for which 7-azaindole competes with other water molecules to form a cyclic hydrogen-bond bridge. The probe is inserted to a coiled-coil protein to selectively probe the water energetics at the surface of the protein [4]. From the measurements of the femtosecond-resolved fluorescence spectra of the fluorescent amino acids installed, the hydration dynamics was also investigated.

References

[1] Bhattacharyya, K. *Chem. Commun.* **2008**, 25, 2848-2857
[2] Zhong, D.; Pal, S. K.; Zewail, A. H. *Chem. Phys. Lett.* **2011**, 503, 1-11
[3] Qin, Y.; Wang, L.; Zhong, D. *Proc. Natl. Acad. Sci. USA* **2016**, 113, 8424-8429
[4] Kwon, O.-H.; Yoo, T. H.; Othon, C. M.; Van Deventer, J. A.; Tirrell, D. A.; Zewail, A. H. *Proc. Natl. Acad. Sci. USA* **2011**, 107, 17101-17106

B26

Chiral Differentiation of Protonated L- and D-Amino Acids by Permethylated β-cyclodextrin: Experiments and Theory

(Department of Applied Chemistry, Kyung Hee Univ., Gyeonggi 446-701, Republic of Korea[a], Department of Chemistry, Sogang Univ., Seoul 121-742, Republic of Korea [b], State Key Lab. of Elemento-Organic Chemistry, Nankai Univ., Tianjin 300071, China[c], Collaborative Innovation Center of Chemical Science and Engineering, Nankai Univ., Tianjin 300071, China[d].)

Sung-Sik Lee[a], Soojin Park[b], Xianglei Kong[c, d*](kongxianglei@nankai.edu.cn), Sungyul Lee[a*](sylee@khu.ac.kr), Han Bin Oh[b](hanbinoh@sogang.ac.kr)

Structures of gaseous permethylated β-cyclodextrin/H^+/H_2O and /H^+/Ala are studied using electrospray, IRMPD spectroscopy and density functional theory calculations. The protonated non-covalent complexes of permethylated β-cyclodextrin and the *D*- or *L*-alanine were mass-selected and investigated by IR laser pulses in the wavelength region of 2650-3800 cm^{-1}. The remarkably different features of the IRMPD spectra for *D*- and *L*-alanine are described, and their origin is elucidated by quantum chemical calculations. We show that the differentiation of the experimentally observed spectral features is the result of different local interactions of *D*- and *L*-alanine with permethylated β-cyclodextrin. The very high Gibbs free energies of the gaseous permethylated β-cyclodextrin/H^+/H_2O and permethylated β-cyclodextrin/H^+/Ala complexes are noted. We focus on the extremely high frequency bands at > 3700 cm^{-1}, assigning them to completely isolated carboxyl group. We also find that the high Gibbs free energy of gas phase permethylated β-cyclodextrin/H^+/H_2O system is due to the presence of separate H^+ and H_2O rather than H_3O^+. These findings are discussed in relation to solution phase host-guest-solvent configurations.

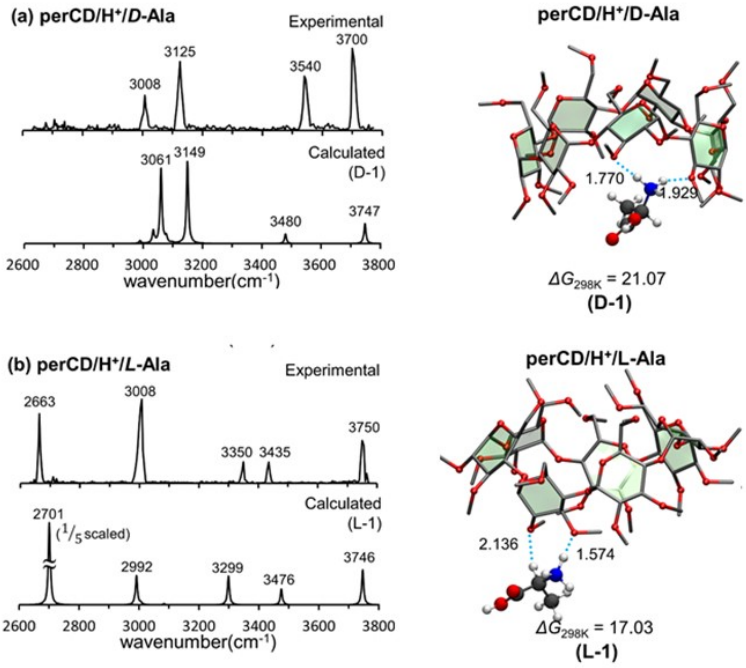

B27

Photodissociation of CF_2ICF_2I and CF_2I_2 in solution probed by femtosecond infrared spectroscopy

(Pusan National Univ.) Seongchul Park, Joohyang Shin, Changwon Yang, Youngshang Pak, and Manho Lim

Photodissociation dynamics of CF_2ICF_2I and CF_2I_2 in solution was investigated by probing the C-F stretching mode using femtosecond infrared spectroscopy after excitation with a 267-nm photon. Dissociation of the first I atom was faster than 0.3 ps after the UV absorption. All of the resulting haloethyl radicals undergo the secondary dissociation with two time constants; the radical from the *anti*-CF_2ICF_2I in CCl_4 and in acetonitrile solutions dissociate with time constants of 175 ± 5 ps and 40 ps, respectively. The radical from *gauche*-CF_2ICF_2I in both solutions dissociates with the same time constant of 7 ± 1 ns. Some portion of the radical from CF_2ICF_2Br geminately rebinds and the remaining forms CF_2CF_2 with a time constant of 160 ns. A photodissociation mechanism that explains the conformer-dependent dissociation rate as well as solvent-dependent dissociation rate was suggested based on a potential energy surface calculated CASSCF.

B28

Hydration Characteristics of a Water Pool in a Nano-Confined System Probed by a Superphotoacid

(Department of Chemistry, School of Natural Science, Ulsan National Institute of Science and Technology (UNIST)[a], Center for Soft and Living Matter, Institute for Basic Science (IBS)[b]) Jae-Heon Park[a], Hak-Won Nho[a] and Oh-Hoon Kwon[a,b*] (ohkwon@unist.ac.kr)

The reverse micellar system is a representative biomimetic molecular system. A reverse micelle consists of a non-polar solvent phase, an interfacial region of surfactant molecular layer and a water pool [1]. The characteristics of a reverse micelle system varies with the size of the reverse micelle, mainly the size of the water pool confined in a nanometer core. The water nanopool can be further distinguished as two different regions; boundary water and free water. In the boundary water region, the water molecules have strong dipole-ion interaction with the surfactant head groups, so the boundary water motion is more restricted than free water motion [2,3]. The motion of water molecules in the free water region becomes similar with that of bulk water.

Here, we investigated the hydration characteristics of a water pool in the Aerosol-OT (sodium bis[2-ethylhexyl] sulfosuccinate) reverse micelle by measuring the fluorescence of cationic superphotoacid, N-methyl-7-hydroxyquniolinium ($NM7HQ^+$) ion in a water nanopool. $NM7HQ^+$ is a strong photoacid with a much lower pKa value when excited by light than in the ground state which triggers the excited-state deprotonation of the cationic $NM7HQ^+$ (C) giving birth to a product, keto form (K). The two prototropic species have different formal charges, which affect residence sites and diffusive motions in the confined environment of the reverse micelle.

The excited-state dynamics of $NM7HQ^+$ was analyzed by measuring picosecond-resolved emission spectra (TRES). The spectral deconvolution of the TRES into the spectra of the two prototropic species allowed for the differentiation of the spectral shift from the excited-state population dynamics. As a result, we could successfully resolve the hydration dynamics in the water pool and correlate it to proton-transfer dynamics. Also, the time-dependent florescence anisotropy measurements revealed the rotational diffusion dynamics of the two prototropic species.

References

[1] Shirota, H.; Horie, K. *J. Phys. Chem. B* **1999**, 103, 1437-1443
[2] Chatterjee A.; Maity B.; Seth D. *Phys. Chem. Chem. Phys.* **2013**, 15, 1894-1906
[3] Kwon O.-H.; Kim T. G.; Lee Y.-S.; Jang D.-J. *J. Phys. Chem. B* **2006**, 110, 11997-12004

Local Mode-Based Infrared Probe Spectra: a Case Study of Formic Acid-Water Clusters and Solutions

(Institute of Theoretical Chemistry, Jilin University) Yang Cong[a], Hui Li[b]
Email: Prof_huili@jlu.edu.cn

A new method based on perturbation theory and statistical method is developed to simulate the IR spectra of clusters and solutions. This approach could be used to quickly predict more accurate spectra corresponding to formic acid C=O stretching in water clusters and condensed states than traditional methods. Vibrational localization method[1] can be used to select the most related modes to the C=O stretching, which is helpful to find a more effective vibrational space in following calculations. *Ab initio* molecular dynamics simulation is used to sample intermolecular configurations of clusters, and quantum treatment based on the perturbation approximation is made following that. Fourier transformation is performed to get the spectrum with not only peak positions but also line shapes. Hence, the method could get an experiment-comparable time-dependent transition frequencies of the system. This method was firstly successfully applied in the study of HCl-water clusters[2]. In this work, we will extend this approach and applied it in studying the IR proble spectra of formic acid-water clusters and solutions.

[1] Christoph R. Jacob, Sandra Luber and Markus Reiher *J. Phys. Chem. B*, 113(18) 6558-6573 (2009)

[2] Rui-Jie Xue, Adam Grofe, He Yin, Zexing Qu, Jiali Gao,and Hui Li. *J. Chem. Theory. Comput.* 13, 191-201 (2017)